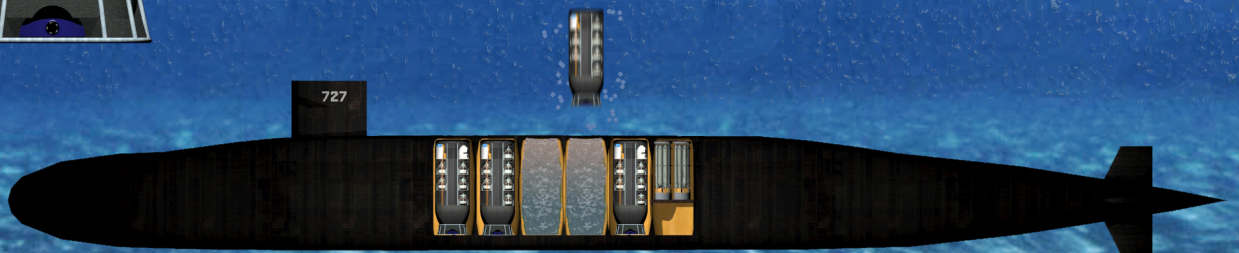
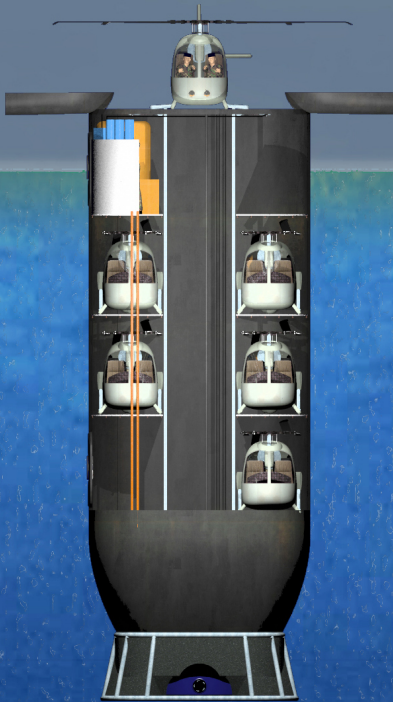
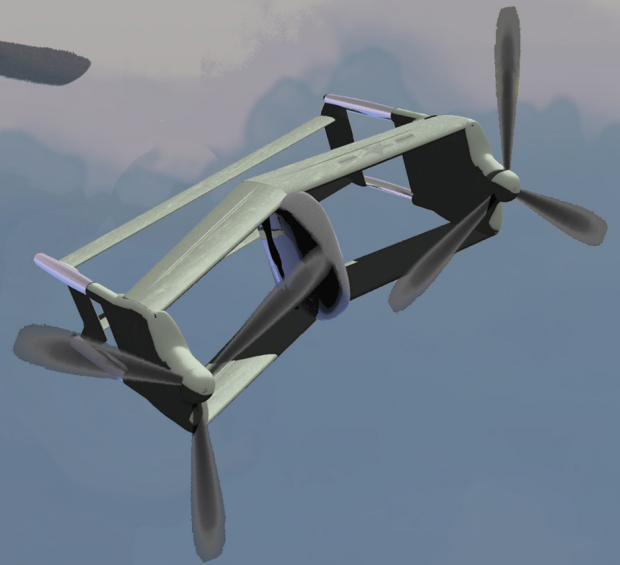


2007 AHS Graduate Design Competition

Cipher, Dragonfly, and Barracuda

Daniel Guggenheim School of Aerospace Engineering
Georgia Institute of Technology



Acknowledgements

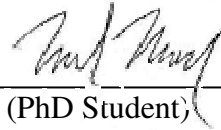
We would like to recognize and thank the following individuals for their special assistance in the completion of this design project:

Dr. Daniel Schrage	Mr. Kshitij Shrotri	Mr. Mike Scully
Dr. Mark Costello	Mr. Emre Gündüz	Mr. John Davis
Dr. Robert Loewy	Mr. Bernard Laurendeau	Mr. Andrew Hahn
Dr. Lakshmi Sankar	Mr. Apinut Sirirojvisuth	Mr. Todd Hodges
Dr. JVR Prasad	Mr. Sumit Mishra	Maj Stephen Suhr
Dr. Suresh Kannan	Mr. Nischint Rajmohan	CPT Eugene Jones
Dr. Han Gil Chae	Mr. Sameer Hameer	Mrs. Amber Stone
Dr. Sandeep Agarwal	Dr. Jieun Ku	Dr. Byung-Ho Ahn
Dr. Adeel Khalid	Dr. Vitali Volovoi	Dr. Dewey Hodges
Dr. Olivier Bauchau		

2007 Georgia Tech Design Team



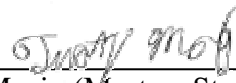
CPT Joseph Davis (Masters Student)



Mark Moore (PhD Student)



Jeremy Bain (Masters Student)



Tim Mosig (Masters Student)



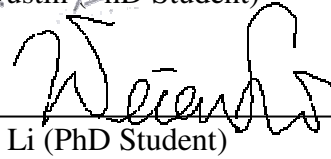
Michael Duffy (Masters Student)



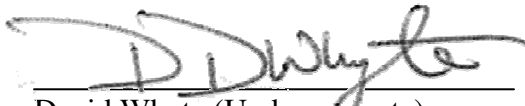
Cedric Justin (PhD Student)



Jeff Staub (Undergraduate)



Wei-En Li (PhD Student)



David Whyte (Undergraduate)



Doug Smith (Undergraduate)

For participating in the 2007 AHS design competition, all graduate students received four hours of academic credit for AE6334 (Rotorcraft Design). All undergraduate students received four hours of academic credit for AE4351 (Rotorcraft Design).

Table of Contents

Table of Tables	v
Table of Figures	vi
Nomenclature	viii
Executive Summary	v
1. Introduction	13
1.1. RFP Summary	13
1.2. Mission and Requirements Analysis.....	14
1.2.1. Stealth	14
1.2.2. Soldier Deployment Rate.....	14
1.3. Overall Evaluation Criteria (OEC)	18
1.3.2. Mission Capability Index for the ARV (MCI_{ARV})	19
1.3.3. Mission Capability Index for the UEV (MCI_{UEV})	19
1.3.4. Availability Index (AI)	19
1.3.5. Maneuverability Index (MI)	20
1.3.6. Autonomous Control Risk Index (ACRI)	20
1.3.7. Life Cycle Cost Index (LCC).....	20
2. Submarine Modification and Launch System Development	22
2.1. Design History and Tradeoffs.....	22
2.1.1. Initial Launch Concept.....	22
2.1.2. Tethered Box.....	23
2.1.3. General Dynamics Missile Capsules	24
2.1.4. Early Barracuda Capsule.....	25
2.2. Barracuda	26
2.2.1. Layout and Systems Overview	27
2.3. Launch Process and Mission.....	28
2.3.1. Capsule Loading and Launch.....	28
2.4. Surface Maneuvers.....	28
2.4.1. Aircraft Loading and Launch.....	29
2.5. Barracuda Launch Deck Stability	29
3. ARV and UEV Concept Selection	30
3.1. Concept Filtering	30
3.2. ARV and UEV Mission Comparison.....	30
3.3. RF Analysis and Aircraft Sizing	31
3.4. Acoustic Signature	33
3.4.1. Acoustic Signature Intensity	33
3.4.2. Aircraft Gross Weight and Disk Loading	33
3.4.3. Number of Rotor Blades	34
3.4.4. Rotor Tip Speed	34
3.4.5. Blade Vortex Interaction.....	35
3.4.6. Acoustic Signature Directivity.....	36
3.4.7. Acoustic Signature Duration.....	36
3.5. Concept Summary.....	36
3.5.1. Tilt Rotor.....	36
3.5.2. Coaxial Helicopter with Aux Propulsion.....	37
3.5.3. Single Main Rotor Helicopter.....	37
3.5.4. Box Wing Tail Sitter.....	37
3.6. Concept Comparison.....	38

3.6.1.	Qualitative Comparison	38
3.6.2.	Overall Evaluation Criteria Comparison	38
4.	Cipher Concept Development	40
4.1.	Main Rotor Radius	40
4.2.	Tandem vs. Side by Side Seating.....	40
4.3.	Hub Design Trade Study.....	41
4.4.	Number of Rotor Blades	42
4.4.1.	Number of Rotor Blades: Automatic Folding Considerations.....	42
4.4.2.	Number of Rotor Blades: Acoustic, Performance, and Structural Considerations.....	44
4.5.	Automatic Blade Folding Design.....	44
4.6.	Tail Rotor Design Selection.....	45
4.7.	Tail Folding Design	45
4.8.	Landing Gear Selection.....	46
4.9.	Landing Gear Design	46
4.9.1.	Gear Configurations.....	47
4.9.2.	Landing Gear Assembly	47
4.10.	Launch Preparations.....	48
5.	UEV Configuration Development	50
5.1.	Dragonfly Design Evolution	50
5.2.	Dragonfly Engine Selection	51
5.2.1.	Dragonfly Engine Placement	52
5.3.	Dragonfly Aerodynamic Design	53
5.3.1.	Dragonfly Airfoil Selection	53
5.3.2.	Dragonfly Wing Type Selection	53
5.3.3.	Dragonfly Induced Drag Estimation.....	54
5.3.4.	Aero-Propulsive Interaction.....	55
5.3.5.	Dragonfly Tail Design	55
5.4.	Dragonfly Rotor Design.....	56
5.4.1.	Dragonfly Rotor Blade Design	56
5.4.2.	Dragonfly Tip Speed Selection.....	57
6.	Performance	58
6.1.	Cipher Flat Plate Drag Breakdown	58
6.2.	Dragonfly Flat Plate Drag Breakdown	58
6.3.	Cipher and Dragonfly Mission Breakdown	59
6.4.	Cipher Autorotative Performance	59
6.5.	Cipher Performance	60
6.6.	Dragonfly Performance.....	61
6.7.	Cipher and Dragonfly Hover Performance.....	61
6.8.	Cipher and Dragonfly Empty Weight Breakdown.....	62
6.9.	Cipher Center of Gravity Travel	63
6.10.	Overall System Reliability	63
7.	Rotor System Design.....	65
7.1.	Cipher Rotor Blade Aerodynamic Design	65
7.1.1.	Airfoil Selection.....	65
7.1.2.	Twist	65
7.1.3.	Taper	66
7.1.4.	Sweep.....	66
7.1.5.	Anhedral.....	66
7.2.	Rotor Blade Structural Dynamic Design	66

7.2.1.	Blade Material.....	66
7.2.2.	Blade Structure.....	67
7.2.3.	Blade Sectional Properties	67
7.3.	Blade Loads Analysis	68
7.4.	Flexbeam Design	69
7.4.1.	Flexbeam Material Selection	69
7.4.2.	Flexbeam Sectional Properties.....	70
7.5.	Flexbeam Loads Analysis	70
7.6.	Fatigue Life Estimation.....	72
7.7.	Rotor Dynamics	73
7.8.	Static Droop Analysis	73
7.9.	Quasi-Static Analysis.....	73
7.10.	Ground Resonance	74
7.11.	Air Resonance.....	75
7.12.	Blade Pitch Control.....	75
8.	Acoustics	76
8.1.	Main Rotor Harmonics	76
8.2.	High Speed Impulsive Noise	77
8.3.	Blade Vortex Interaction.....	77
8.4.	Tip Speed Reduction.....	77
8.5.	Computational Analysis.....	77
8.6.	Computational Acoustic Analysis.....	78
8.7.	Acoustic Results.....	79
9.	Propulsion.....	80
9.1.	Cipher Engine Selection	80
9.2.	Engine Installation Losses	80
9.3.	Transmission Design.....	81
9.4.	Drive System Mounts	82
10.	Structural Design	83
10.1.	Finite Element Analysis.....	83
10.2.	Fuselage Structural Design	85
10.3.	Dragonfly Landing Gear	85
10.4.	Flotation Capability	85
10.5.	Static Tip Analysis.....	87
11.	Stability and Control Analysis.....	88
11.1.	Cipher Trim Analysis.....	88
11.2.	Cipher Maneuverability	89
11.3.	GUST Modeling.....	89
11.3.1.	Autonomous Control.....	90
11.3.2.	Open Control Platform.....	91
11.3.3.	Adaptive Neural Network.....	93
11.4.	Control Interface	93
11.5.	Dragonfly Hover to Forward Flight Transition Analysis	96
12.	Cost Analysis	97
12.1.	Submarine Retrofit Cost Estimate	97
12.2.	Capsule Cost Estimate	97
12.3.	Autonomous Flight Control System Cost Estimate	98
12.4.	Acquisition Cost Estimate.....	98
	Conclusions.....	100

Table of Tables

Table 1-1: ARV Mission Profile.....	14
Table 1-2: UEV Mission Profile.....	14
Table 1-3: Mission timeline for four generic ARV concepts with different cruise speeds	16
Table 1-4: Effect of Cruise Speed on Number of Soldiers Deployed to OBJ	16
Table 2-1: Barracuda Deployment Times	28
Table 2-2: Sea State 3 Stability	29
Table 3-1: "A Priori" Design Parameters	31
Table 3-2: Performance Estimates	31
Table 3-3: Design Parameters for the Helicopter and Tail Sitter for the UEV Mission.....	33
Table 3-4: Performance Comparison for the Helicopter and Tail Sitter as UEV Concepts	33
Table 3-5: Qualitative Comparison of Design Concept.....	38
Table 3-6: OEC Comparison of ARV and UEV Concept Combinations.....	38
Table 4-1: Crew Seating Arrangement Trade Study.....	40
Table 4-2: Rotor Hub Trade Study	41
Table 4-3: Folded Width of Folding Configurations	43
Table 4-4: Blade Folding Decision Matrix	44
Table 4-5: Landing Gear Type Trade Study.....	46
Table 4-6: Pugh Matrix of Landing Gear Folding Types	47
Table 4-7: Cipher Startup Times.....	48
Table 5-1: Comparison of Turboshaft and Turbo-Diesel Installations.....	53
Table 5-2: Induced Drag Reduction from Wingtip Mounted Propellers	55
Table 6-1: Cipher Drag Buildup	58
Table 6-2: Dragonfly Drag Buildup.....	59
Table 6-3: Cipher Mission Summary.....	59
Table 6-4: Dragonfly Mission Summary	59
Table 6-5: Cipher and Dragonfly Weight Breakdown.....	62
Table 6-6: Barracuda Failure Sources.....	63
Table 6-7: Cipher Failure Sources	63
Table 7-1: Material Properties of Possible Composite	67
Table 7-2: Sectional Properties of Rotor Blade	68
Table 7-3: Test Cases.....	68
Table 7-4: Sectional Properties of Flexbeam.....	70
Table 7-5: Rotor Frequencies	73
Table 8-1: Acoustic Sources	76
Table 9-1: Cipher Uninstalled Engine Data.....	80
Table 9-2: Dragonfly Turbo Diesel Uninstalled Data.....	81
Table 9-3: Transmission Design Requirements.....	81
Table 9-4: Gear Dimensions	82
Table 10-1: Crash Test Stress Results.....	84
Table 10-2: Cipher Tip Over Angle.....	87
Table 11-1: GUST Flightplan and Cipher Flight Results.....	90
Table 11-2: Autonomy Level.....	90
Table 11-3: List of Touch Screen Pages	94
Table 12-1: ARV and UEV Acquisition Costs (2007 Year Dollars).....	99
Table 12-2: Total Aircraft Development Cost.....	99

Table of Figures

Figure 1-1: Quality Function Deployment	17
Figure 1-2: Morphological Matrix	21
Figure 1-3: Design Flow	21
Figure 2-1: Initial Submarine Modification	22
Figure 2-2: First LARS, Version 1	22
Figure 2-3: Unfolded Capsule Platform	23
Figure 2-4: First LARS, Version 3	23
Figure 2-5: Sideward Tilt in Sea State 3	23
Figure 2-6: LARS v2.1	24
Figure 2-7: General Dynamics Capsule Launch Sequence	24
Figure 2-8: LARS v2.2 Capsule	25
Figure 2-9: LARS v2.3 Capsule and Cross Section Comparison	26
Figure 2-10: Barracuda Capsule	27
Figure 2-11: Troops Loaded on Lower Deck	28
Figure 3-1: Possible ARV and UEV Concept	30
Figure 3-2: RF Program Algorithm	32
Figure 3-3: Acoustic Signature of Different Concepts Near the Objective	34
Figure 3-4: Acoustic Signature of Coaxial vs. Single Main Rotor Helicopter	35
Figure 3-5: XV-15 Acoustic Signature	35
Figure 3-6: TOPSIS Analysis of Concept Combinations for the ARV and UEV	39
Figure 4-1: Rotor Hub Components	42
Figure 4-2: Possible Rotor Blade Folding Configurations	43
Figure 4-3: Variation of Gross Weight with Solidity	44
Figure 4-4: 65dBA Contours	45
Figure 4-5: Sachs ZFG Rotational Damper	47
Figure 4-6: NEMA 34 Stepper Motor	48
Figure 4-7: Cipher Folding Systems	49
Figure 5-1: Dragonfly Development Progression	50
Figure 5-2: Turbo-Diesel Fuel Flow Comparison to Conventional Spark-Ignition Engines	51
Figure 5-3: Comparison of Turboshaft and GSE Turbo-Diesel SFC at a 200 HPW Size	52
Figure 5-4: Optional Cross-shaft for Engine-Out Flight Capability	53
Figure 5-5: Oswald Efficiency Factor for Various Wing Types	53
Figure 5-6: NASA ASH-17 Airfoil Drag Polar Compared to Popular Low Speed Airfoils at a Typical Cruise Reynolds Number of Five Million	54
Figure 5-7: Optimized Vortex Lattice Load Distribution	54
Figure 5-8: Non-Linear and Linear Twist Comparison at the Hover and Loiter Flight Conditions	56
Figure 5-9: Dragonfly Power Required at Cruise and Loiter Tip Speeds	57
Figure 6-1: HV Diagram and Autorotative Rate of Decent	60
Figure 6-2: Cipher Rate of Climb	60
Figure 6-3: Cipher Power vs. Airspeed and Power vs. Altitude (ISA and Max Gross Weight)	60
Figure 6-4: Dragonfly Forward Flight Performance	61
Figure 6-5: Cipher (left) and Dragonfly (right) HOGE Performance	61
Figure 6-6: Center of Gravity Travel	63
Figure 6-7: Petri Net for a Barracuda Capsule	64
Figure 6-8: Petri Net for a Cipher Aircraft	64
Figure 7-1: Nonlinear Twist Distribution	65
Figure 7-2: Rotor Blade Tip Design	66
Figure 7-3: Blade Section Design	67

Figure 7-4: Tsai-Wu Stress for Blade Root Cross Section	68
Figure 7-5: Tsai-Wu Strain for Blade Root Cross Section	69
Figure 7-6: Flexbeam Cross Section	70
Figure 7-7: Tsai-Wu Stress for Flexbeam Cross Section	71
Figure 7-8: Tsai-Wu Strain for Flexbeam Root Cross Section	71
Figure 7-9: Goodman Diagram for CYTEC 5250-4 IM7/6K	72
Figure 7-10: Goodman Diagram for Graphite/RP46	72
Figure 7-11: Main Rotor Static Droop	73
Figure 7-12: Fan Plot	74
Figure 7-13: Ground Resonance Plot	74
Figure 7-14: Rotor Blade Pitch Control	75
Figure 8-1: Computational Surface Grid	78
Figure 8-2: Vorticity Contours at 5 Degrees	78
Figure 8-3: Calculated Acoustic Footprints at Maximum Gross Weight (65dBA Contour)	79
Figure 9-1: RFP Engine SFC Compared to Current Engines with 20% SFC Improvement	80
Figure 9-2: 3 Stage Planetary Gear Planetary Transmission Concept	81
Figure 9-3: Final Transmission Assembly	81
Figure 9-4: Engine and Rotor System Mounts	82
Figure 10-1: CAD (left) and ABAQUS (right) Landing Gear Models	83
Figure 10-2: ABAQUS Stress Analysis	84
Figure 10-3: Structural Analysis Foldout	86
Figure 10-4: Cipher and Dragonfly Tip Over Analysis	87
Figure 11-1: Required Anti-torque	88
Figure 11-2: Trimmed Rotor Controls and Body Attitudes	89
Figure 11-3: Cipher Maximum Angular Rates	89
Figure 11-4: Mission Plan from Satellite Image to Entering into Computer and Flown Path	90
Figure 11-5: Autonomous Control Flow Diagram	91
Figure 11-6: Main Menu Screen	93
Figure 11-7: Split Screen View	93
Figure 11-8: 3-D Moving Map	94
Figure 11-9: Cockpit Layout Foldout	95
Figure 11-10: Dragonfly Transition	96
Figure 11-11: Dragonfly Transition Corridor	96

Nomenclature

ABFS	Automatic Blade Folding System
AC	Air Conditioning
ACRI	Autonomous Control Risk Index
ACS	Autonomous Control System
ADS	Aeronautical Design Standard
AGMA	American Gear Manufacturers Association
AHS	American Helicopter Society
AI	Availability Index
AIAA	American Institute of Aeronautics and Astronautics
AR	Aspect Ratio
ARV	Approach and Recovery Vehicle
ASDS	Advanced Seal Delivery System
BAPS	Ballistic Air Protection
BoB	Blade over Blade
BVI	Blade Vortex Interaction
CAA	Computational Aeroacoustics
CATIA	Computer Aided Three Dimensional Interactive Application
CBEM	Combined Blade Element Momentum
CFD	Computational Fluid Dynamics
CG	Center of Gravity
DARPA	Defense Advanced Research Projects Agency
FAA	Federal Aviation Agency
FAR	Federal Aviation Regulation
FLIR	Forward Looking Infrared
GPS	Global Positioning System
HOGE	Hover Out of Ground Effect
HP	Horsepower
HSI	High Speed Impulsive Noise
IR	Infrared Radiation
IRP	Intermediate Rated Power
LARS	Launch and Recovery System
LCC	Life Cycle Cost
MADM	Multi-Attribute Decision Making
MATLAB	Matrix Laboratory
MCI	Mission Capability Index
MCP	Maximum Continuous Power
MI	Maneuverability Index
MRP	Maximum Rated Power
MTOW	Maximum Takeoff Weight
NACA	National Advisory Committee for Aeronautics

NASA	National Aeronautics and Space Administration
NM	Nautical Mile
NOE	Nap of the Earth
NOTAR	NO TAIL Rotor
OBJ	Objective
OCP	Open Control Platform
OEC	Overall Evaluation Criteria
OGE	Out of Ground Effect
POL	Petroleum Oil and Lubricants
QFD	Quality Function Deployment
RDT&E	Research Development Testing and Experimentation
RF	Ratio of Fuel
RFP	Request for Proposal
RPM	Rotations per Minute
SbS	Side by Side
SFC	Specific Fuel Consumption
SI	Stealth and Survivability Index
SIETEC	Self Injection Engine Technology
SLS	Sea Level Standard
SOF	Special Operations Forces
SPN	Stochastic Petri Nets
SSBN	Submersible Ship Ballistic Missile
SSCN	Submersible Ship Aircraft Carrier
SSGN	Submersible Ship Guided Missile
STVD	Symmetric Total Variation Diminishing
TOPSIS	Technique for Order Preference by Similarity to Ideal Solution
TURNS	Transonic Unsteady Rotor Navier-Stokes
UAV	Unmanned Aerial Vehicle
UEV	Unmanned Escort Vehicle
VABS	Variational Asymptotic Beam Sectional Analysis
VTOL	Vertical Takeoff and Landing

Executive Summary

In response to the 2007 American Helicopter Society's (AHS) Request for Proposal (RFP), the Cipher, Dragonfly, and Barracuda have been designed to provide Special Operations Forces (SOF) with covert deployment and support from an Ohio Class submarine.¹ The RFP, sponsored by Sikorsky Aircraft, outlines the need for compact rotorcraft that are launched from submerged submarines to execute covert and clandestine missions in denied, hostile, or politically sensitive regions to achieve military, diplomatic, informational, or economic objectives. Cipher is an extremely compact single main rotor NOTAR helicopter approach and recovery vehicle (ARV) optimized for low acoustic signature and submarine operations. Dragonfly is a unique box wing tail sitter unmanned escort vehicle (UEV) optimized for low acoustic signature and low speed and low power endurance. Barracuda is a multilevel self propelled launch capsule capable of launching aircraft from a modified submarine to the surface.

Mission Requirements

The primary ARV mission outlined in the RFP involves launching a fleet of ARV's from a submerged submarine operating at periscope depth, cruising at low altitudes to distances up to 140nm, performing a mid-mission hover out of ground effect, and returning back to the submarine. The ARV must be operated by two SOF soldiers not trained as pilots that will be dropped off at the tactical objective 140nm from the submarine. Therefore, it is implied that the ARV should be able to conduct approach and landings to unimproved surfaces. The UEV has a similar mission, but instead of hovering and landing at the objective, it must be able to conduct a mid-mission loiter for a least three hours in support of the SOF soldiers at the objective. Both aircraft must be capable of hovering OGE 6000ft/95F and be capable of reprogrammable autonomous flight. The primary metric used to judge system value is the total number of soldiers that can be deployed to a range of 140 nm from a single SSCN submarine in a six hour window while providing UEV support at the 140 nm range. Each ARV may transport only two SOF soldiers during each lift, but the ARV may fly back to the submarine autonomously to make additional lifts during the six hour window. A primary mission goal is to remain undetected throughout the entire mission.

Submarine Modification

The designs of the submarine modification and launch system were done iteratively and in parallel with the designs of the ARV and UEV. Through nine fully developed submarine modifications and launch design iterations and many more aircraft design iterations, the team selected to utilize the space of four existing missile silos to design a 44ft tall by 16.67ft by 16.67ft rounded corner launch chamber

containing a single Barracuda Launch Capsule. The existing radius of single missile silo was kept as the radius of the rounded corner of the new launch chamber. Since, up to 20 existing missile silos may be used, this gives the possibility of up to five Barracudas for a single submarine. Each Barracuda is capable of storing six aircraft for a maximum total of 30 aircraft (28 Ciphers, 2 Dragonflies) per submarine. However, this modular submarine retrofit provides the possibility of a lower cost, reduced capacity option of only modifying four missile silos for a single Barracuda (six aircraft).

Barracuda Design Features

Stability: Upon reaching the surface, the Barracuda must provide a stable takeoff and landing platform for the Ciphers and Dragonflies. Therefore, the design of the Barracuda was based on a General Dynamics study of stable sea platforms². The most stable sea platform is a long thin tube with a very low center of gravity well below the surface of the water (similar to a buoy). Surface floating capsules are susceptible to surface conditions. The Barracuda is 42ft long by 16.67 ft by 16.67 ft rounded square with a large lead weight at the bottom. This results in an angular tilt of less than 2° and an up and down motion of only 1ft per 4.47 seconds. NFES 1885, Interagency Helicopter Operations Guide, recommends a minimum of 15ft by 15ft landing pad for Type 3 helicopters which represent the size of the Cipher and Dragonfly.³ It also recommends avoiding landing on slopes greater than 5°. Dragonfly meets both of these requirements providing a stable takeoff and landing platform.

Propulsion and Navigation: The Barracuda is a self propelled free capsule that uses differential GPS navigation augmented with extremely low power short range beacons and a series of four Voith Schneider propellers for precise directional control. This greatly enhances the security of the submarine by giving it the ability to depart the launch area after launching the capsules. This design is superior to tethered launch designs which cause the submarine to be stationary and vulnerable for the entire 6 hour launch and recovery operation. The Barracuda is capable of an underwater rendezvous and recovery at a location different from the launch site. The depth of the Barracuda is controlled using a 9966 gal ballast tank and bilge system. All Barracuda systems are powered by a 2000 kWh high energy to volume rechargeable battery bank.

Aircraft Packing and Operations: The aircraft packing efficiency and aircraft launch operations of the Barracuda is a trade between maximizing the number of aircraft stored in the Barracuda and the feasibility of aircraft movement, soldier and equipment storage, aircraft maintenance, logistics, and safety. The Barracuda has four aircraft storage decks and an upper launch deck that is accessible only when the Barracuda hatch is opened on the surface. Each storage deck stores two aircraft, but half of the upper deck is dedicated to the Barracuda control station and half of the lower deck is dedicated to crew and equipment storage for the second mission lift (second trip to objective). The center of the capsule is

dedicated for an elevator that transports the aircraft to the launch deck. The floor of the elevator becomes the center of each deck floor when the elevator is on that level. The aircraft are pushed onto the elevator through the use of caster wheel on the landing gear. This results in 6 aircraft on each Barracuda. This was a realistic reduction from previous iterations that attempted to store 10 or more aircraft per capsule.

Cipher Design Features

Stealth: Cipher is a five bladed single main rotor helicopter designed to be extremely compact for the confined operations inside a submarine while maintaining a high degree of stealth necessary for covert Special Operations. Based on the Ratio of Fuel (RF) extended VTOL sizing methodology, the single main rotor helicopter provides the lightest and lowest disk loading aircraft configuration capable of meeting the ARV requirements. This causes it to be the quietest concept during the approach and landing to the objective which is the most critical portion of its mission. The Cipher uses an advanced NOTAR tail that dramatically reduces the acoustic signature by eliminating the interaction between the main rotor wake and the tail rotor. It uses advanced swept, tapered, anhedral rotor blade tips to eliminate High Speed Impulsive noise in forward flight and reduce the Blade Vortex Interaction during descent. Since Cipher's rotor blades must be folded for storage on the Barracuda, the main rotor mast is positioned as far forward on the aircraft as possible to maximize the length of the rotor blades in order to keep the disk loading and acoustic signature low. The engine exhaust is dual ducted out both sides with IR suppressors to reduce the exhaust temperature and IR signature. The small size of the Cipher and its superior maneuverability as a result of its bearingless rotor with large equivalent hinge offset reduce the visual and radar vulnerability.

Performance: The Cipher main rotor blades are a combination of SC1094R8 (inboard) and SC1095 (outboard) airfoils with nonlinear twist optimized using blade element and CFD models for improved performance. The engine was sized based on the high hot hover requirement using the engine specified in the RFP and a three stage planetary transmission was designed for minimum weight. With a max range speed of 124 kts for the mission sizing conditions, and considering the launch timeline, each Cipher can make two lifts to the objective during the 6 hour mission window. With 28 total Ciphers, this results in 112 total soldiers deployed to the objective with a reliability confidence of 94% based on Stochastic Petri Net analysis with regressed equipment failure models and battle damage history data.

Hub Design: In order to reduce the ground footprint, the rotor blades, tail, and landing gear are folded automatically. The main rotor hub is a bearingless design based on the Hanson hub. The major difference between the Cipher hub and the Hanson hub is that the swash plate was moved from the top of the hub to just above the transmission to provide access for maintenance on the confined space

Barracuda. The bearingless design greatly reduces the maintenance required with dampers and hinges. It also provides superior control power and maneuverability through a large equivalent hinge offset. The blade folding hinges are outboard of the flex beams and are rigidly locked in place with stepper motors.

Folding Skid Landing Gear: The Cipher folding skid landing gear uses a set of four knuckles directly attached to the aircraft load path. These knuckles are locked in place with a set of hydraulic pins that are actuated similar to an automotive break system. The pins are designed to shear at critical loads during a crash sequence. The knuckles contain rotational dampers that help cushion the descent rate after the pins shear making the Cipher more survivable in a crash. Additionally, after a normal landing, these dampers allow for the controlled motorless descent of the aircraft during the landing gear folding sequence. Once on the ground, the pins are hydraulically disengaged, and the aircraft slowly descends under its own weight while the dampers slow the rate of descent (approx three seconds to descend). During takeoff, the skids are extended and the pins lock in place after the aircraft is airborne. Therefore, the motors required for folding and unfolding only need to move the weight of the skid and not the aircraft.

Autonomous Control System: The control systems for both the Cipher and Dragonfly use an open control platform with an adaptive neural network. In normal operations, the flight computer autonomously flies a pre-programmed trajectory, and a flight control stick provides the SOF soldiers with override capability in an emergency. The flight control system interprets the inputs of the flight control stick and allows the soldiers to maneuver the aircraft within the programmed flight envelope in the control system. A series of four reconfigurable touch screens provide the capability of pre-programming and reprogramming trajectories at any point in the mission using 2D/3D moving map interfaces. The touch screens also provide reconfigurable pages for external imagery, video surveillance from the Dragonfly, and several general informational and communications modules. Ballistic Air Protection (BAPS) was placed beneath the crew and the flight computer to protect the crew and sensitive control and navigation systems. This adds 100 lbs of empty weight to the Cipher which slightly degrades the performance, but it is necessary for mission reliability and vulnerability reduction.

Dragonfly Design Features

General: The Dragonfly is a dual rotor box wing tail sitter designed for a low acoustic signature and great loiter efficiency. The incredibly low acoustic signature in loiter is achieved by flying in airplane mode during loiter at an extremely low power setting (146HP) and low rotor tip speed (220 ft/sec). The airplane mode allows for noise to be directed primarily outward instead of downward towards the objective. In order to minimize the power required (and thus acoustic signature) during loiter, the airspeed should be very slow. This forces the wing area to be very large to avoid stalling. The box wing

configuration provides the simplest and most efficient method for maximizing wing area given a confined space. The tail area must also be very large to provide adequate control since the moment arm from the tail to the CG is small. The large wing and tail area give the Dragonfly a very unusual shape, but they provide a very efficient and quiet UEV design. The Dragonfly has a retracting tail and two three bladed gimbaled rotors that fold automatically for compact storage on the Barracuda.

Stealth: The combination of noise directivity using the airplane mode, low loiter power setting, and low rotor tip speed make the Dragonfly the quietest VTOL aircraft of its weight and size. The dual turbo-diesel engines of the Dragonfly have exhaust temperatures much smaller than turbine engines, so the IR signature is greatly reduced. The shape of the Dragonfly provides a very small radar section and at its max range rotor tip speed (375 ft/sec) and in airplane mode, the Dragonfly is considerably maneuverable in high speed flight.

Performance: The turbo-diesel engine was chosen above the RFP turbine engine because of its superior SFC in low power settings (0.42 lb/(hp-hr)) and reduced engine exhaust signature. In order to reduce the number of UEV's required for the 6 hour continuous coverage, the Dragonfly was designed for a 6 hour loiter instead of 3 hours. Two Dragonflies are still maintained as part of the aircraft fleet on a single SSCN for redundancy, but only one is required to meet the mission specified in the RFP. While the turbo-diesel is considerably heavier than the turbine, the difference in fuel required for the six hour loiter more than makes up for the difference in engine weight by more than 100 lbs. The 140kt max range airspeed for the mission sizing conditions make the Dragonfly faster than the Cipher, so it can reach the objective early for tactical reconnaissance without delaying the operational timeline.

Autonomous Control: The Dragonfly uses the same control system with open control platform and adaptive neural network as the Cipher. It can be pre-programmed for a mission and it can receive trajectory changes from a variety of entities to include the Cipher, SOF soldiers on the objective, satellite downloads, and modular external control stations. It is equipped with obstacle avoidance software and IR and radar missile threat detection and evasion algorithms.

Data Summary

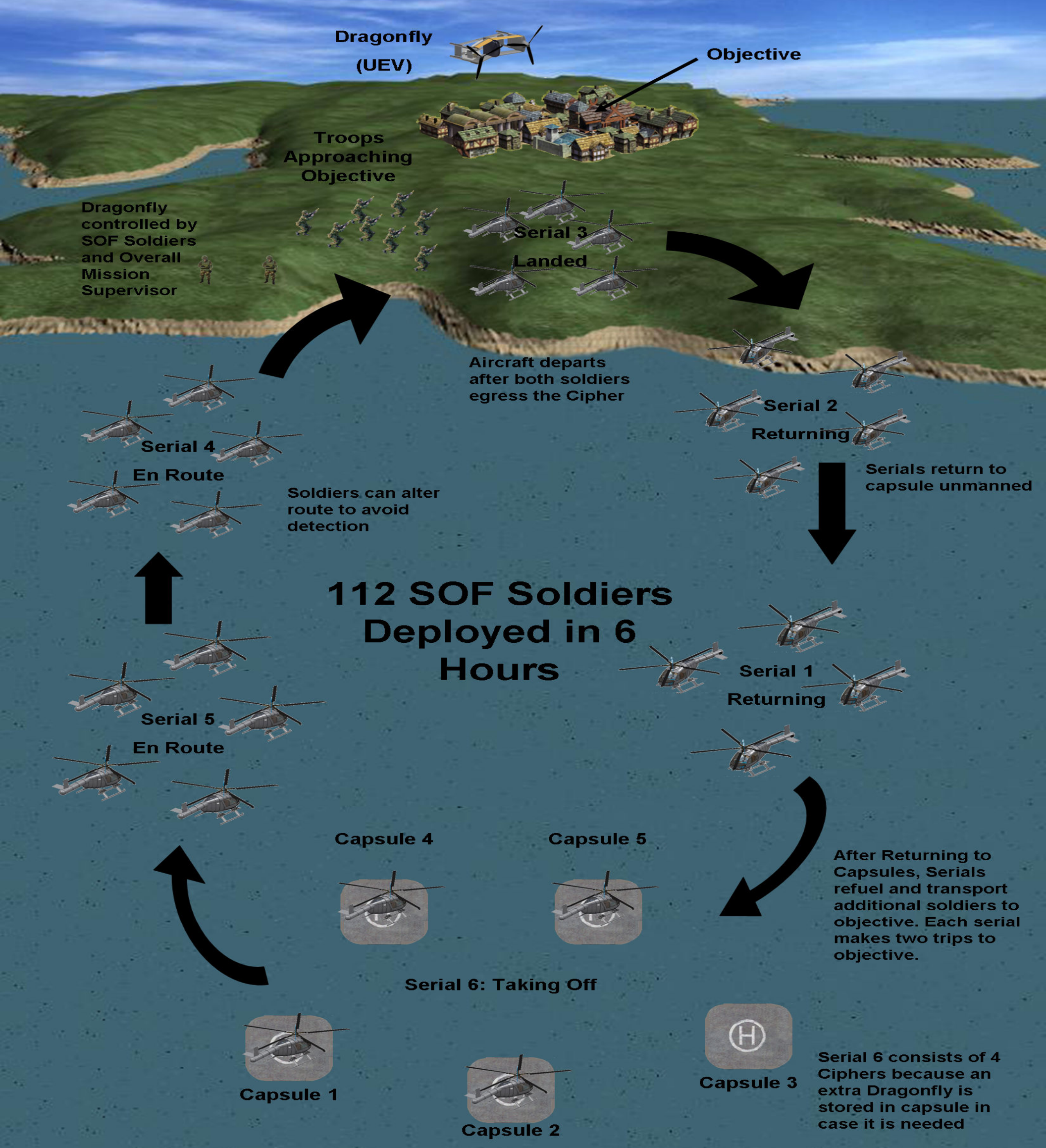
Cipher ARV		Dragonfly UEV	
Vehicle Dimension		Vehicle Dimensions	
Length (ft)	18.67	Length (ft)	28.01
Folded Length (ft)	15.67	Folded Length (ft)	15.50
Height (ft)	8.72	Height (ft)	10.04
Folded Height (ft)	7.00	Folded Height (ft)	7.00
Width (ft)	6.90	Width (ft)	13.50
Folded Width (ft)	4.89	Folded Width (ft)	4.90
Main Rotor		Rotors Data	
Radius (ft)	11.67	Radius (ft)	2x6.75
Number of Blades	5	Number of Blades	2x3
Solidity	0.085	Solidity	0.115
Tip Speed (ft/sec)	650	Tip Speed (ft/sec)	variable
Taper Ratio	1:5/8 at r=0.95	Taper Ratio	1:0.5 at r=0.8
Airfoils	SC1095, SC1094R8	Airfoils	VR8
Shaft Tilt (deg)	3 forward, 1 left	Shaft Tilt (deg)	-
Disk Loading (lb/ft ²)	6.59	Disk Loading (lb/ft ²)	10.36
Twist Rates (deg)	-18, 25 at r=0.95	Twist Rates	-55, -16 at r=0.7
Weights		Weights	
Gross Weight (lb)	2819	Gross Weight (lb)	2966
Empty Weight (lb)	1680	Empty Weight (lb)	1701
Fuel Weight (lb)	338	Fuel Weight (lb)	665
Payload (lb)	800	Payload (lb)	600
Performance (SLS at MTOW)		Performance (SLS at MTOW)	
Cruise Speed (kts)	124	Cruise Speed (kts)	140
Max Airspeed (kts)	129	Max Airspeed (kts)	144
Endurance Airspeed (kts)	65	Endurance Airspeed (kts)	91
HOGE (ft)	9437	HOGE (ft)	7500
Max ROC (ft/min)	1768	Max ROC (ft/min)	1197
Range (nm)	320	Range (nm)	874
Endurance (hr)	4	Endurance (hr)	10.27
Engine		Engine	
MRP (SLS) (hp)	496	Total Power (hp)	452
MRP (6000ft/95F) (hp)	329	SFC at MRP lb/hr/hp	0.47
SFC at MRP (SLS) lb/hr/hp	0.412	Transmission Rating (hp)	452
Transmission Rating (hp)	329	Wing	
		Span (ft)	15.5
		Area (ft ²)	80
		Airfoil	ASH-17

Proposal Requirements Matrix

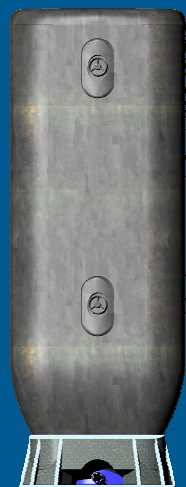
	Status	Section
RFP Objectives		
Primary Objective – The design of an advanced manned Approach and Recovery Vehicle (ARV) that is capable from operating from a submersible vehicle in support of Special Operations Forces	✓	4
Secondary Objective – The design of an advanced Unmanned Escort Vehicle (UEV) that is capable of supporting the operations of the ARV	✓	5
Primary Goal – Develop an efficient launch and recovery system that uses only the internal volume of 20 existing SSCN missile silos and will enable the ARV/UEV to be launched and recovered while the SSCN is at periscope depth (~50 ft)	✓	2.2
Primary Mission Requirements		
Primary Goal – Remain undetected throughout the entire mission	✓	8.4
Primary Metric – The total number of SOF soldiers that can be deployed to a range of 140 nm from a single SSCN in a 6 hour time window (with only two soldiers per ARV per trip) while providing UEV support at the 140 nm range location	✓	6.10
Primary design mission for the ARV involves launching from a single SSCN operating at periscope depth, cruising at low altitude to distances up to 140 nm, performing a mid-mission HOGE (4 minutes), and returning back to the submarine.	✓	6.3
Primary design mission for the UEV involves launching from an SSCN operating at periscope depth, cruising at low altitude to distances up to 140 nm, performing a mid-mission loiter (3 hours), and returning back to the submarine.	✓	6.3
Launch and Recovery Requirements		
The vehicles shall be capable of launching within 30 minutes of receipt of tasking.	✓	2.3, pg 9
The vehicles shall be capable of launching within 10 minutes after being positioned on the water surface.	✓	4.10
Following landing, the vehicles shall be capable of receding beneath the water’s surface within 10 minutes.	✓	2.3, 4.10
Common ARV / UEV Requirements		
Vertical takeoff and landing capability	✓	6.7
Hover out of ground effect capability at 6000ft / 95F	✓	6.7
If blades/wings need to be folded, automatic folding should be employed	✓	4.5, 4.7, 4.9, 10.3
Automatic takeoff and landing system should be used for normal launching and recovery of the vehicles, both at sea and on land.	✓	11.3
A manual interface should be incorporated to enable takeoff aborts and/or recovery wave-offs in the event of emergencies.	✓	11.4
Capability to automatically recovery to pre-designated locations during an emergency	✓	11.3, 11.4
Utilize advanced susceptibility reduction techniques. Minimize visual, IR, radar, and particularly acoustic signatures.	✓	8, 9.2

Utilize vulnerability reduction techniques to limit effects of combat damage	✓	6.8, 11.3
Aircraft should be able to be rolled-on/rolled-off a C-130J aircraft	✓	pg 10, 4.8
Avionics weight = 300lbs / Contingency weight = 5% of empty weight	✓	6.8
100% mission capable in global environments including maritime, artic, tropical, and desert	✓	10.2
Impervious to the effects of salt water	✓	10.2
Able to remain afloat in sea state 3 for not less than 30 minutes	✓	10.4
High degree of availability and reliability	✓	6.10
Qualitative estimate of acquisition and direct operating cost	✓	12
ARV Specific Requirements		
Operable by personnel who are not trained as pilots	✓	11.4
Payload = 800 lbs (2 crewmembers at 270 lbs each and 260 lbs mission equipment)	✓	6.3
Lighting compatible with night vision devices	✓	11.4
Crashworthy fuel system	✓	6.8
Mission configurable to allow for transport of one or both of the crew as injured	✓	11.4
Mission equipment capabilities consistent with IR/ low light imaging, all weather day-night pilotage, over the horizon jam resistant communication, net-centric services (RTI exchange), and wireless communications between other ARV and personnel up to 100 meters	✓	11.4
UEV Specific Requirements		
Payload = 600 lbs	✓	6.8
Capable of operating via pre-programmed instructions, or operator initiated instructions, providing EO and IR sensors and laser designation capability	✓	11.3
Capable of programming mission planning data prior to launch	✓	11.3
Capable of re-planning the mission while in flight	✓	11.3
Tactical data link to provide C4 and data exchange	✓	11.3
Embedded VHF and UHF radio relay capability	✓	11.3

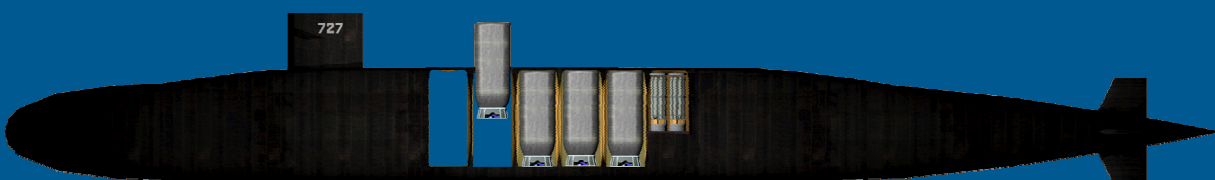
Overall Mission System of Systems



Capsule carrying six aircraft moves to surface



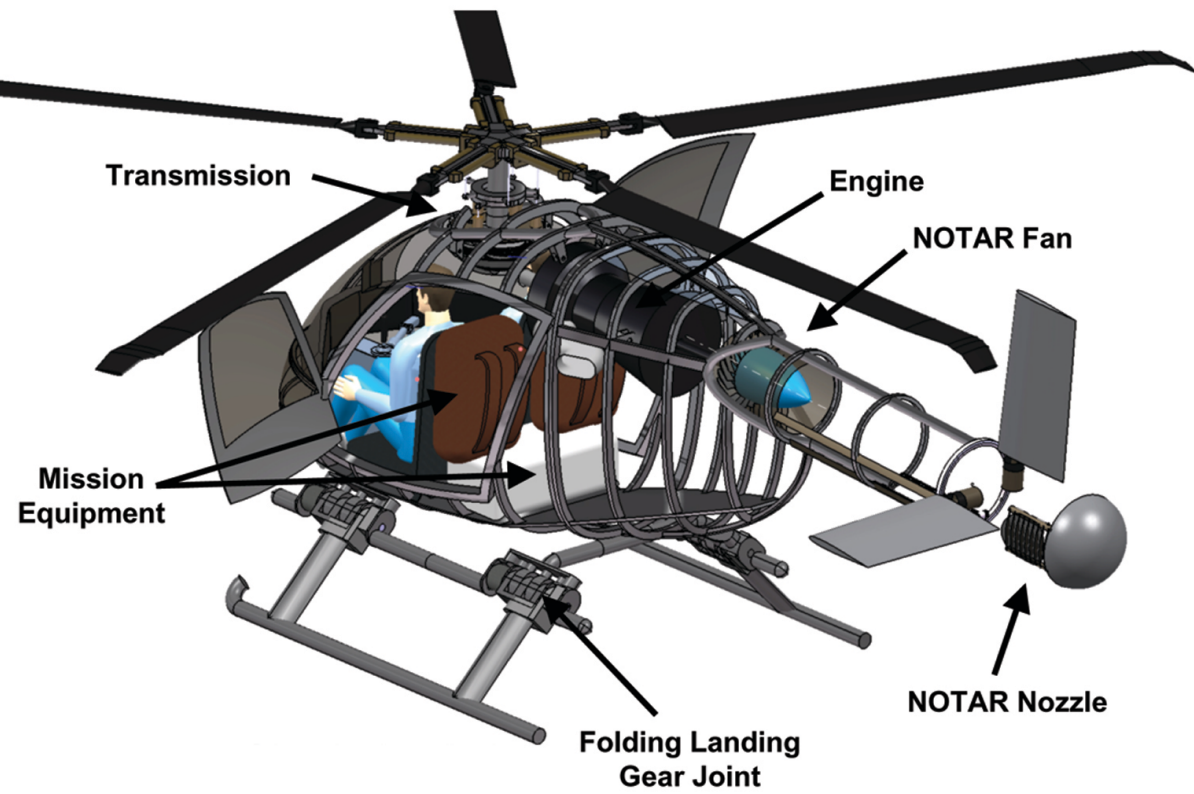
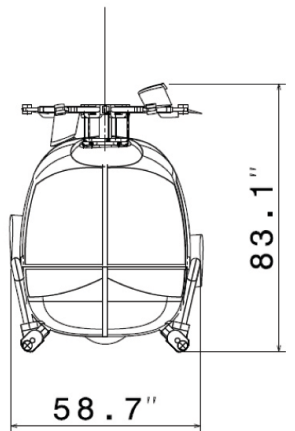
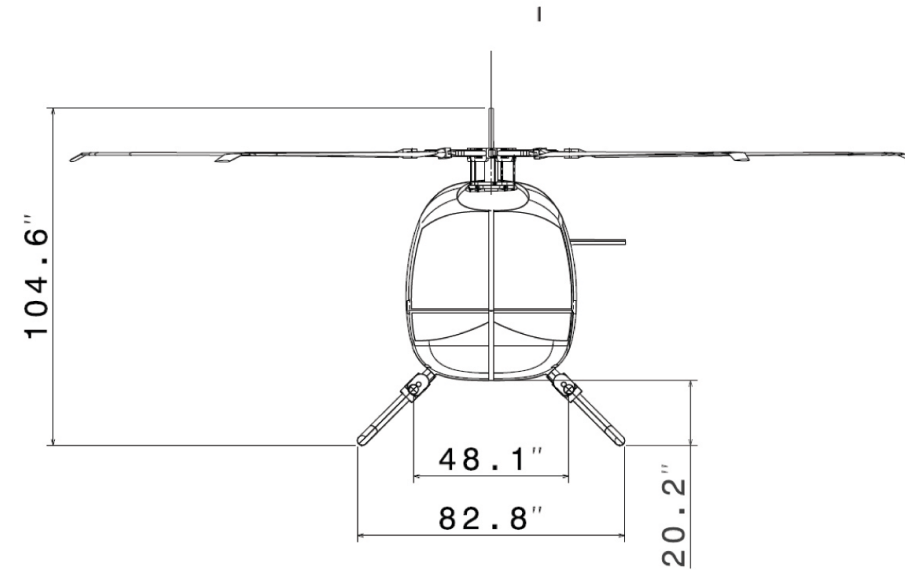
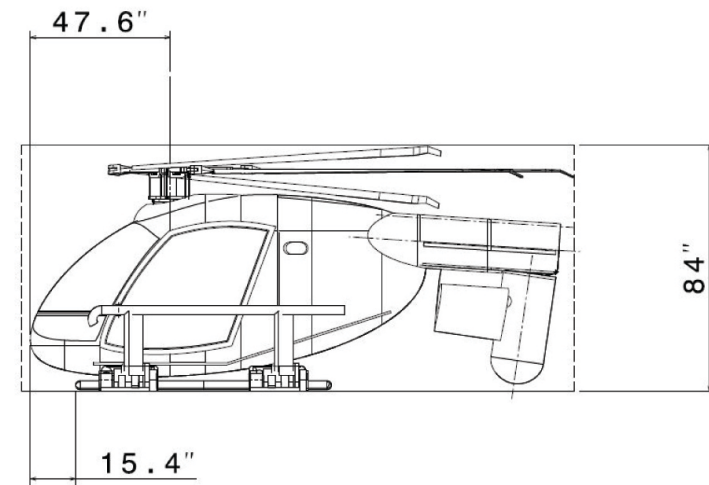
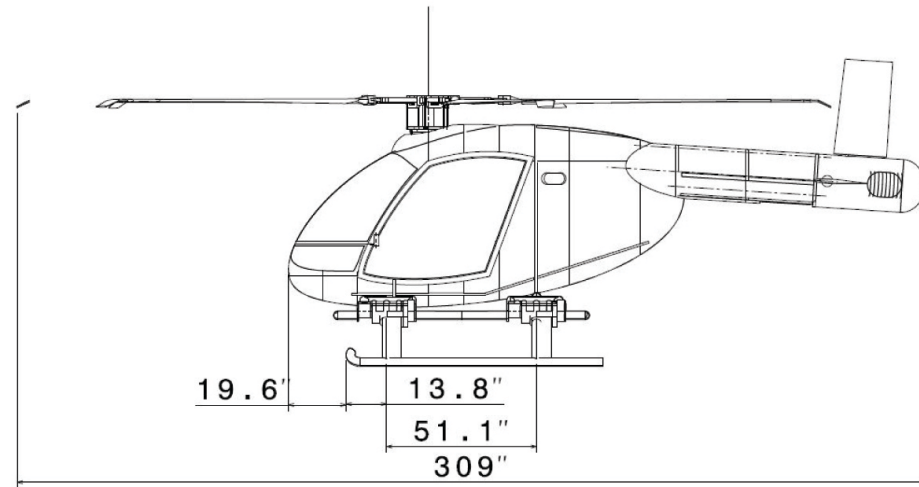
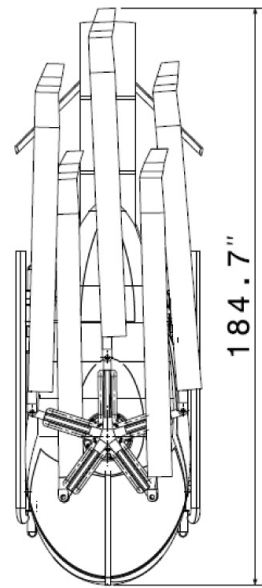
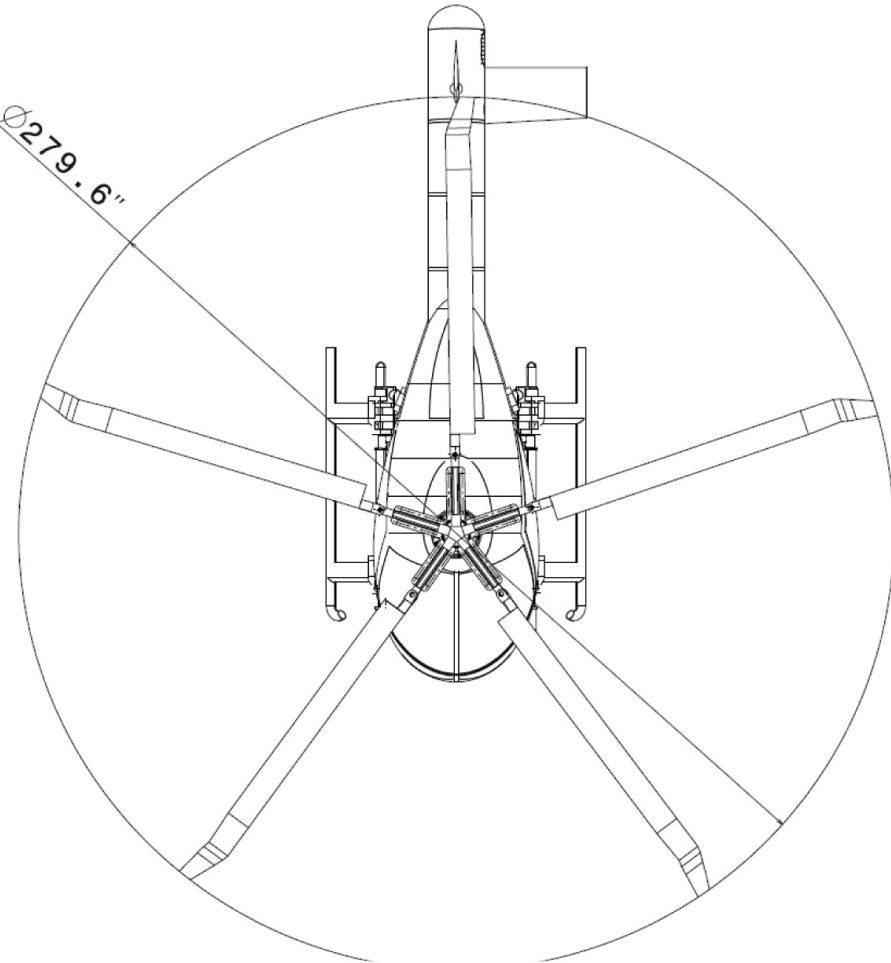
Capsule Launches from Ohio Class SSCN Submarine



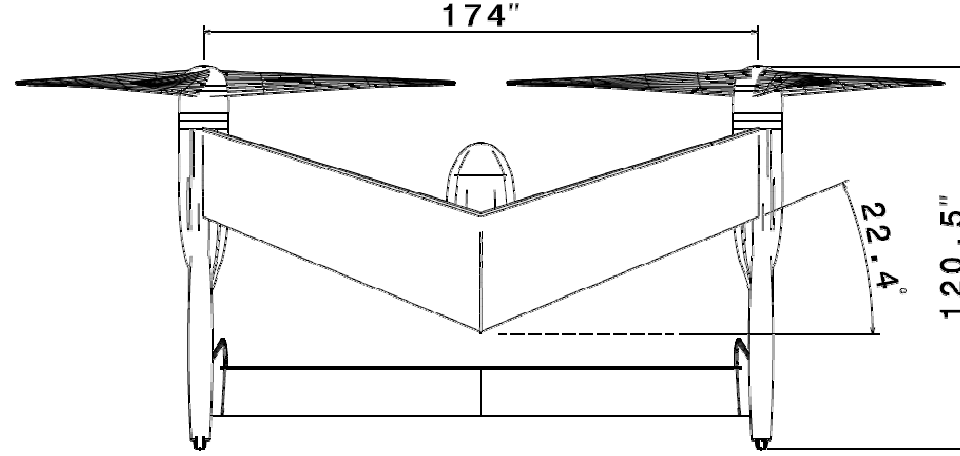
Mission Timeline

- 00:00:00 - Receipt of Mission
- 00:16:00 – Capsule Loaded and Sealed
- 00:20:30 – Capsule Reaches Surface
- 00:23:00 – First Aircraft Reach Launch Deck
- 00:32:00 - Serial 1 Takes off, each successive Serial follows 10 minutes later
- 01:39:00 – Serial 1 Arrives at Objective
- 02:46:00 – Serial 1 Refuels at Capsule
- 02:56:00 – Serial 1 Takes off
- 04:03:00 – Serial 1 Arrives at Objective
- 05:10:00 – Serial 1 Returns to Capsule

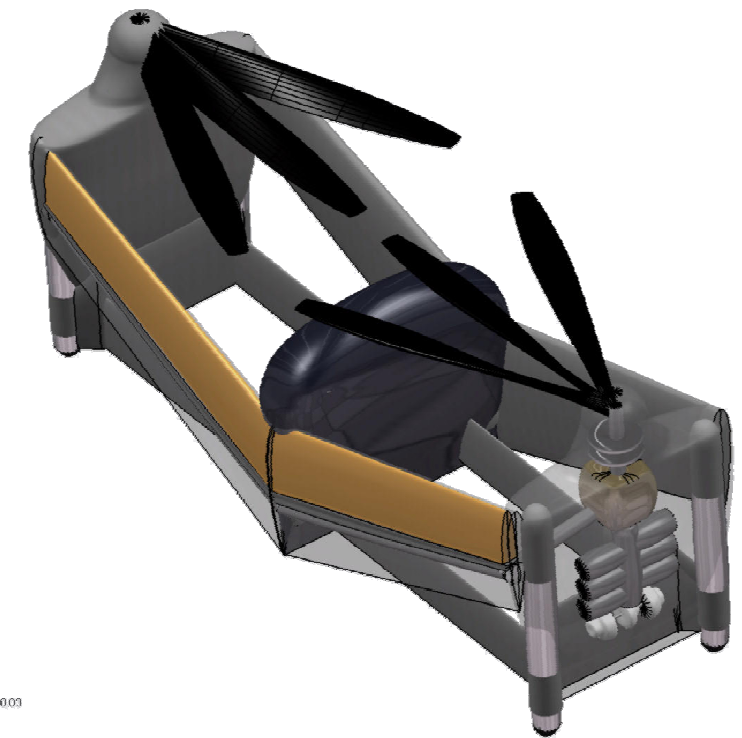
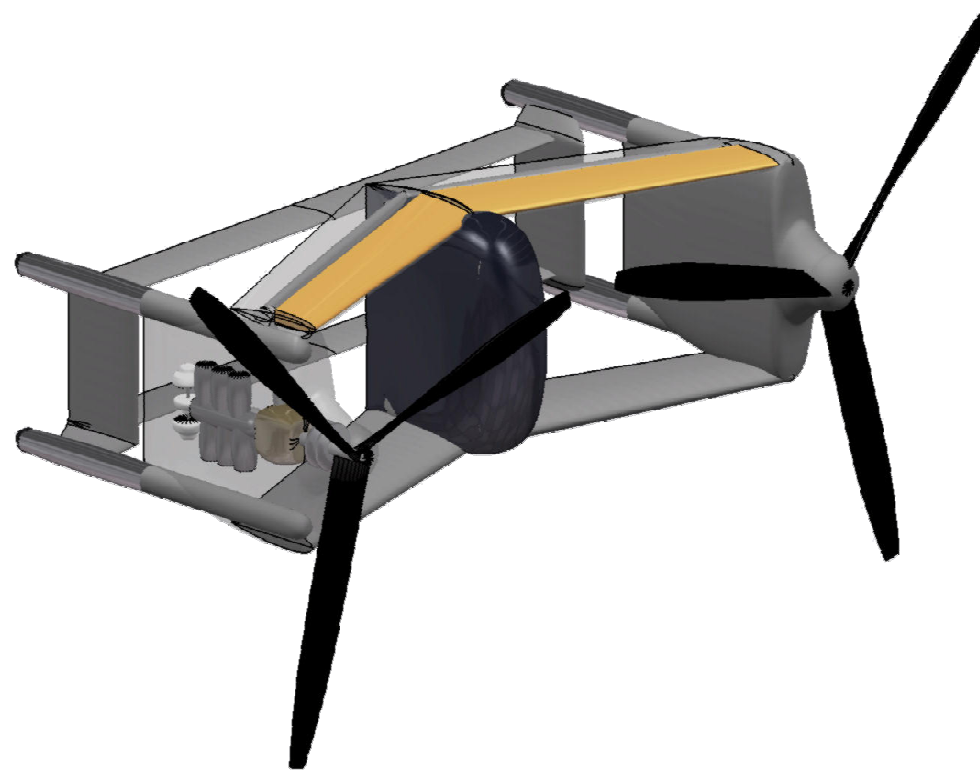
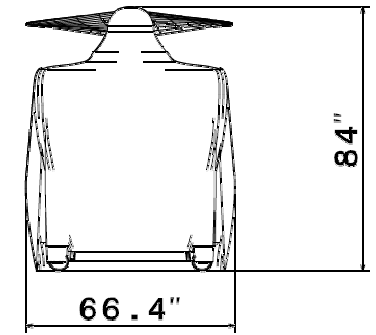
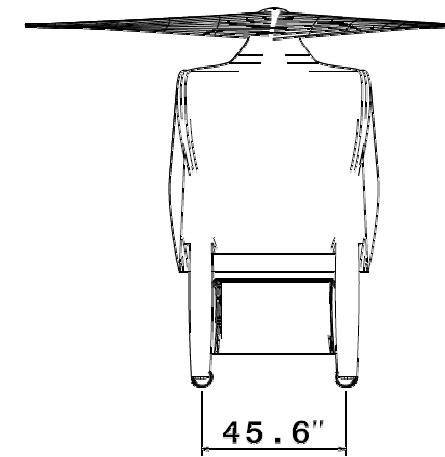
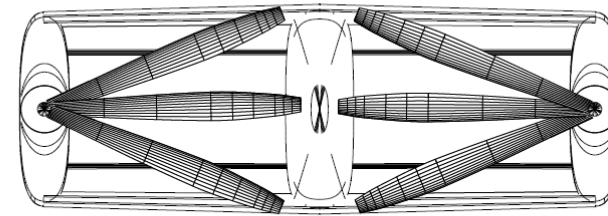
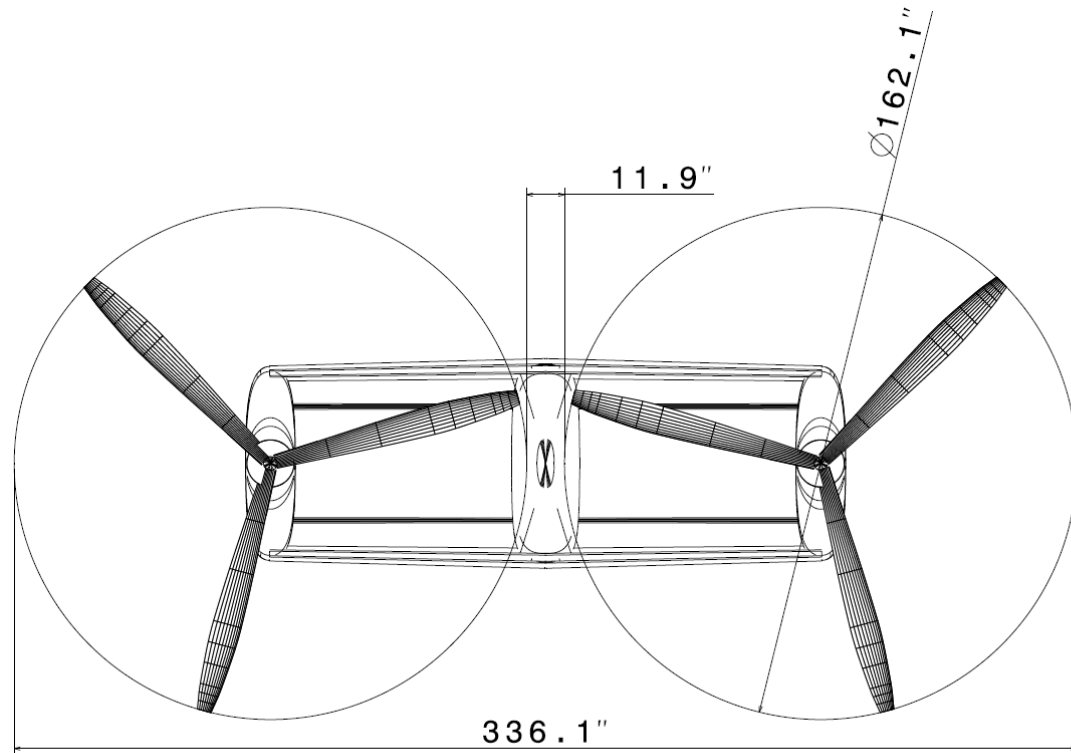
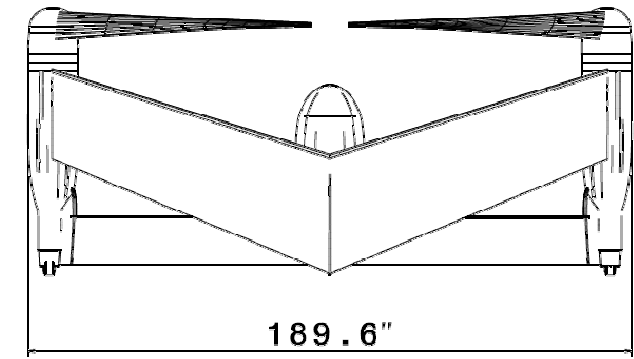
Cipher - ARV



Dragonfly - UEV



Front view
Scale: 1:25



Barracuda Capsule Cutaway

Hydraulic Roped Elevator

- 2 x 1500 psi pistons
- Moves 15000 lbs in 10s

Upper Capsule Access Hatch

- ## Fuel Pump and Tank
- Capacity: 3600 lbs
 - Flow Rate: 350 GPM

Capsule Management Console



Waiting and storage area w/ access hatch for up to 12 SOF troops and their equipment

Lead Counterweight
Weight: 242365 lb



Voith Schnieder Propellor (x4)
Allows precise multi-directional navigation

Main Capsule Doors
-Pressure resistant
- Watertight

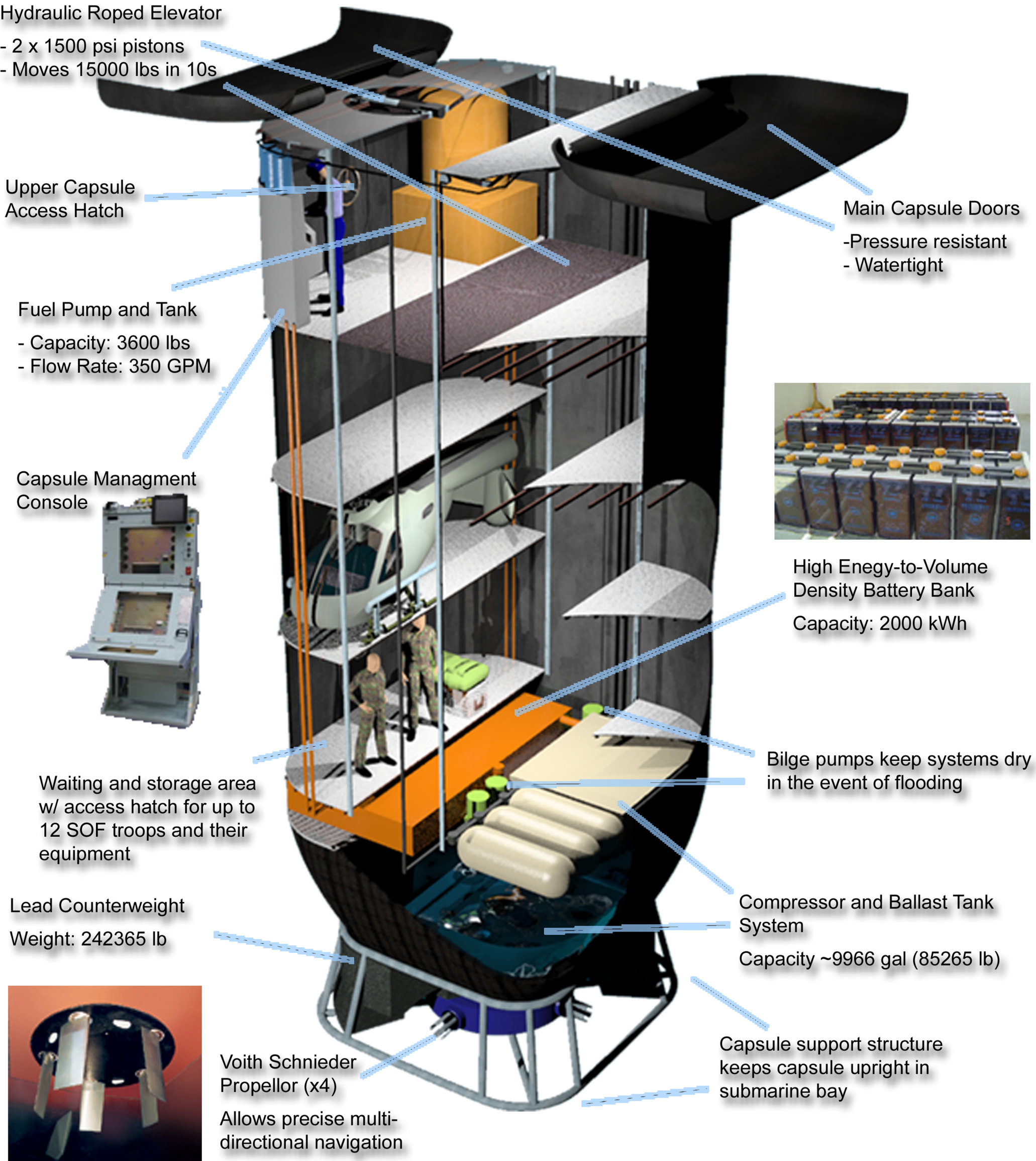


High Energy-to-Volume Density Battery Bank
Capacity: 2000 kWh

Bilge pumps keep systems dry in the event of flooding

Compressor and Ballast Tank System
Capacity ~9966 gal (85265 lb)

Capsule support structure keeps capsule upright in submarine bay



1. Introduction

1.1. RFP Summary

The purpose of this RFP is to design a fleet of vertical takeoff and landing (VTOL) aircraft that are launched from and recovered to a submerged Ohio Class submarine using the volume of the Trident missile compartments.¹ The design consists of the aircraft launch and recovery system as well as the modifications and space allocation of the submarine.

Two aircraft designs were required – a manned Approach and Recovery Vehicle (ARV), and an Unmanned Escort Vehicle (UEV). Both aircraft must launch from the submerged submarine, be capable of hover out of ground effect (HOGE) at 6000ft/95F, and fly to a tactical objective 140 nm away.

The ARV must be operated by two Special Operations Forces (SOF) soldiers who are not trained as pilots. The payload is 800 lbs including the SOF soldiers. From an AHS question response, “It is highly undesirable to generate design solutions with larger payloads.”⁴ The two SOF soldiers will egress the ARV at the objective. The ARV should be able to conduct a tactical approach and landing to unimproved surfaces, takeoff, and return to the submarine autonomously. The UEV does not land at the objective, but must remain in loiter at the objective in support of the SOF soldiers for three hours before returning to the submarine. All aircraft must be able to recovery to the submerged submarine at the completion of the mission. All aircraft should remain undetected throughout all phases of the mission. The mission profiles for the ARV and UEV are shown in Table 1-1 and Table 1-2.

The primary metric used to judge system value is the total number of SOF soldiers that can be deployed to a range of 140 nm from a single SSCN in a six hour time window while providing UEV support at the 140 nm range location. Since the payload of a single ARV cannot be increased, the design solution should be very compact, allowing the maximum number of aircraft to be stored on the submarine. The aircraft should also have a high cruise speed allowing it to make multiple trips to the objective, and the launch and refuel operations should be as efficient as possible. UEV coverage must be provided in support of the SOF soldiers throughout a six hour mission window, so either one UEV must be able to remain on station for the entire six hours or a second UEV must be launched to relieve the first UEV on station. Since stealth is also a major design consideration, the solution to this RFP is a delicate balance

between two highly conflicting design requirements – **deploying a large number of soldiers to the objective and maximizing stealth.**

Table 1-1: ARV Mission Profile

Segment	1	2	3	4	5	6	7	Units
Type	Idle	HOGE	Cruise	HOGE	Cruise	HOGE	Reserve	-
Speed	0	0	V_{br-99}	0	V_{br-99}	0	V_{be}	ktas
Time	4	2	-	4	-	2	20	Min
Range	-	-	140	-	140	-	-	Nm
Altitude	0	0	0	0	0	0	0	ft
Temperature	102.92	102.92	102.92	102.92	102.92	102.92	102.92	°F
Engine Rating	IRP	MRP	MCP	MRP	MCP	MRP	MCP	-

Table 1-2: UEV Mission Profile

Segment	1	2	3	4	5	6	7	Units
Type	Idle	HOGE	Cruise	Loiter	Cruise	HOGE	Reserve	-
Speed	0	0	V_{br-99}	V_{be}	V_{br-99}	0	V_{be}	ktas
Time	4	2	-	180	-	2	20	Min
Range	-	-	140	-	140	-	-	Nm
Altitude	0	0	0	0	0	0	0	ft
Temperature	102.92	102.92	102.92	102.92	102.92	102.92	102.92	°F
Engine Rating	IRP	MRP	MCP	MRP	MCP	MRP	MCP	-

1.2. Mission and Requirements Analysis

1.2.1. Stealth

The three main modes of detection are radar, visual/IR, and audible. Radar detection avoidance for rotorcraft is best achieved through minimizing the size of the aircraft and more importantly, flying tactically at lower altitudes. A smaller aircraft is also beneficial to avoiding visual and IR detection. Acoustic signature, however, is highly dependent upon concept selection and is the most important stealth parameter for rotorcraft missions. Specifically, acoustic signature is most important near the objective where the threat is the greatest and the aircraft is the most vulnerable. **Therefore, minimizing the acoustic signature of the ARV and UEV near the objective is the most heavily weighted design consideration.**

1.2.2. Soldier Deployment Rate

The ARV payload cannot be increased so the number of soldiers deployed to the objective in a 6 hour window will depend on the efficiency of the launch and refuel operation, the cruise speed, and the

packing efficiency of aircraft. Rotorcraft cruise airspeed is roughly a direct function of disk loading. However, increasing the disk loading also increases the empty weight of the aircraft because of the larger engine required to hover. This increases aircraft size decreasing the packing efficiency. With a very densely packed submarine design, aircraft repositioning, maintenance, and launch operations become more cumbersome. Therefore, trades must be made for a balanced, safe, and feasible design solution.

The simplest method to launch aircraft is to design vehicles that launch and recover without the use of a separate launch capsule. However, an amphibious design concept was viewed as an impossibility due to the increased skin weight required to withstand the pressure load and difficulty integrating air breathing propulsion. Another launch method is to dedicate a capsule to each individual aircraft; this design increases the number of capsules and is far less efficient than a design where each capsule stores multiple aircraft

All feasible launch solutions for this problem require the use of capsules that store multiple aircraft. This results in serials (groups) of aircraft that are separated by the time it takes to launch subsequent serials. When the first serial returns for refuel, the obvious place to refuel is the pad from which it took off. Therefore, once the first serial returns for refuel, the launch operations from that pad must be complete. This means that all aircraft required for launch operations using a given launch system must be launched before the first serial returns for refuel. There is not enough time between serials returning for refuel to launch additional serials.

Due to the launch and refuel scheduling, the effect of increasing cruise speed is greatly reduced. If an aircraft's speed is increased, it will arrive at the objective sooner, but it will also return to the submarine sooner, which means there is less time to launch subsequent serials. This means that even though the ARV is faster, there will be fewer of them in the air. When viewed from the objective, once the first serial arrives, subsequent serials will arrive at constant intervals. The additional soldiers deployed for a faster concept is only increased by the number of additional serials that a faster concept can get to the objective before the first serial of the slower concept arrives. Table 1-1 shows the mission timeline for three generic ARV concepts with different cruise speeds. It is assumed that the launch time required for the first serial is thirty minutes, and each subsequent serial launches twenty minutes later.

Table 1-4 shows the results of soldiers deployed for each concept in Table 1-3. The time required for refuel is assumed to be ten minutes, and the serial size is three aircraft.

Table 1-3: Mission timeline for four generic ARV concepts with different cruise speeds

100 Kt Cruise Speed ARV		200 Kt Cruise Speed ARV		300 Kt Cruise Speed ARV	
Time	Event	Time	Event	Time	Event
00:30	Serial 1 Takeoff	00:30	Serial 1 Takeoff	00:30	Serial 1 Takeoff
00:50	Serial 2 Takeoff	00:50	Serial 2 Takeoff	00:50	Serial 2 Takeoff
01:10	Serial 3 Takeoff	01:10	Serial 3 Takeoff	01:02	Serial 1 Lands at OBJ
01:30	Serial 4 Takeoff	01:16	Serial 1 Lands at OBJ	01:10	Serial 3 Takeoff
01:50	Serial 5 Takeoff	01:30	Serial 4 Takeoff	01:30	Serial 4 Takeoff
01:58	Serial 1 Lands at OBJ	01:50	Serial 5 Takeoff	01:32	Serial 1 Begins Refuel
02:10	Serial 6 Takeoff	02:00	Serial 1 Begin Refuel		Cycle continues
02:30	Serial 7 Takeoff		Cycle continues		
02:50	Serial 8 Takeoff				
03:10	Serial 9 Takeoff				
03:24	Serial 1 Begin Refuel				
	Cycle continues				

Table 1-4: Effect of Cruise Speed on Number of Soldiers Deployed to OBJ

	100 Kt Cruise	200 Kt Cruise	300 Kt Cruise
Serial 1 Lands at OBJ	01:58	01:16	01:02
Mission Time Remaining	04:02	04:44	04:58
Total Serials to OBJ	13	15	16
Total Aircraft to OBJ	39	45	48
Total Soldiers to OBJ	78	90	96

Notice that while increasing the cruise speed does increase the total number of soldiers deployed, it is not very substantial. Shortening the launch and refuel times and increasing the serial size would increase the difference in soldiers deployed for different airspeeds increases, but the gain is still not very substantial. Therefore, the impact of airspeed is not as significant as other engineering considerations for the ARV mission capability.

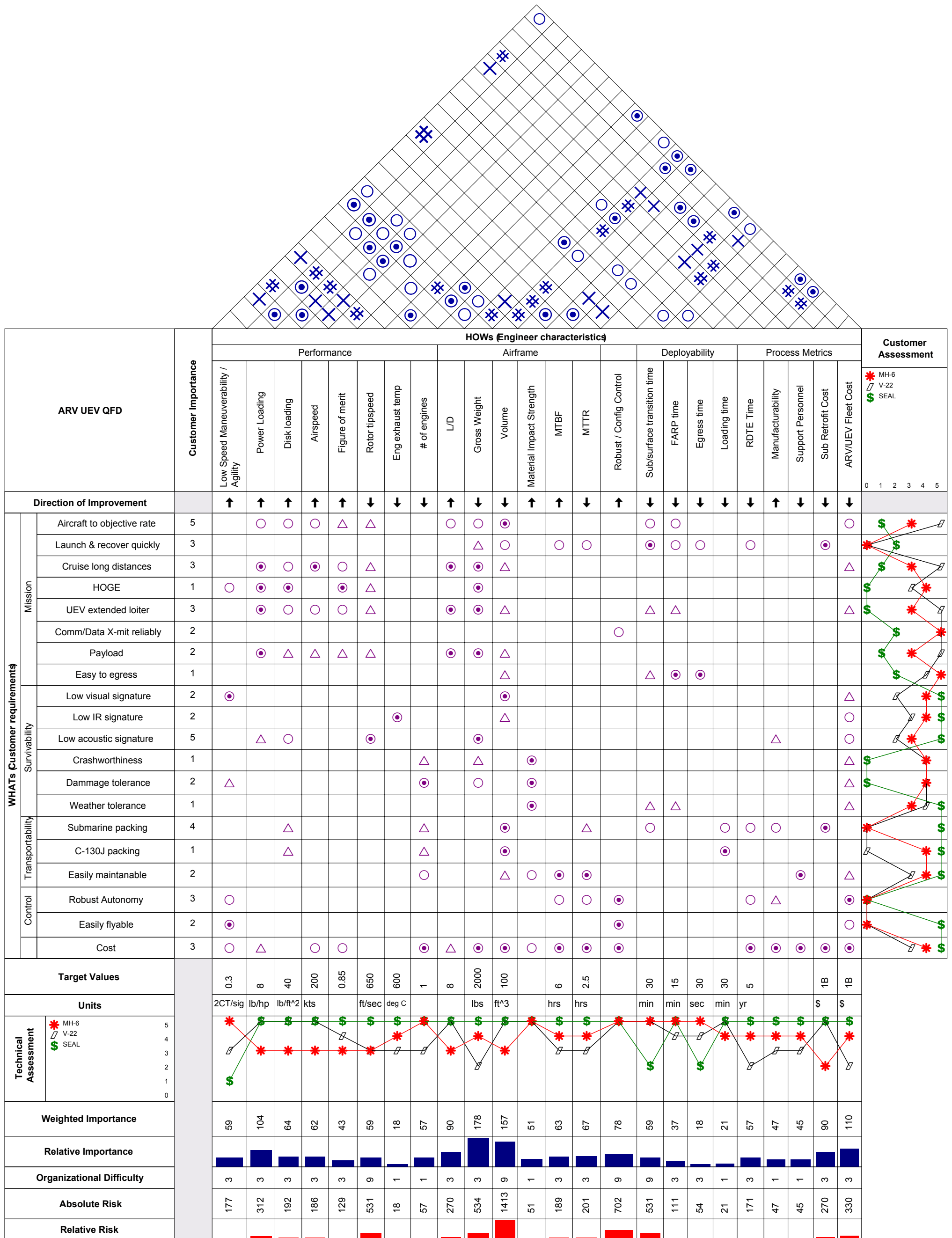


Figure 2-1: Quality Function Deployment

1. QFD shows the top three risk related engineering considerations to be Aircraft Packing Volume, Robust Configurable Autonomous Control, and Gross Weight.
2. Since no other aircraft have been designed to conduct this RFP mission, three competitive assessments were made with systems that are be capable of conducting similar missions (i.e. insertion of SOF soldiers to tactical objectives from sea based vessels). The “Seal” represents the current seal underwater vehicle described in the RFP. The MH-6 and the V-22 represent these aircraft launched from a concealed cargo ship. This competitive assessment helps define gaps in technology. These gaps help place weighting on the risk of engineering considerations.

1.3. Overall Evaluation Criteria (OEC)

$$OEC = \frac{2.5SI + 2.0MCI_{ARV} + 1.5MCI_{UEV} + 1.5AI + 1.0ACRI + 0.5MI}{9 + LCC}$$

where all indices are values of 0 to 1, and

SI = Stealth and Survivability Index

MCI_{ARV} = ARV Mission Capability Index

MCI_{UEV} = UEV Mission Capability Index

AI = Availability Index

ACRI = Autonomous Control Risk Index

MI = Maneuverability Index

LCC = Life Cycle Cost Index

1.3.1. Stealth and Survivability Index (SI)

A simple index for survivability may be defined as follows:

$$\text{Survivability Index (SVI)} = 1 - P_D \times P_H \times P_K$$

where P_D = Probability of Detection, P_H = Probability of Being Hit if Detected, P_K = Probability of Being Killed if Hit

P_K is a qualitative estimate based on system robustness and redundancy. P_H will depend upon size, IR signature, paint color, engine and other minor features. P_D is divided into radar, visual/IR detection, which are based on aircraft size, and audible detection which is based on acoustic signature.

Acoustic signature for the ARV is most important during the approach to the objective. Since the ARV is required to hover and land at the objective, the rotor system will be projecting noise downward during the approach regardless of the selected concept. Also, because the aircraft is descending during the approach, the rotor blades will pass through or near the previous blade's tip vortex of the rotor and produce Blade Vortex Interaction (BVI) noise which increases the overall noise level by 6-8 dBA⁵.

Since the UEV does not hover or land at the objective, the downward propagation of noise may be reduced by taking advantage of noise directivity. The UEV can avoid the BVI noise since it does not have to conduct a descent approach and landing at the objective. For these reasons the acoustic signature of the UEV should be quieter than that of the ARV. The MD520N is currently the quietest FAA certified turbine helicopter.⁶ Therefore aggressive design goals for the noise levels of the ARV and UEV are to have a lower acoustic footprint than the MD520N.

The perceived noise levels of the ARV and UEV are considered for the quantification of the probability of being detected audibly (P_{DA}) since both aircraft will be at the objective during the mission. Therefore, an index for P_{DA} is defined as follows:

$$P_{DA} = 1 - \left[1 - \left(\frac{\text{Noise Level}_{ARV} - \text{Noise Level}_{GOAL}}{10} \right) \right] \times \left[1 - \left(\frac{\text{Noise Level}_{UEV} - \text{Noise Level}_{GOAL}}{10} \right) \right]$$

Stealth Index (STI) = 1 - P_D where P_D is the same value given for the survivability index

Since this operation is clandestine/covert, being detected by the enemy may result in a mission failure. Detection eliminates deniability which is often a primary mission goal for Special Forces operations. Therefore, stealth is weighted more heavily than survivability so a combined stealth and survivability index may be defined as follows:

$$SI = 0.8(1 - P_D) + 0.2(1 - P_D P_H P_K)$$

1.3.2. Mission Capability Index for the ARV (MCI_{ARV})

The performance mission of the ARV is defined as the number of soldiers deployed to the objective in six hours. This is highly dependent on the submarine modification and launch system. It was determined that while unfeasible, it is possible to deploy a maximum of 350 soldiers in 6 hours. Therefore, to get the MCI to a scale of 0 to 1, the MCI_{ARV} is defined as follows.

$$MCI_{ARV} = \frac{\text{SOF soldiers to OBJ in 6 hours}}{350}$$

1.3.3. Mission Capability Index for the UEV (MCI_{UEV})

$$MCI_{UEV} = \frac{0.92 + \frac{\ln(0.84x)}{x^{2.5}}}{\# \text{ UEV required for 6 hour loiter}}$$

$$\text{where } x = \frac{\text{UEV 99\% max range speed}}{\text{ARV 99\% max range speed}}$$

In order to provide adequate reconnaissance; the UEV must arrive at the objective before the ARV. This means that a UEV with a cruise speed greater than the cruise speed of the ARV is highly desired. The function of the numerator models this situation with a severe penalty for lower cruise speed and a limited benefit for increasing cruise speed significantly beyond that of the ARV.

1.3.4. Availability Index (AI)

$$AI = \frac{MTBF}{MTBF + MTTR}$$

MTBF = mean time between failure and will be based on historical trends for the different concepts

MTTR = mean time to repair and will also be based on historical trends, but it will also take into account the increased repair time due to service volume available on the submarine.

$$MTTR = MTTR_{optimum} \times \frac{\text{Service Volume Available}}{\text{Optimum Service Volume}}$$

where, $MTTR_{optimum}$ = the MTTR with optimum service volume available

1.3.5. Maneuverability Index (MI)

$$MI = \frac{\text{Control Power}}{\text{Damping}}$$

Control Power is a function of the pitch, roll, and yaw derivatives $L_{\delta a}$, $M_{\delta e}$, $N_{\delta p}$, and Damping is a function of the pitch roll and yaw damping derivatives L_p , M_q , N_r . The control power is primarily increased with an increase in equivalent hinge offset.

1.3.6. Autonomous Control Risk Index (ACRI)

$$ACRI = \text{Concept Experience} \times \text{Damping}$$

This index is primarily based on concept experience and the stability and control damping derivatives. A vehicle that is highly maneuverable generally has lower damping and therefore is less stable and requires a more in-depth autonomous control system.

1.3.7. Life Cycle Cost Index (LCC)

This index is a function of the system cost including submarine retro fit and launch mechanism and both aircraft. The submarine retrofit cost greatly eclipses the vehicle cost and is therefore weighted more.

1.4. Morphological Matrix

Figure 1-2 shows the morphological matrix that links from (“how”) to all of the sub functions (“whats”). This represents the pools from which possible feasible design solutions may be obtained through feasibility filtering, OEC comparison, qualitative Pugh comparison, and Multi-Attribute Decision Making (MADM). These comparisons were used to select the submarine modifications and launch concepts as well as ARV and UEV configuration selections.

Subfunction		Alternatives					No. of Option
		1	2	3	4	5	
Sub Hanger	Launch Tube Type	Use 1 Tube	Use 2 Tubes	Use 4 Tubes			3
	Vehicle Storage Type	In-Tube	In-Hanger				2
	Number of ARVs	50	40	30	20	10	5
	Number of UEVs	1	2	3	4	5	5
Mission	Launch Vehicle	Free capsule	Tethered capsule	Extending launch tube	Self-Submerging		4
	Platform Type	Inflatable	Unfolding Rigid	Hybrid Fold/Inflate			3
	Stabilize Platform	None	Passive Ballasts	Active			3
	Resupply Vehicle	Return to Sub	Jettison Fuel/SOF				2
	Stealth	Shape Opt	Absorbant Material				2
Configuration	Configuration Type	Tailsitter	Helicopter	Deflected slipstream	Tilt Duct	Tilt-Rotor	7
	Seat Layout	sitting	prone	pivoting	None		4
	Material	Aluminium	Composite	Hybrid			3
Control System	Autonomous System Type	Autopilot	Autonomous	Haptic			3
	Control linkage type	Mechanical	Digital	Optical			3
	Control Mechanism	Swashplate	Control Surfaces	Pneumatic			3
Systems	Landing Gear Type	Skids	3 Wheel- Nose/Main	3 Wheel - Taildragger	Wheeled Floats	Inflatable	5
	Wing Structure Type	Fixed	Inflatable	Folding	None		4
Propulsion System	Compound Propulsion	Propeller	Ducted Propeller	Fan	None		4
	Rotor Type	Single	Co-axial	Dual	Overlapping	None	5
	Disloading	Low	Med	High			3
	Number of engines	1	2	3	4		4
	Number of rotor blades	0	2	3	4	5	5
	Hub type	Teetering	Articulated	Hingeless	Bearingless	None	5
	Tipspeed	600	650	700	750		4
Total Number of Combinations							2E+13

Figure 1-2: Morphological Matrix

1.5. Design Flow

Figure 1-3 shows the flow block diagram used in this design. The capsule modification and vehicle concept selection were done iteratively and simultaneously. The analysis tools were used to generate a more detailed and accurate design. They were used to more accurately calculate the weight and performance of the aircrafts and to guide the decision making.

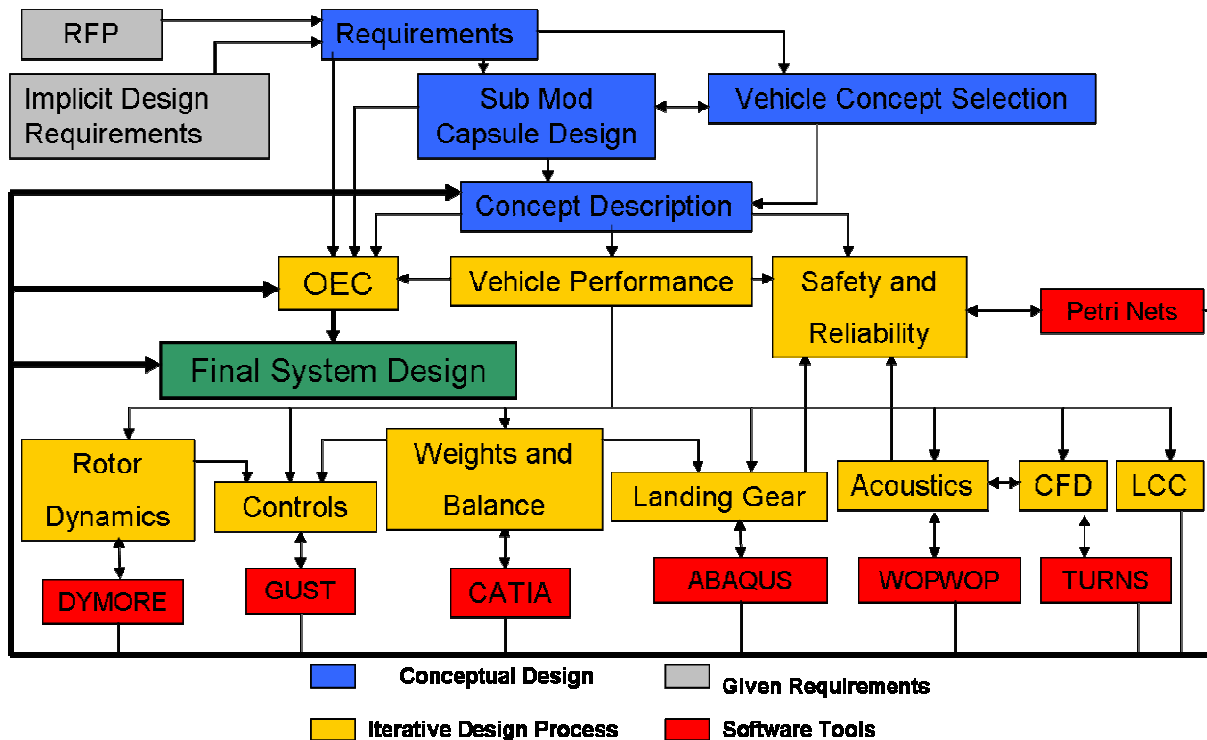


Figure 1-3: Design Flow

2. Submarine Modification and Launch System Development

The necessity of aircraft operations from a submerged submarine drives the ARV and UEV designs and other mission considerations, thus limiting the aircraft deploying system. Aircraft are required to takeoff and land on a small platform regardless of the type of launch system chosen. The launch design is coupled to the aircraft design in the iterative design process. Currently, the modified Ohio Class submarines can carry 102 SOF soldiers⁷. This provides a general design goal for the number of soldiers that the new system should be able to deploy to the objective.

2.1. Design History and Tradeoffs

2.1.1. Initial Launch Concept

The preliminary Launch and Recovery System, LARS, concept focused on the submarine modifications, instead of launch and recovery, with two main considerations; leave the majority of the missile tubes intact, or replace the entire available volume with hangar space. Concepts of both types were developed.

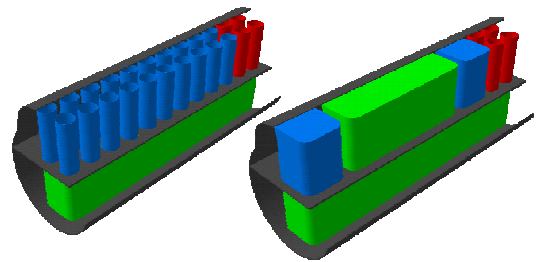


Figure 2-1: Initial Submarine Modification Considerations

The first LARS, shown in Figure 2-2, was similar to the second of two submarine concepts and had a three floor design implementing two elevators and four launch chambers, with each chamber containing one “bubble capsule.” The launch chambers comprised the top floor, with storage in the middle floor and POL storage and maintenance at the bottom. Folded aircraft would be loaded from the second floor onto the elevators and into the capsules in the launch chambers. Each capsule is tethered to the submarine to facilitate recovery and assist in stability, and is unfolded into a launch platform once reaching the surface. With spacing being a concern, two adjacent capsules would not be used simultaneously, allowing only two capsules to be on the surface at a time.

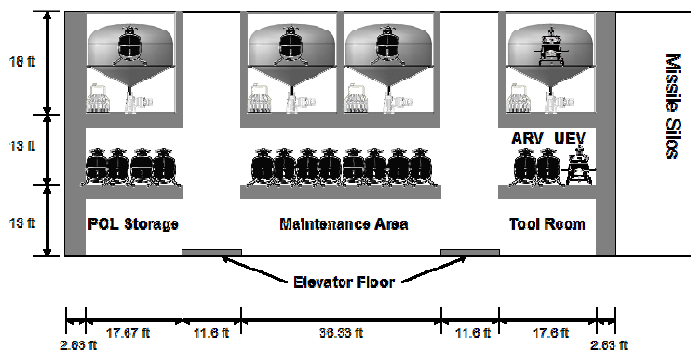


Figure 2-2: First LARS, Version 1

Returning aircraft would land on a deployed capsule once the aircraft using it for launch has cleared the area. After the aircraft returns to the capsule, the capsule would close and withdraw into the submarine.

This design had many problems. First, the returning aircraft would cause a severe bottleneck while other aircraft are being refueled. This would mandate that returning aircraft would have to fly in a holding pattern till the capsule area is clear. Secondly, even with the fastest ARV for this LARS, the maximum SOF troops delivered in six hours would be thirty due to the large time delay in loading the capsule and deploying to and from the water surface.

2.1.2. Tethered Box

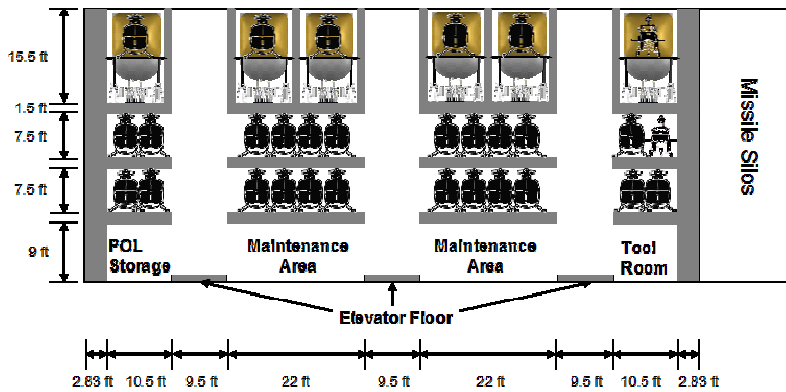


Figure 2-4: First LARS, Version 3

Building on the previous LARS, a “Tethered Box” concept, operationally similar to the “bubble capsule”, was explored. The main differences are that three elevators service four floors and six launch chambers. This system can launch three aircraft simultaneously, while carrying nearly twice as many aircraft (thirty to eighteen), thus deploying more SOF

troops. This capsule has inflatable airbags on its outer surface to support the panels upon unfolding. Three capsules would be released together and joined on the surface to create a large stable platform as shown in Figure 2-5. The “tethered box” LARS can deliver four SOF troops to the objective during the first flight and six troops in each subsequent flight. A total of 78 SOF troops would be deployed at the objective within six hours. The aircraft can also land simultaneously, leading to a quicker refueling cycle. There is a high degree of complexity during launch operations involving four floors and three elevators similar to that on an aircraft carrier. This design would also require several sailors on the surface at all times assisting in the assembly of the platform. The large fixed platform severely limits the stealth of the operation.

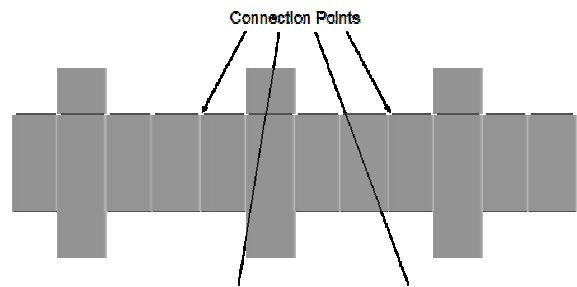


Figure 2-5: Unfolded Capsule Platform

The capsule requires long watertight seals on its six edges. The launch chamber door size and

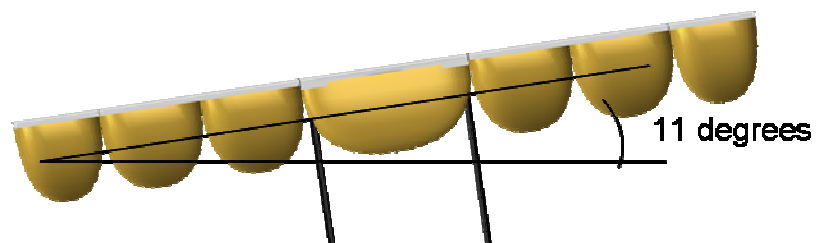


Figure 2-3: Sideward Tilt in Sea State 3

shape posed a similar problem. Also, the surface time required by the capsules and their physical attachment to the submarine presented possible dangers to the submarine, either when discovered or needing to maneuver away from the launch site. The surface stability during sea state three showed an eleven degree side slope which is above the limit of most aircraft as shown in Figure 2-3

2.1.3. General Dynamics Missile Capsules

This design was constructed specifically to counter the issues of the “tethered box” concept and is based on a General Dynamics Sea Stabilization Concept². This LARS left all missile tubes intact, launching capsules containing ARVs and UEVs to the surface, each of which contained two vehicles. A free capsule allows the capsule to operate independently of the submarine, which reduces the security risk to the submarine. Leaving the missile silos intact presents the low cost solution since the submarine retrofit cost will be greater than aircraft cost.

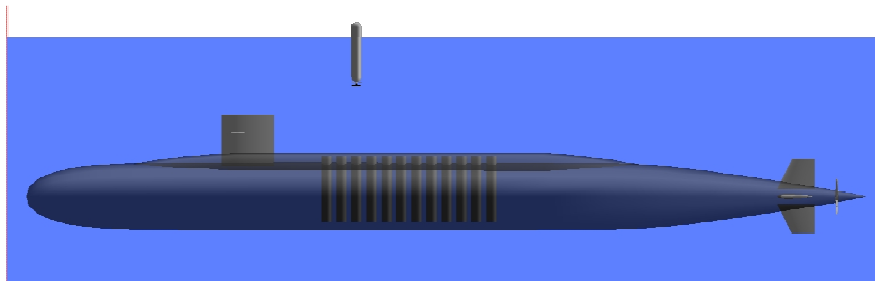


Figure 2-6: LARS v2.1

The capsules would navigate to the surface and return to the submarine through use of directional thrusters, GPS positioning, and communications technologies. This would also prevent capsule collision or deploying too close due to other capsules in the water at any given time. The ascent/descent, buoyancy, and stability of a capsule would be controlled through a combination of ballast tanks and a lead weight engineered to translate down in order to move the capsule’s CG. Once stabilized on the surface, the hatch at the top end of the capsule would open, beginning the launch process. Designing a

VTOL aircraft to deploy from this capsule requires a unique design as shown in Figure 2-7. The aircraft are removed from the capsule through a chain and rail drive system, rotating the aircraft 90° once fully removed from the capsule. While on rail support, the blades and fuselage would unfold

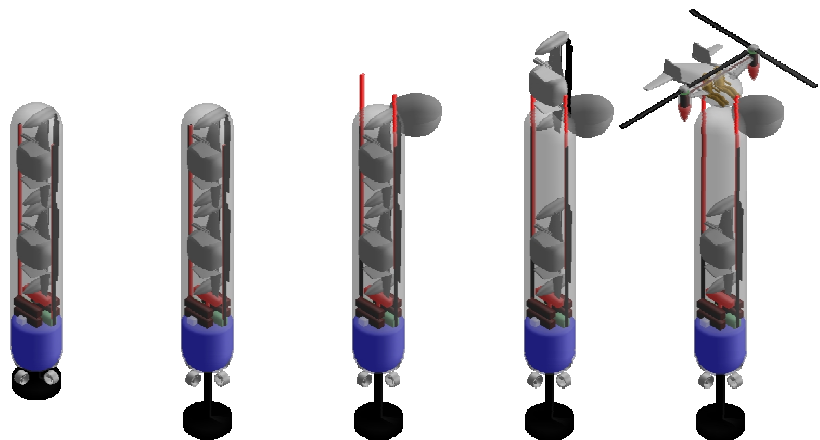


Figure 2-7: General Dynamics Capsule Launch Sequence

and the aircraft would takeoff. Retrieval would be in reverse sequence of launch. With all twenty capsules launched, this system could deploy 158 SOF troops. However, this design presents places severe requirements on the aircraft design. The aircraft storage and mechanical deploying mechanics are very complex. The most significant problem is that the aircraft could not safely and reliably land back on the capsule. Consequently, any concept involving launch from and landing on the missile tubes was considered infeasible.

2.1.4. Early Barracuda Capsule

Still resembling the previous LARS in many ways, this was the first in a series of hybrid concepts, combining benefits and functions of the “bubble capsule,” the “tethered box,” and the General Dynamics capsule. The tubular capsule shape and capsule launch and stabilization process remained the same. However, the capsule was widened to a diameter equal to two missile tubes, resulting in a total of five capsules stored on the submarine. This was done so that the ARVs/UEVs could be stored in a horizontal position, resulting in additional internal space. Four aircraft are stored in each capsule on four moveable platforms fixed to a drive system. After the topmost ARV took off, the floor would translate up and flip or rotate out of the way, allowing the next platform to translate up for the launching of the second ARV. This process would repeat until all aircraft were launched. Operationally, this system is not as effective, as only eight SOF troops can be deployed initially to the objective, with a total of 72 troops, assuming all aircraft deployed. This design allows for more flexibility in aircraft design. The elevator system requirement that all decks be raised and flipped increases the complexity and failure rates. Secondly, there are serviceability issues with the capsule systems being difficult to access and no designated service/storage area availability for inoperable vehicles. This design would require any malfunctioning aircraft to be ditched into the sea. Lastly, the geometry of the capsule resulted in wasted space and an insufficient ballast tank.

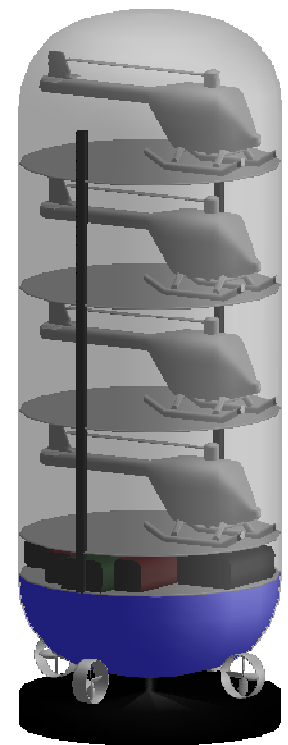


Figure 2-8: LARS 2.2 Capsule

The LARS v2.3, shown in Figure 2-9, eliminated the translating of the entire capsule decks and used a single elevator shaft. Also, it was determined that the shape, weight and inertia of this capsule negated the need for a translating lead weight, reducing the system complexity. The capsule systems were moved to one of the upper decks of the capsule for easy accessibility in the event of an emergency or

maintenance. This upper deck was also designated as the launch preparation/maintenance deck, increasing system viability.

The last and most important change was that of capsule geometry. The spherical hatch shape of previous capsules was somewhat unrealistic and wasted precious vertical space within the capsule. This shape was replaced with a flatter, less bulky hatch shape. Also, until this point, all of the second series of LARS capsules possessed a circular cross-section, the diameter being either one or two missile tubes. Keeping only one quarter of the missile tubes and installing flat panels in between, the capsule could be designed to a “rounded square” shape, allowing more capsule volume. With these changes,

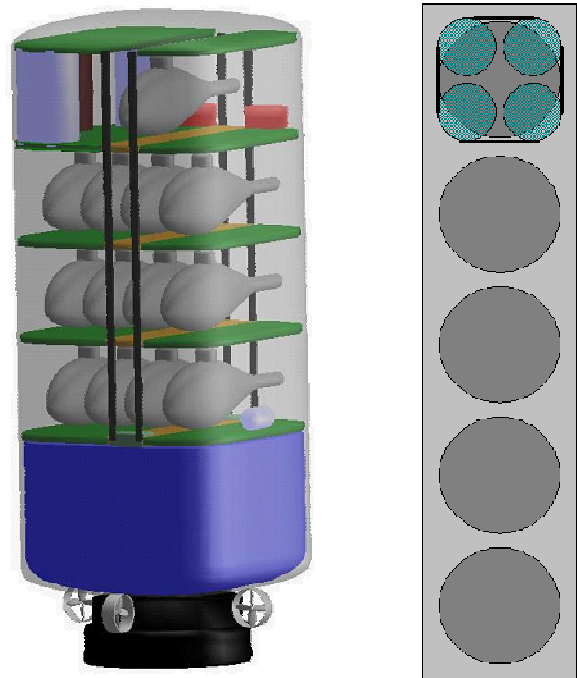


Figure 2-9: LARS 2.3 Capsule and Cross Section Comparison

the capsule in Figure 2-9 was designed that could store thirteen aircraft. Each vehicle would be designed to fold to fit in the given space (2.5 ft x 7 ft x 16 ft), and would unfold after reaching the launch deck. The elevator was designed to have three floors that move collectively. This would allow for an aircraft to be stored on each deck allowing for an additional three aircraft. Thirteen aircraft could be stored on each capsule. This system could deploy 256 soldiers. The drawbacks of this design would be that additional soldiers would need to be located outside the capsule. The elevator design would require that an aircraft on the bottom level would have to be moved eight times to reach the surface.

2.2. Barracuda

The final LARS, designated Barracuda, was both the end result of several stages of iterations and a combination of the two initial LARS developments. To compromise between submarine modifications and ARV simplicity, this system divides the available submarine bay volume into five chambers, from each of which a Barracuda capsule can be launched. The chambers as well as the capsules have a rounded square cross-section, with a slight outward curvature on the “flat” surfaces, to make maximum use of the volume while retaining pressure resistance. It is capable of operating independent of the carrier sub for the mission length before recharging is necessary.

2.2.1. Layout and Systems Overview

The general layout of the Barracuda can be seen in Figure 2-10. The capsule is divided into four floors for aircraft and crew storage while batteries, propulsion, and a ballast system occupy the space below the bottom floor. A hydraulic rope driven elevator operates along the center of the capsule to move SOF troops and ARVs/UEVs from floor to floor in ten seconds under normal load. Access to the capsule while it is in the submarine is gained by two side hatches. The top side hatch opens into the launch prep area and control room, while the bottom hatch opens onto the bottom floor, in a waiting/storage area for SOF troops and their equipment. The top of the capsule is sealed by a pair of pressure/water resistant doors. These doors are similar to the submarine bay doors and are operated by four motors (two per door) located on the launch deck. Located across on the launch prep deck is the fuel pump and tank for servicing the aircraft. The tank can hold approximately 3600 lbs of fuel (530 gal), and the pump is capable of a rate of 350 GPM.

Once the capsule is launched, propulsion is provided by four Voith Schneider Propellers located on the sides of the capsule towards the bottom⁸. Together, these propellers allow precision thrust in any lateral direction, essential for navigation to and from the launch chambers and proper spacing of capsules once above the water's surface. A receiver at the bottom center of the capsule works in tandem with a buoyant beacon tethered in each launch chamber to

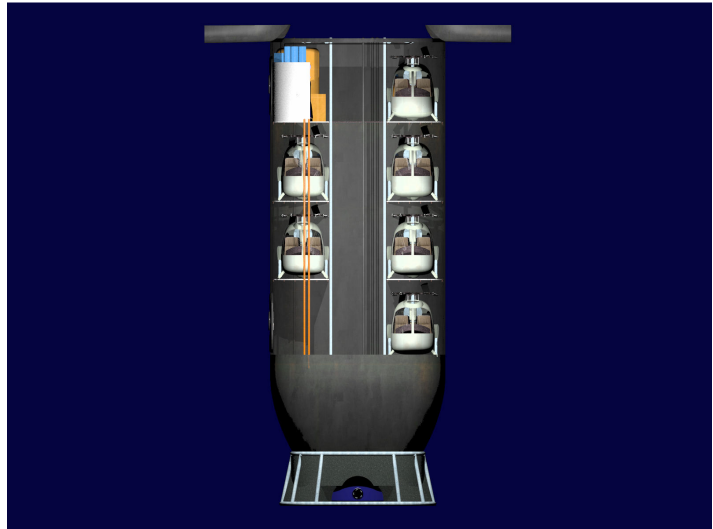


Figure 2-10: Barracuda Capsule

allow the Barracuda to return to a launch chamber at mission completion. Both propulsion and navigation are managed at the capsule control station, located on the launch prep deck, by a capsule officer. Capsule stability and buoyancy are maintained and adjusted by a large lead weight at the bottom of the capsule and a ballast system. The lead weight comprises more than a third of the capsule weight when the capsule is completely full (aircraft, personnel, fuel, equipment, ballast), and slightly less than half when empty. It is also shaped so as not to hamper the function of the propellers. The ballast system uses valves to regulate the inflow of water and compressed air to force water from the ballast tank. When necessary, the compressor operates while the capsule is at the surface to fill its storage tanks. Submarine power is provided by an array of 66 batteries, which can provide enough energy to run the

Barracuda capsule's systems for at least twelve hours before returning to the submarine. The batteries are charged through a cable link running through the open bottom hatch while the capsule is stored in the submarine. The area containing the batteries and compressor is kept dry by bilge pumps in case of flooding.

2.3. Launch Process and Mission

2.3.1. Capsule Loading and Launch

Upon tasking receipt, the SOF troops and capsule officers onboard the submarine load into the five stowed Barracuda vessels through the launch prep deck access hatches. The mission equipment for the first lift is pre-loaded into the aircraft. The mission equipment for the second lift is pre-positioned at the bottom deck of the Barracuda. Soldiers for the second lift enter the capsule on the bottom deck and wait with their mission equipment as shown in Figure 2-11. Soldiers for the first lift board the elevator and are taken to their aircraft.

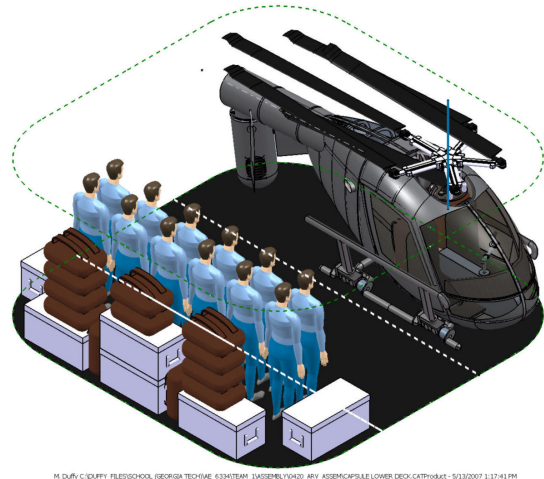


Figure 2-11: Troops Loaded on Lower Deck

Capsules would be launched in a similar manner to launching a missile. The launch chamber is flooded with the capsules having valves on their ballast tanks closed; this will prevent water from entering and allow the capsules to begin surfacing immediately after the bay is flooded.

2.4. Surface Maneuvers

Once on the surface, the capsule officer is responsible for adjusting and maintaining the buoyancy and height of his respective capsule through use of the ballast tank and propellers. Since all five capsules may be deployed at once, the capsule officer must use the propellers to maintain a safe distance from other capsules in order to allow multiple Barracudas to operate simultaneously. Once height, spacing and buoyancy are stabilized at the water's surface, the Barracuda main doors can be opened. The ballast

Table 2-1: Barracuda Deployment Times

Volume of Capsule	9450 ft ³
Water Weight Displaced	604,800 lbs
Capsule Weight Empty	466,781 lbs
Capsule Weight Full	514,661 lbs
Ballast Tank Volume	2200 ft ³
Full Ballast Weight	140,8000 lbs
Minimum Time to Rise 50' (full)	23.89s
Minimum Time to Rise 50' (empty)	18.39s
Minimum Time to Sink 50' (full)	35.97s
Minimum Time to Sink 50' (Empty)	147.80s

tank was sized so that the Barracuda can raise and lower itself when full and empty. This provided the limit on the aircraft height.

2.4.1. Aircraft Loading and Launch

Once the main doors are open, the aircraft on the top deck of each capsule is loaded onto the elevator and brought to the launch deck. The aircraft is then unfolded and launched. The first serial consists of four Ciphers and one Dragonfly. Once the first serial has departed, the elevator then descends to load another aircraft. This process is repeated until all the aircraft are launched. Once the capsule has been emptied, its main doors can be closed and it can retreat below the waves to wait for the first Cipher returning from the objective. After all aircraft and SOF troops have been returned to the capsules, the capsules’ ballast tanks can be filled, and using the propellers and navigation equipment, the capsule officer can navigate the Barracuda back into the submarine.

2.5. Barracuda Launch Deck Stability

The minimum landing platform size for a type three helicopter is 15x15 ft square according to the NFES Interagency Helicopter Operations Guide³. To meet this requirement, the Barracuda has a 16x16ft rounded square landing platform. The surface stability of the Barracuda was analyzed to make sure it meets acceptable stability requirements. The interagency guide mandates the maximum side slope landing of 5^o³. The maximum angular tilt is less than 2^o in sea state three.

Table 2-2: Sea State Three Stability

Capsule Weight	514,661 lbs
Weight of Replaced Missiles	521,084 lbs
Wave Height	4 ft
Weight of Wave Water Displaced	51,446 lbs
Rate of Up/Down Acceleration	0.0996ft/sec ²
Time to Rise 1 foot	4.47s

3. ARV and UEV Concept Selection

3.1. Concept Filtering

The morphological matrix in Figure 1-2 gives twenty trillion different combinations of ARV, UEV and launch design configuration. The following requirements served as the first filters for reducing the number of feasible ARV concept configurations that are capable of performing the mission described in the RFP. The ARV must be able to land on unimproved surfaces in order to deploy the two SOF soldiers at the objective. This requirement eliminates concepts with disk loadings greater than 30 lb/ft². The SOF soldiers should be able to egress quickly from the ARV once on the objective. Since the ARV will be used in tactical flight scenarios, it should be able to conduct Nap of the Earth (NOE) flight maneuvers such as NOE decelerations, pinnacle landings, etc. The requirement to egress quickly on the objective and fly NOE eliminates a tail sitter concept. This led to three best aircraft configurations that could meet the ARV mission requirements: a single main rotor helicopter, a coaxial helicopter with aux prop, and a tilt rotor. Since the UEV is not required to land at the objective, the box wing tail sitter and ducted fan concepts became possibilities for the UEV only. The ducted fan was eliminated because a low disk loading ducted rotor system cannot be folded compactly and a high disk loading ducted fan acoustic signature would be too high.

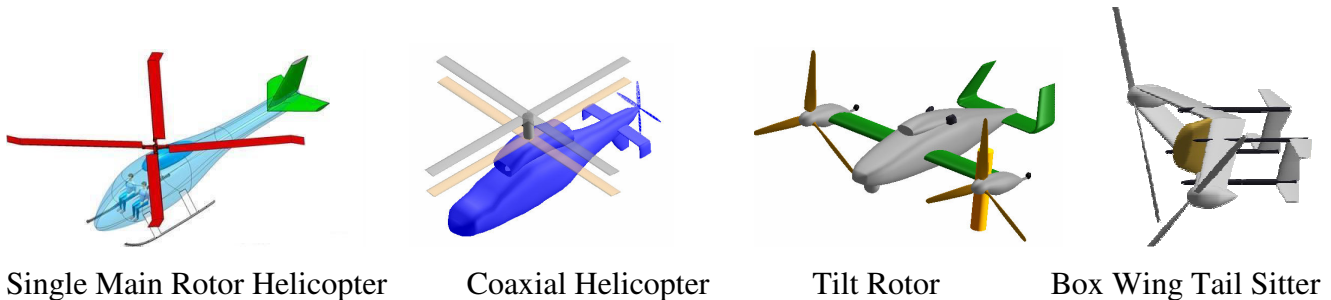


Figure 3-1: Possible ARV and UEV Concepts

3.2. ARV and UEV Mission Comparison

Using the same configuration for both the ARV and UEV would be beneficial in terms of aircraft fleet cost and commonality of parts. However, the enormous cost of retrofitting the submarine is an order of magnitude higher than the cost of the vehicles. This makes the cost of a separate vehicle much less important than achieving mission success. Also, the driving force behind submarine based operations is stealth, so maximizing the stealth of both vehicles is of great importance. A relatively high degree of stealth could be accomplished by launching missions from a concealed cargo ship. This would be much simpler than launching from a submarine, though, it would not provide the same extremely high level of

stealth. The use of a submarine launched system implies that stealth of both vehicles should be maximized. This gives credence to selecting different aircraft configurations for the ARV and UEV to maximize mission performance.

3.3. RF Analysis and Aircraft Sizing

An RF (Ratio of Fuel) performance program was developed that could model almost any type of VTOL rotorcraft configuration. This program was developed in two major iterations. The first iteration simultaneously computed the minimum gross weight and performance of a single main rotor helicopter, a coaxial helicopter, and a tilt rotor given the missions for the ARV and the UEV and a set of “a priori” data for each aircraft.^{9,10,11,12} The second iteration allows a user to define attributes and functions of the aircraft to construct any type of rotorcraft configuration. Table 3-2 summarizes the performance results given the “a priori” inputs of Table 3-1. The empty weight fractions of each concept were reduced for the UEV mission due to increased fuel required and lack of crew.

Table 3-1: "A Priori" Design Parameters

A Priori Design Parameters	Units	Single Main Rotor Helicopter		Coaxial Helicopter		Tilt Rotor	
		ARV	UEV	ARV	UEV	ARV	UEV
Disk Loading	lb/ft ²	6	6	10	10	20	20
Empty Weight Fraction	ND	0.55	0.535	0.6	0.585	0.65	0.55
Equivalent Flat Plate Drag	ft ²	5	5	6	6	4	4
Rotor Solidity	ND	0.1	0.1	0.1	0.1	0.1	0.1
Tip Speed	ft/sec	650	650	650	650	650	650
Downwash Factor	ND	0.03	0.03	0.05	0.05	0.08	0.08
Aux Prop Percent Thrust	ND	NA	NA	100	100	NA	NA
Wing Span	ft	NA	NA	NA	NA	15	15
Wing Aspect Ratio	ND	NA	NA	NA	NA	5	5

Table 3-2: Performance Estimates

Performance Parameter	Units	Single Main Rotor		Coaxial Helicopter		Tilt Rotor	
		ARV	UEV	ARV	UEV	ARV	UEV
Minimum Gross Weight	lbs	2430	2344	2918	3029	4188	5402
Hover Power 6000ft/95F	HP	293	283	415	430	990	1278
99% Max Range Airspeed	kts	118	117	132	134	234	265
99% Max Range Airspeed Power	HP	214	206	303	316	1148	1666
Max Endurance Airspeed	kts	64	61	73	70	140	150
Max Endurance Airspeed Power	HP	134	121	191	181	482	672
Empty Weight	lbs	1336	1254	1751	1772	2722	3079
Total Fuel Weight	lbs	272	448	336	601	616	1583

The results of the program show that the single main rotor helicopter is the lightest configuration for the ARV mission and is lighter than all concepts other than possibly the box wing tail sitter for the UEV.

The aerodynamic properties of the proposed box wing tail sitter UEV concept were too complicated for the first iteration RF program. Therefore, the RF program was modified to include the following new and advanced features.

A blade element model with a Prandtl tip loss model was added which allows for blades with nonlinear twist, multiple tapered sections, and multiple airfoil sections along the span of the blade.⁹ It was also used to model a rotor in vertical climb. An empty weight model was created based on weight equations from Prouty, NASA, and the military.^{10,13} A wing model which allows for different wing and airfoil designs such as box wings and sweep was added. A better model of intermeshing/coaxial rotors was used.⁹ A feature that allowed for changing tip speeds during the mission was also added. The RF program was used to compare the sizing and performance of the single main rotor and tail sitter concepts for the UEV mission. The results are summarized in Table 3-4.

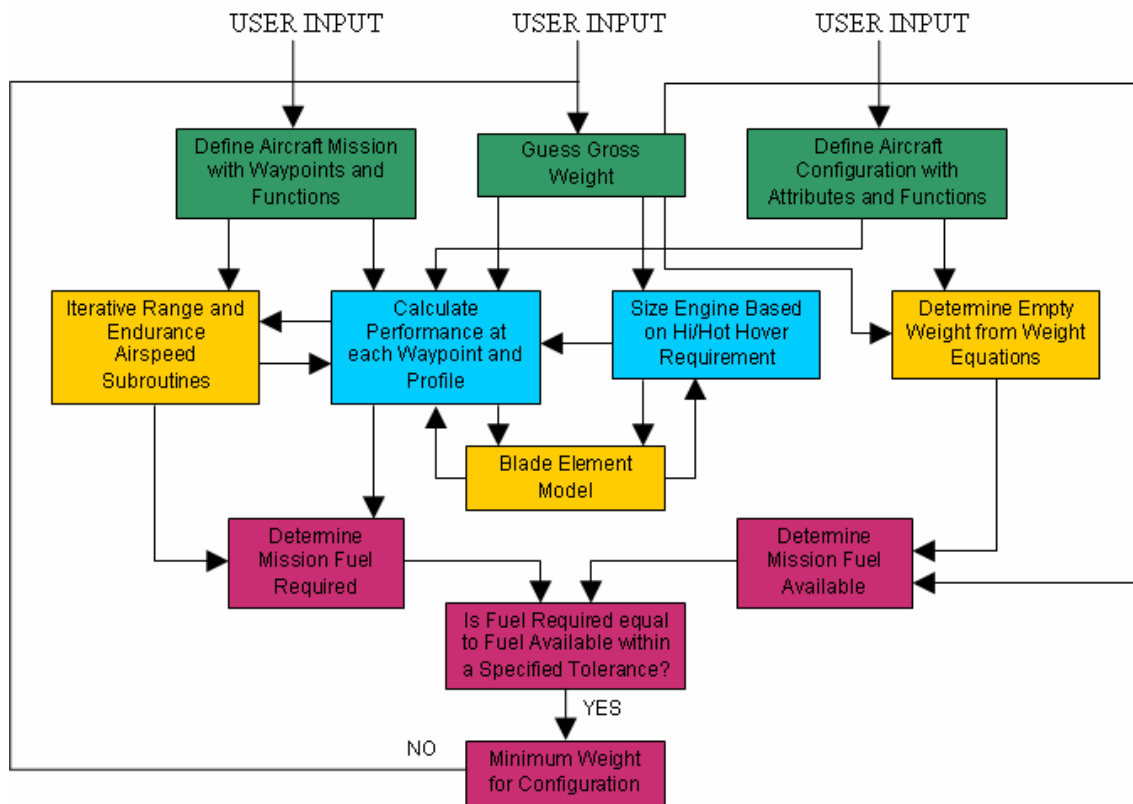


Figure 3-2: RF Program Algorithm

Table 3-3: Design Parameters for the Helicopter and Tail Sitter for the UEV Mission

Design Parameters	Units	Single Main Rotor Helicopter	Box Wing Tail Sitter
Disk Loading (calculated)	lb/ft ²	6.2	9.1
Empty Weight Fraction (calc)	ND	0.56	0.61
Equivalent Flat Plate Drag (calc)	ft ²	7.1	1.15
Rotor Solidity	ND	0.085	0.115
Hover Tip Speed	ft/sec	650	600
Cruise Tip Speed	ft/sec	650	375
Loiter Tip Speed	ft/sec	650	220
Downwash Factor	ND	0.03	0.0105
Wing Area	ft	n/a	80

Table 3-4: Performance Comparison for the Helicopter and Tail Sitter as UEV Concepts

Performance Parameter	Units	Single Main Rotor Helicopter	Box Wing Tail Sitter
Minimum Gross Weight	lbs	2650	2606
Hover Power 6000ft/95F	HP	273	378
99% Max Range Airspeed	kts	120	142
99% Max Range Airspeed Power	HP	261	239
Max Endurance Airspeed	kts	63	83
Max Endurance Airspeed Power	HP	155	110
Empty Weight	lbs	1471	1580
Weight of Total Fuel Required	lbs	577	347

3.4. Acoustic Signature

The most heavily weighted design consideration is minimizing the acoustic signature of the ARV and UEV near the objective. Fundamentally, the key factors that contribute to the human perception of noise are the intensity, duration, and directivity. Figure 3-3 shows a graphical comparison of the rotor acoustic signature intensity and directivity of the four concepts.

3.4.1. Acoustic Signature Intensity

Generally, if the magnitude (intensity) of an omni-directional noise source is increased by 6 dB, the distance from the source at which the source can be heard is doubled. The equivalent perceived acoustic signature intensity of rotorcraft is a function of gross weight, disk loading, number of rotor blades, rotor tip speed, and BVI.

3.4.2. Aircraft Gross Weight and Disk Loading

All VTOL concepts accelerate air downwards to produce thrust. According to simple momentum theory, this velocity is proportional to the square root of disk loading.⁹ The acoustic intensity (dBA) produced is proportional to the six power of this velocity for low velocity values.^{14,15} Therefore,

acoustic power increases with an increase in disk loading to the third power. Therefore, minimizing gross weight and disk loading will reduce the acoustic signature of the aircraft. **According to the RF sizing, for the ARV mission, the single main rotor helicopter is the lightest weight and lowest disk loading aircraft configuration during the approach to the objective and is therefore the quietest in low speed flight.**

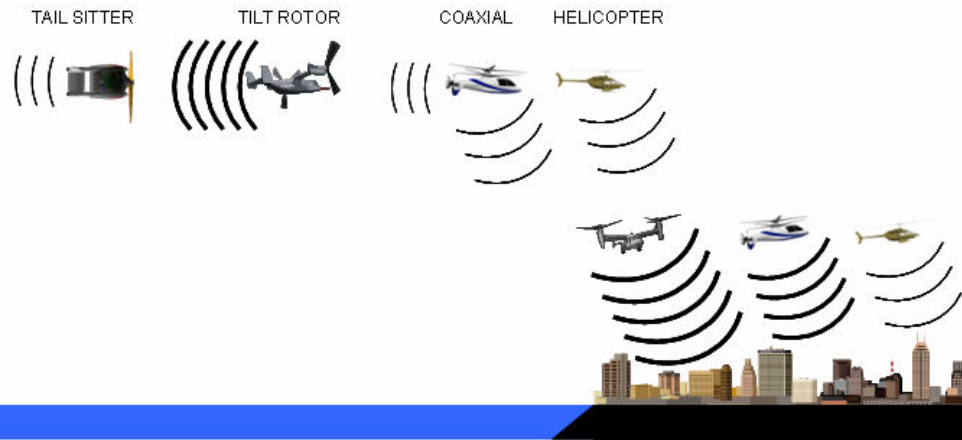


Figure 3-3: Acoustic Signature of Different Concepts Near the Objective

3.4.3. Number of Rotor Blades

Increasing the number of rotor blades per rotor decreases the magnitude of the noise, and increases the frequency of the noise which reduces the perceived noise. Higher frequency noise attenuates more quickly in the atmosphere. While a tilt rotor and a coaxial rotor may have more blades than a single main rotor helicopter, the load on one of their rotor disks is approximately the same as that of a single main rotor, except their disk loading is higher. Therefore, the acoustic signature of a single rotor disk of a tilt rotor or a coaxial rotor is still higher than that of a single main rotor. Accounting for the second rotor increases the overall rotor acoustic signature by 3 dB. There is no compelling reason that a single rotor disk of a tilt rotor or coaxial helicopter would have more blades than a single main rotor. Therefore, the coaxial helicopter and tilt rotor gain no advantage over the helicopter by increasing the number of blades.

3.4.4. Rotor Tip Speed

Rotor tip speed may be the single most important factor that determines rotor acoustic signature. As the tip speed is lowered, the acoustic signature is reduced significantly. Also, the tip vortex strength is lowered which reduces BVI noise during the approach to the objective. However, there is no compelling reason why the tip speed in hover and low speed flight should benefit one ARV concept over another. The tip speed can be lower for a coaxial helicopter or tilt rotor than for a single main rotor

helicopter while the aircraft is flying at cruise speed on the way to the objective. However, acoustic signature is much more important near the objective.

Since the UEV does not have to land at the objective, a UEV configuration that employs a reduced tip speed is preferred. Both the tilt rotor and the tail sitter concepts can lower their tip speeds in loiter because their wings produce lift while the rotors are only responsible for thrust. The tilt rotor is unable to reach low loiter speeds because of the high weight and limited wing area.

3.4.5. Blade Vortex Interaction

A crucial component of noise during the approach to the objective is the BVI noise. This occurs when a rotor blade passes through the tip vortex of the previous blade. BVI is unavoidable during the approach and landing to the objective. This can be reduced with active control such as active flaps or passive methods such as swept anhedral rotor tips. Any concept with intermeshing or overlapping rotors such as tandem or coaxial will suffer from BVI during all modes of flight and the approach noise will be compounded. For this reason, the acoustic signature of the coaxial rotor will almost always be greater than that of a single main rotor helicopter as shown in Figure 3-4.¹⁶ Figure 3-5 shows the rise in noise as a tilt rotor goes through transition due to BVI¹⁷. For a single main rotor helicopter, a major source of noise is the interaction between the main rotor vortices and tail rotor blades. This is the primary reason

NOTAR and fenestron helicopters are quieter than those with a standard tail rotor.

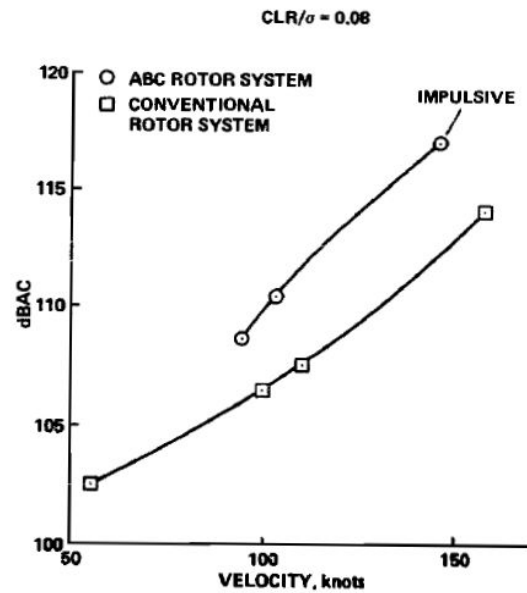


Figure 3-4: Acoustic Signature of Coaxial vs. Single Main Rotor Helo

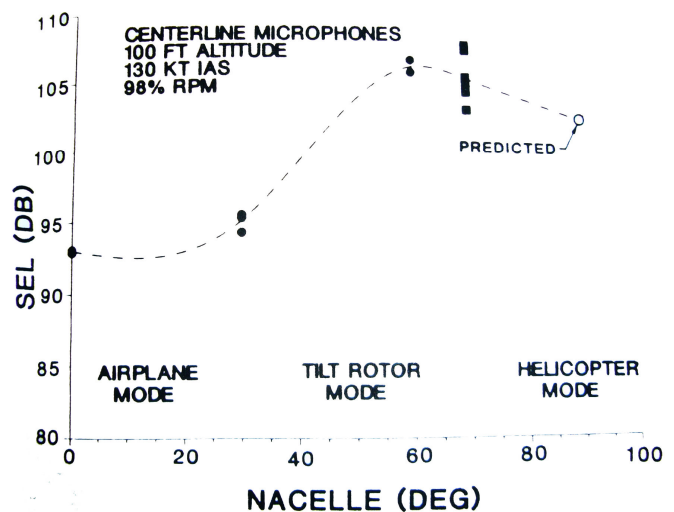


Figure 3-5: XV-15 Acoustic Signature

3.4.6. Acoustic Signature Directivity

Most sources (like aircraft) are not omni-directional, so the directivity of the noise must be considered. A rotor system parallel to the surface of the earth like a single main rotor helicopter projects noise down towards the earth with a smaller component projected forward. Rotors that are tilted 90 degrees like an airplane propeller tend to project a larger component outward. This helps reduce the amount of noise that is projected down towards the earth. Figure 3-5 shows 10dB decrease in noise for an XV-15 in airplane mode vs. helicopter mode.¹⁷ For the UEV concept, this is very beneficial, because the aircraft does not have to land near the objective. Therefore, the quietest UEV concept will be one in which the rotor is tilted 90 degrees so that less noise is projected towards the objective.

3.4.7. Acoustic Signature Duration

A noise source is more likely to be detected by humans the longer the noise source is active. This emphasizes the requirement for the soldiers to be able to egress the ARV quickly on the objective. Since the UEV is required to remain over or near the objective for up to three hours with continuous coverage for up to six hours, the long duration of the noise cannot be avoided. Therefore, the UEV acoustic signature intensity must be minimized to compensate for this. This is another reason why the UEV must be optimized for acoustic signature independently of the ARV concept selected.

3.5. Concept Summary

3.5.1. Tilt Rotor

The tilt rotor was disappointing. It has improved range performance over a helicopter at the expense of hover performance and higher weight. The prospect of having an ARV with a high cruise speed was initially attractive in order to get more SOF soldiers to the objective. However, the high cruise speed is the only advantage of the tilt rotor, and the number of soldiers deployed to the objective is more sensitive to the launch process than the aircraft cruise speed since the payload is fixed to two SOF soldiers. Due to the space constraints on the submarine, the wing span of the tilt rotor is limited to 16 ft. This means that the rotor diameter could only be about 7 ft, which results in a disk loading of about 20 lb/ft². This causes the tilt rotor to be the noisiest ARV concept considered. The prospect of using the tilt rotor as a UEV to take advantage of noise directivity also became a disappointment. Due to the short wing span, the loiter speed would have to be considerably high making the loiter efficiency very poor. The fuel weight and thus gross weight of the aircraft becomes substantial. This negates the noise benefit gained from directivity.

3.5.2. Coaxial Helicopter with Aux Propulsion

The coaxial helicopter is not as fast as the tilt rotor, but it is faster than a helicopter. It is not as light or quiet as a helicopter, but it's lighter and quieter than a tilt rotor. For a complicated problem where compromise is required, the coaxial was considered a strong possibility for a balanced design. Its major disadvantage is the BVI noise during the approach to the objective.

3.5.3. Single Main Rotor Helicopter

The single main rotor helicopter is the quietest ARV concept during the approach to the objective due to its low disk loading and low gross weight. It is the slowest concept, so it will not be able to deploy as many soldiers to the objective, but it is smaller, so more aircraft will be able to fit on the submarine. There is an experience factor associated with a helicopter concept that will reduce the overall design risk. Very few tilt rotors or coaxial rotor helicopters have been manufactured, but many single main rotor helicopters have been manufactured. The cost of production and risk of autonomous integration would be smaller.

3.5.4. Box Wing Tail Sitter

While the box wing tail sitter could not be used for the ARV it makes a great candidate for the UEV because the UEV does not have to land at the objective. The box wing configuration allows for a larger wing area which results in a much slower loiter speed. This means that the thrust required from the main rotor is quite small and therefore, the tip speed can be reduced significantly. Many of the RF sizing iterations for the tail sitter used tip speeds as low as 200 ft/sec, whereas the single main rotor tip speed could not be lowered below about 550 ft/sec. The tail sitter also benefits from acoustic directivity. **Therefore, because of the low tip speed and directivity of noise, the box wing tail sitter is the quietest UEV concept.** The main disadvantage of the tail sitter concept is that it requires the development of a second aircraft concept. This results in a poor life cycle cost index, and it also eliminates the ability to use common parts for both aircraft. However, The decision to launch from the submarine places the weighting on mission accomplishment and stealth much higher than the weighting on cost. Also, a successful compact VTOL UEV with a great loiter efficiency and minimal acoustic signature could be a valuable national asset that is used for many applications outside of those mentioned in the RFP. This could justify much of the additional developmental cost required for a second concept. Therefore, because the box wing tail sitter can be much quieter and more efficient than other concepts during loiter, it makes a very strong candidate for the UEV concept.

3.6. Concept Comparison

3.6.1. Qualitative Comparison

Table 3-5: Qualitative Comparison of Design Concept

Engineering Consideration	Single Main Rotor	Coaxial Helicopter	Tilt Rotor	Tail Sitter (UEV Only)
Approach Noise	++	-	--	n/a
Gross Weight	+	0	--	++
Cruise Speed	-	+	++	+
Low Speed Maneuverability	+	+	-	--
High Speed Maneuverability	0	++	++	+
Ease of Soldier Egress	++	++	0	n/a
Complexity	++	0	-	-
Industry Experience	++	-	+	--
Reliability	++	+	-	0
Autonomous Control Risk	++	+	0	-
Life Cycle Cost	++	+	--	-
Loiter Noise	+	0	0	++
Loiter Efficiency	+	0	--	++

3.6.2. Overall Evaluation Criteria Comparison

Given the three possible ARV concepts (single main rotor helicopter, coaxial helicopter, tilt rotor) and the four possible UEV concepts (the three ARV concepts plus the tail sitter), the OEC was used to evaluate the 12 different combinations of ARV and UEV concepts.

$$OEC = \frac{2.5SI + 2.0MCI_{ARV} + 1.5MCI_{UEV} + 1.5AI + 1.0ACRI + 0.5MI}{9 + LCC}$$

Table 3-6: OEC Comparison of ARV and UEV Concept Combinations

OEC VALUES		ARV CONCEPTS		
		Helicopter	Coaxial	Tilt Rotor
UEV CONCEPTS	Helicopter	0.83	0.70	0.61
	Coaxial	0.77	0.69	0.56
	Tilt Rotor	0.59	0.51	0.49
	Tail Sitter	0.85	0.73	0.59

Based on the OEC, the helicopter/tail sitter combination has the highest rating followed closely by the helicopter/helicopter combination. However, this is only one possible weighting configuration. Adjusting the weightings tends to change the order of concepts combinations. Therefore, for a more thorough comparison, the top four combinations were selected for comparison using TOPSIS

(Technique for Order Preference by Similarity to Ideal Solution). This program allows up to ten different weightings for each index and finds the Euclidean distance from the ideal solution. Figure 3-6 shows a radar plot of the four concept combinations. The ideal or optimal point is the center of the plot.

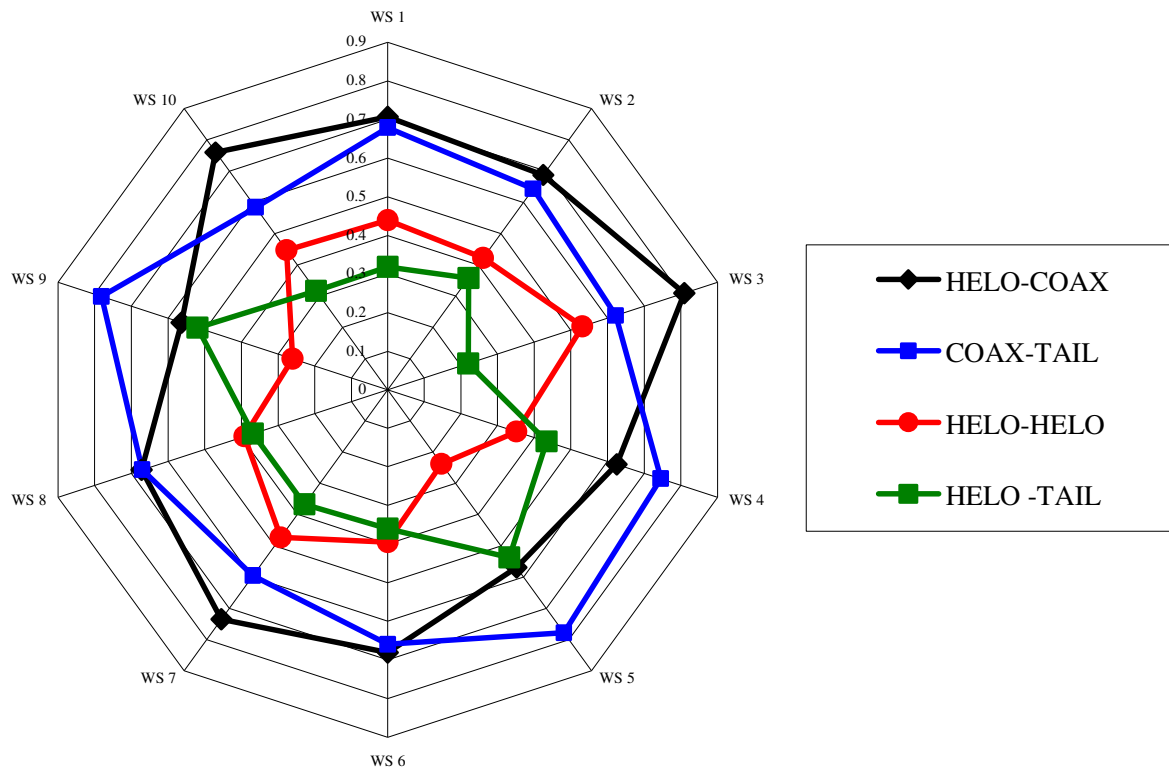


Figure 3-6: TOPSIS Analysis of Concept Combinations for the ARV and UEV

Based on the results of the OEC values and the TOPSIS Analysis, **the single main rotor helicopter was selected for the ARV concept and the box wing tail sitter concept was selected for the UEV concept.** This combination pair will provide the highest level of stealth which is the most heavily weighted design consideration of the RFP. Note that the ARV could be easily modified to conduct the UEV mission, by simply removing the cockpit area and adding a Robinson Auxiliary Fuel System. This requires minimal additional engineering analysis and would be a lower cost alternative. However, the box wing tail sitter is recommended for superior mission performance and stealth.

4. Cipher Concept Development

A number of trade studies were conducted to finalize the design of Cipher. Throughout this process the two primary design goals were compactness and low acoustic signature. This impacts the seating configuration, rotor hub type, and automatic folding design.

4.1. Main Rotor Radius

The main rotor radius was desired to be as large as possible to reduce the hover power required, overall weight, and acoustic signature. Due to the Barracuda dimension trades, the folded aircraft is required to have a length of no more than 15ft, 8 inches. To increase the diameter of the rotor, the mast needed to be placed as close to the nose as possible. The CG of the aircraft needs to be maintained near the mast during all loading configurations for ease of control. The minimum distance from the nose to the mast was determined to be four feet resulting in a main rotor radius of 11ft, 8 inches and a maximum disk loading of 6.63 lbs/ft².

4.2. Tandem vs. Side by Side Seating

A detailed trade study was conducted to determine the appropriate crew seating locations. The main choices were between a tandem and a side by side seating arrangement. The tandem seating arrangement reduces the equivalent flat plate drag of the fuselage in nearly half, allowing for a higher cruise speed. Tandem seating would also allow for an additional helicopter to be placed on each deck of the capsule. To take advantage of this, the landing gear and hub would also have to be less than three feet wide when stored in the capsule, which would have eliminated a hingeless rotor hub. The benefits of a side by side configuration are that the two soldiers can interact with each other easier, they have better visibility, and increased flexibility in landing gear and hub type design. These trades are reflected in Table 4-1. A side by side seating arrangement was chosen for the Cipher.

Table 4-1: Crew Seating Arrangement Trade Study

Criteria	Importance	Tandem	Side by Side
High Cruise Speed	1	5	3
Landing Gear Width	3	1	5
Hub Type Flexibility	5	3	5
Crew Coordination	3	3	5
Number of Aircraft on Capsule	5	5	3
Maximum Rotor Diameter	5	3	5
Total		72	98

4.3. Hub Design Trade Study

In order to select an appropriate hub type, four hub types were investigated: teetering/gimbaled, articulated, hingeless, and bearingless. In order to decrease acoustic signature, at least four rotor blades are required effectively ruling out a teetering or gimbaled rotor. Based on the Barracuda design, there is little room available to inspect/repair/maintain the aircraft; therefore minimizing the required maintenance is the most important aspect of the hub design. The Barracuda also requires blade folding, and as a requirement of the RFP, any blade folding must be automatic. Therefore, the ease of implementing an automatic blade folding system was considered. As the Cipher is required to complete its mission undetected, flying NOE near the mission objective is important, therefore the maneuverability of each hub type is also important.

An articulated rotor system has flapping, feathering, and lead-lag hinges. The effective hinge offset is less than that of a hingeless or bearingless rotor system, resulting in lower maneuverability. The hinges of an articulated rotor require more maintenance than the hingeless or bearingless rotor. The lead-lag hinge of an articulated rotor requires a damper to prevent air and ground resonance issues, which complicates the blade folding process.

The hingeless rotor has no flapping or lead lag hinge, but still has a feathering hinge. The in-plane and flapping moments are absorbed by a flexbeam. Due to a larger effective hinge offset the hingeless hub has increased maneuverability over the articulated hub. The feathering hinge requires significantly less maintenance than an articulated hub. Blade folding requires an in-plane hinge, so it would be necessary to add a folding hinge. However, this hinge may rigidly lock when in flight.

The bearingless rotor hub type has no flapping, lead-lag, or feathering hinges. The flapping and lead-lag moments are absorbed by a flexbeam and feathering control is accomplished with inputs are input by torque tubes. The maneuverability of a bearingless rotor is approximately equivalent to the hingeless rotor. The key benefit of the bearingless rotor type is that because there are no hinges or bearings, considerably less maintenance is required. Similar to the hingeless hub, a hinge is required to fold blades. Based on the decision matrix, a bearingless hub type was chosen for the Cipher.

Table 4-2: Rotor Hub Trade Study

Category (Weight)	Maintenance (5)	Ease of Folding (3)	Maneuverability (3)	Cost (1)	Total
Articulated	1	3	1	5	22
Hingeless	3	1	3	3	30
Bearingless	5	1	3	1	38

The bearingless hub design consists of three major parts: the folding hinge, the flex beam, and the torque tube. The hub designed for the Cipher is based on of the Hanson hub, which due to its fewer parts decreases rotor weight to five percent of gross weight versus seven to ten percent for hingeless and articulated hub types¹⁸.

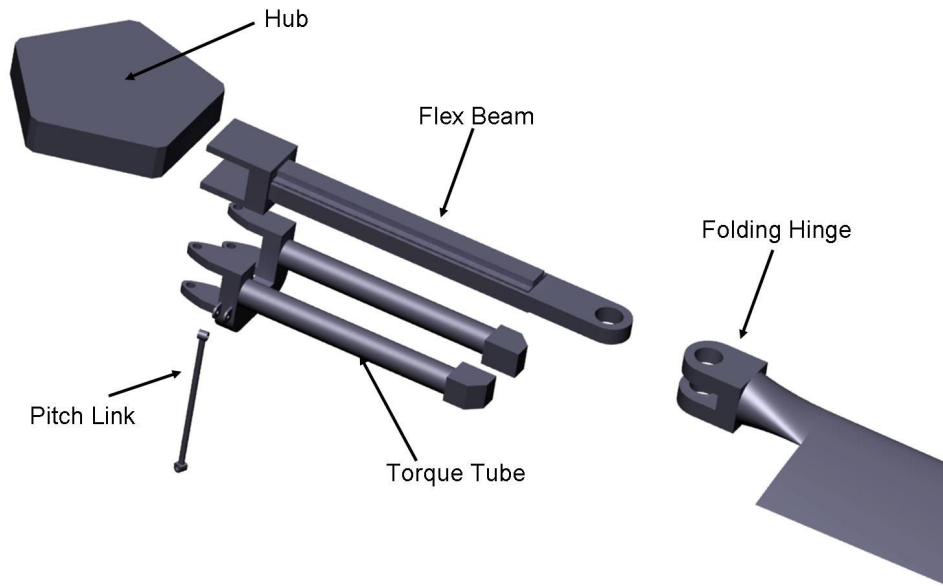


Figure 4-1: Rotor Hub Components

4.4. Number of Rotor Blades

4.4.1. Number of Rotor Blades: Automatic Folding Considerations

Key design parameters for the Cipher are a low acoustic signature and a small storage volume. This leads to a conflict where a design with more rotor blades is better for acoustic signature, but worse for storage volume. It is required to automatically fold the rotor blades so that the aircraft has a small storage volume while still maintaining the necessary rotor blades for acoustic purposes. Based on RFP requirements, the blade folding must be operated automatically. This requires that several features be added to the rotor system. An automatic blade folding system (ABFS) requires a blade folding actuator, blade hinge lock, rotor lock, and a rotor brake¹¹.

The Cipher’s ABFS uses a stepper motor that functions as both the actuator and the blade hinge lock. When folding/unfolding, the stepper motor moves the blade to the appropriate position; once the blade is in that position, the stepper motor locks it in place keeping the blade in that position throughout flight. In order to correctly fold the rotor blades, the blades must be positioned in the correct orientation based on number of blades. This is accomplished with the use of a rotor brake and a rotor lock.

To determine the optimum number of blades and method of folding, a trade study looked at two different folding methods with four, five, and six blades. The key features were ease of folding, performance, acoustic signature, and the folded width. The folding methods studied were side by side (SBS) and blade over blade (BOB).

In SBS folding, the blades on the forward side of the hub center fold on the same plane as the blades aft of the hub center. This means that the forward blades cannot fold inside of the aft blades. This increases the folded width of the vehicle, but is simpler than BOB folding. If BOB folding is used,

then the forward blades are folded such that they pass under the aft blades in order to minimize the folded width. This is accomplished by tilting the folding hinges on the forward blades at an angle so that they rotate on a different plane than the aft blades. For a given hinge offset of twenty percent, it is possible to compute the folded width of each configuration as shown in Table 4-3 and Figure 4-1.

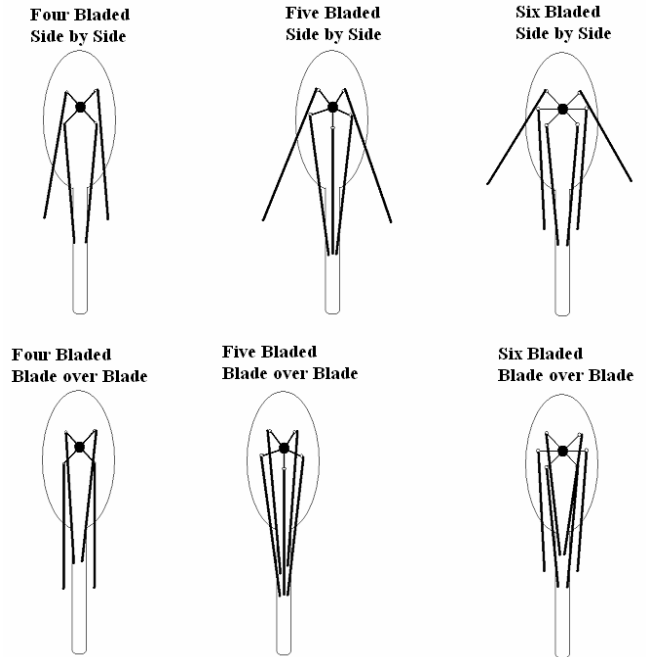


Figure 4-2: Possible Rotor Blade Folding Configurations

Table 4-3: Folded Width of Folding Configurations

	Four Blades	Five Blades	Six Blades
Side by Side Folding (SBS)	0.4594R	0.954R	1.2474R
Blade over Blade Folding (BOB)	0.2828R	0.3804R	0.4R

Six BOB requires the folding of six blades with two folding out of plane. Six SBS requires the folding of six blades with no blades folding out of plane. Both five and four BOB require the folding of four blades with two folding out of plane. Five and four SBS require the folding of four blades with no out of plane folding. It is imperative that the width of the folded hub to be less than that of the fuselage, which corresponds to a folded width of 0.3857R. Only four BoB and five BOB meet this criterion. Based on the results in Table 4-4, five rotor blades folded Blade over Blade was chosen for the Cipher balancing aerodynamic, performance, structural, and folding considerations.

Table 4-4: Blade Folding Decision Matrix

Category (Weight)	Acoustics (5)	Performance (2)	Complexity (3)	Width (4)	Total
4 SBS	1	5	5	3	42
4 BOB	1	5	3	5	44
5 SBS	3	3	5	1	40
5 BOB	3	3	3	5	50
6 SBS	5	1	3	1	40
6 BOB	5	1	1	3	42

4.4.2. Number of Rotor Blades: Acoustic, Performance, and Structural Considerations

To reduce the acoustic signature, it is desired to increase the number of rotor blades to reduce the amplitude of the main rotor harmonic signature and increase the frequency. Each rotor blade is required to produce less thrust than a same weight aircraft with fewer rotor blades. Adding rotor blades adds the additional weight of the blade and hub attachments. The aspect ratio of rotor blades is generally between ten and twenty. Very high aspect ratio blades lack the structural stiffness for the high air loads and torsional rigidity. The effect of increasing solidity on gross weight is shown in Figure 4-3. Increasing to six blades requires a higher solidity and higher gross weight while maintaining an aspect ratio below twenty. Five rotor blades and a solidity of 0.85 were chosen yielding an aspect ratio of 18.724. This is very similar to the BO-105 which has a similar bearingless hub design and blade aspect ratio of 18.158¹⁹.

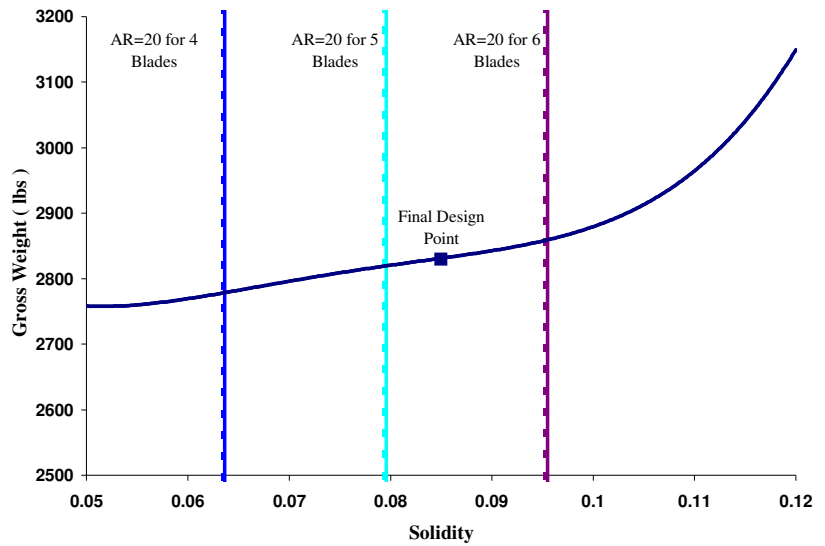


Figure 4-3: Variation of Gross Weight with Solidity

4.5. Automatic Blade Folding Design

The folding actuator was sized to produce the required torque to rotate the blade 144° to the appropriate location and is shown in Figure 4-7. Each blade has a mass of 0.48 slugs and the folding process takes ten seconds, which gives a required torque of 1.095 ft lbs and a shaft rotation of 2.4 rpm. For aerodynamic reasons, the size and weight of the motor should be minimized. There are dozens of motors currently on the market that meet these specifications; these are generally on the scale of one to two inch diameter and weigh less than one pound. However, the motor dimensions only account for a

percentage of the hinge dimensions. Most of the weight is in the hinge in which the motor is encased. Based on empirical data of other vehicles that have employed automatic blade folding, the total weight of the blade folding system is two percent of empty weight, or forty pounds.²⁰ Since blade one is stationary, the folding hinge is replaced with a dummy hinge which is the same size and weight as the other hinges but has no motor and is a completely rigid structure. The folding hinges of blades three and four are tilted ten degrees so that the blades can fold under blades two and five. Blades three and four rotate 144 degrees in ten seconds, blades two and five rotate 72° degrees in five seconds.

4.6. Tail Rotor Design Selection

An anti torque trade study was conducted between a traditional tail rotor, a fenestron, and a NOTAR. The primary selection criterion was acoustic signature. While modulating the tail rotor blade spacing can reduce the main rotor tail rotor interaction, fenestron and NOTAR designs are significantly quieter. The fenestron design also uses varied blade spacing and a higher number of blades. Due to the higher number of blades and enclosing, a fenestron operates at higher frequencies than standard tail rotors. Higher frequency noise attenuates easier in the atmosphere than low frequency.

By not having any exposed rotating blades, it does not interact with the main rotor wake. The exhaust nozzle does add jet noise and sideward directivity but the overall acoustic signature is reduced. The tail boom is less susceptible to ground fire as it does not have a drive shaft running through it. The air going through the boom is low pressure so punctures do little damage to performance. An example of the acoustic advantage of the NOTAR is shown for a MD520N in Figure 4-4²¹. Not having an exposed tail rotor also improves ground safety. This is especially important due to the confined launch platform.

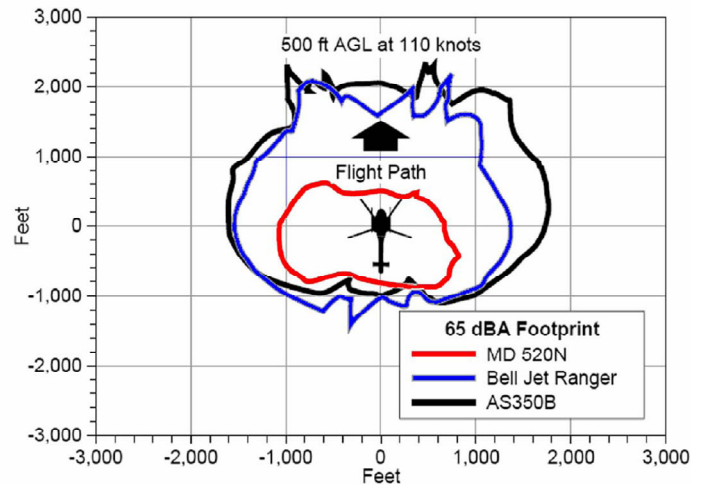


Figure 4-4: 65dBA Contours

4.7. Tail Folding Design

Tail fold is achieved using five motors, a track, and a ring that transmits thrust via a tapered roller bearing as shown in Figure 4-7. The tail fold sequence is a four step process: First, a single motor rotates the aft section of the tail down 110°, so that the vertical and horizontal tails are positioned under the tail boom. Next, a pin is electronically released and two inboard motors draw the tail down ~90°.

After the tail is under the boom, a second set of outboard motors draw the whole tail under the boom along a slider track. The whole process takes less than sixty seconds.

4.8. Landing Gear Selection

Operations on a submarine place a high priority on compact storage size. Many current helicopters that have compact storage requirements have folding main rotor blades and folding tail. These helicopters do not generally have a height restriction beyond what is required for air transportability in a C-17. The RFP has a 9 ft height requirement to be transportable inside a C-130. Operating on a submarine places storage restrictions in all three dimensions. In order to increase the number of aircraft on each level of the capsule, the aircraft is required to be no wider than the 4.5 foot fuselage. In order to reduce the height to allow a third level to the capsule, the landing gear was required to be folded.

Table 4-5: Landing Gear Type Trade Study

Parameter	Weight	Retractable Tricycle Wheeled	Fixed Tricycle Wheeled	Fixed Skid	Retractable Skid	Folding Skid
Capsule Mode Height	0.30	10	4	2	10	10
Internal Space Req.	0.20	4	10	10	2	10
Weight	0.15	3	6	10	5	5
Simplicity	0.05	3	6	10	5	6
Maintenance	0.10	3	5	10	3	7
Crash Worthiness	0.20	8	10	7	5	6
Weighted Totals		6.3	6.9	7.0	5.7	7.95

In Table 4-5, these factors are weighted along with other important parameters such as weight, simplicity of design, and maintenance. A ground maneuverability requirement for capsule design stipulates a caster system for all landing gear configurations, even tricycle systems. Followed closely by fixed skids and fixed tricycle gear, the weighted totals specify **folding skid gear as ultimately fitting the design criteria best.**

Without the height restriction, the fixed skid ostensibly provides the most adequate characteristics, reinforced by the multitude of light rotorcraft with fixed skids. Despite having several ideal characteristics, it fails miserably within the most important, and thus most heavily weighted, parameter: Capsule Mode Height.

4.9. Landing Gear Design

After choosing the landing gear type, many features remained undetermined. Foremost, the joint of the landing gear and subsequent automatic folding procedure had to be established. Three methods of

folding were considered: kneeling camel style, folding in underneath the fuselage, and folding out and up finishing flush with the fuselage. Four main criteria were developed to establish the most ideal system.

Table 4-6: Pugh Matrix of Landing Gear Folding Types

	Kneeling	Folding Out	Folding In
Take-off Stability	-	+	-
Increased height during storage	-	+	+
Increased width during storage	+	-	+
Folding Ease	+	+	-

Take-off stability refers to the decreased width that results in taking-off from a kneeling or folded position. Only the skid that folds out could provide increased stability in this configuration. Since it was a primary concern to fit three aircraft on each capsule deck, the second and third rows take into account the effects of overall width and height of the helicopter when the skid is folded. In the fourth and final row, gravity’s effect on the natural development of folding is measured. In both the kneeling and folding-out gears, gravity naturally works with the descent of the aircraft, as opposed to the folding-in case when the inherent spreading tendency of landing skids will have to be overcome. Overall, the table clearly demonstrates the folding-out skid has the greatest advantage and therefore, was employed.

4.9.1. Gear Configurations

The landing gear has three main configurations during the mission profile as shown in Figure 4-7. Inside the capsule the gear must be folded at all times. During unfolding on the launch deck, the gear will descend via stepper motor to lie parallel to the ground. The CIPHER takes off from this position and during the initial stages of flight the gear is lowered into its final flight and landing position and lock in place with hydraulically actuated pins.

4.9.2. Landing Gear Assembly

Figure 4-7 has a close-up and exploded view of a single gear joint including a parts list. Also shown is the complete landing skid with no fuselage present. The most important components are the upper and lower skids themselves. These will be discussed in particular detail within the crash analysis. The three non-skid components are the pin, damper and motor. The pin, with a 0.75 inch diameter, screws into



Figure 4-5: Sachs ZFG Rotational Damper

the last interlocking member of the lower skid. Thus, it rotates with the lower portion of the skids. The two pictures represent the remaining two parts of the joint, a rotational damper and stepper motor; both of which would be mounted on the upper skid. The ZF Sachs AG rotational damper pictured uses advanced sealing technology that provides a motor-less descent in the transition from the flight to the folded configuration over a three second time period.

The stepper motor only has to raise the lower skid and does not have to carry the weight of the aircraft at anytime. This allows the stepper motor, represented here by the NEMA 34, to be smaller in size and weight. A stepper motor is the ideal choice in this design because of its ability to keep an accurate angular position. This is important, primarily, to ensure the landing gear locks in the desired position and does not endanger the crew, and alternatively, to ensure no fuselage damage is incurred during automatic folding. The locking mechanism in the upper gear has eight hydraulically actuated pins that lock the lower gear into position during the flight and landing. Four pins are inserted from each side of the two surrounding interlocking faces.



Figure 4-6: NEMA 34 Stepper Motor

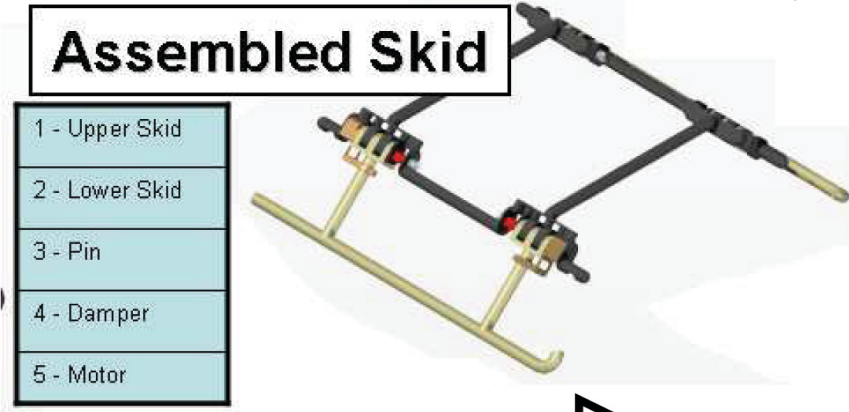
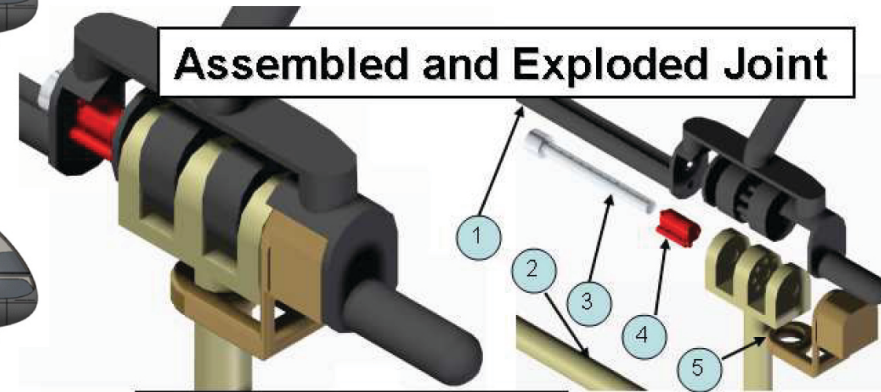
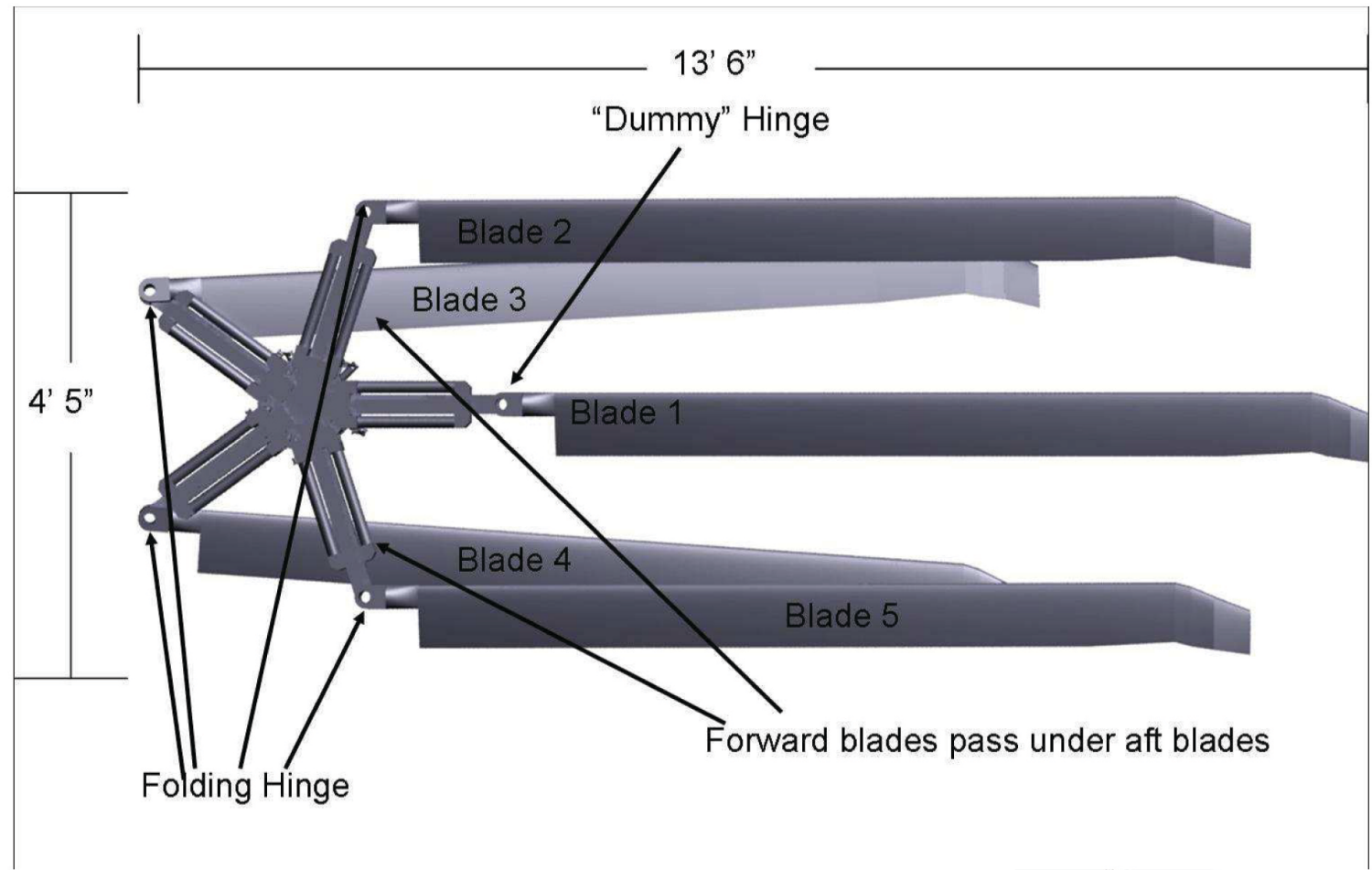
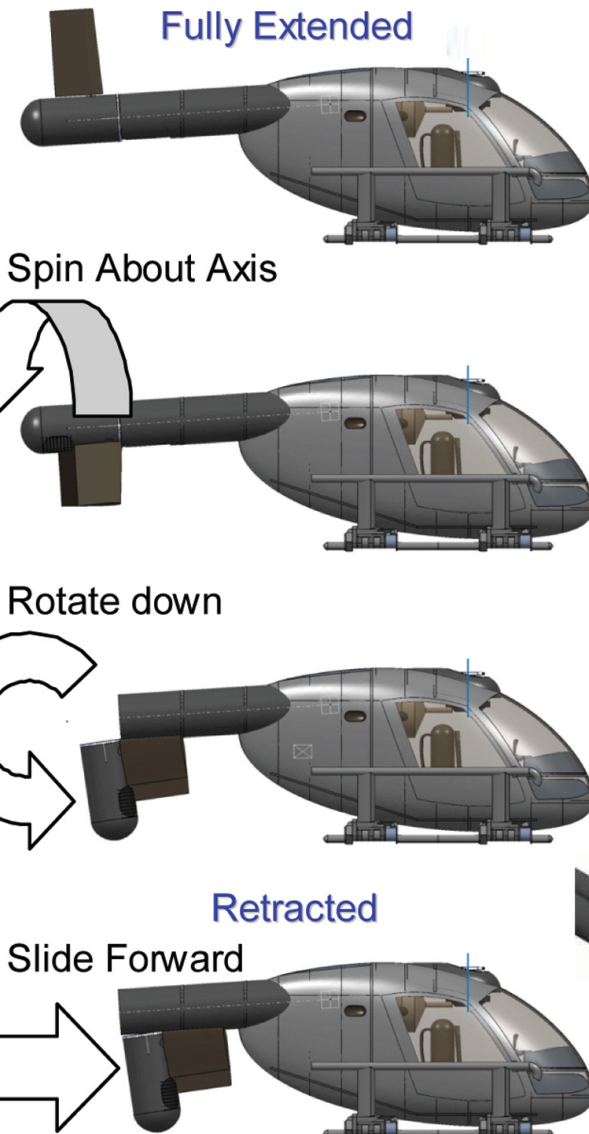
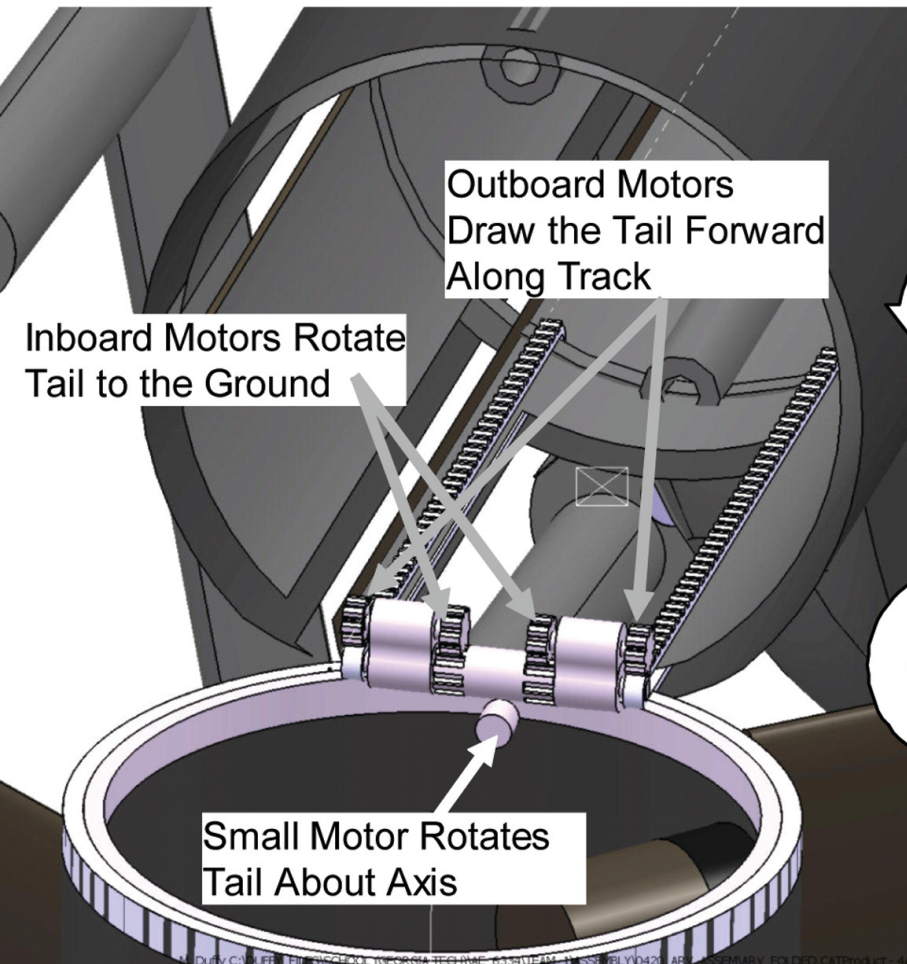
4.10. Launch Preparations

Cipher is ready to launch from the deck of the Barracuda after nine minutes on the launch deck as shown in Table 4-7. The process is repeated on landing.

Table 4-7: Cipher Startup Time

Event	Total Time Elapsed
Cipher reaches launch deck	0 min
Rotor Blades unfold, landing gear folds down, tail boom unfolds	1 min
Crew and payload loaded	2 min
Preflight Startup Sequence and Engine Startup	4 min
Engine Reaches Idle	5 min
Takeoff	9 min

Figure 4-7: Cipher Folding Systems



Capsule Deck

5. UEV Configuration Development

5.1. Dragonfly Design Evolution

The dual rotor side-by-side boxwing tail sitter evolved during the design iteration as shown below in Figure 5-1. The main elements of the design progression were determining the rotor diameter, wing size, engine type, and horizontal tail size.

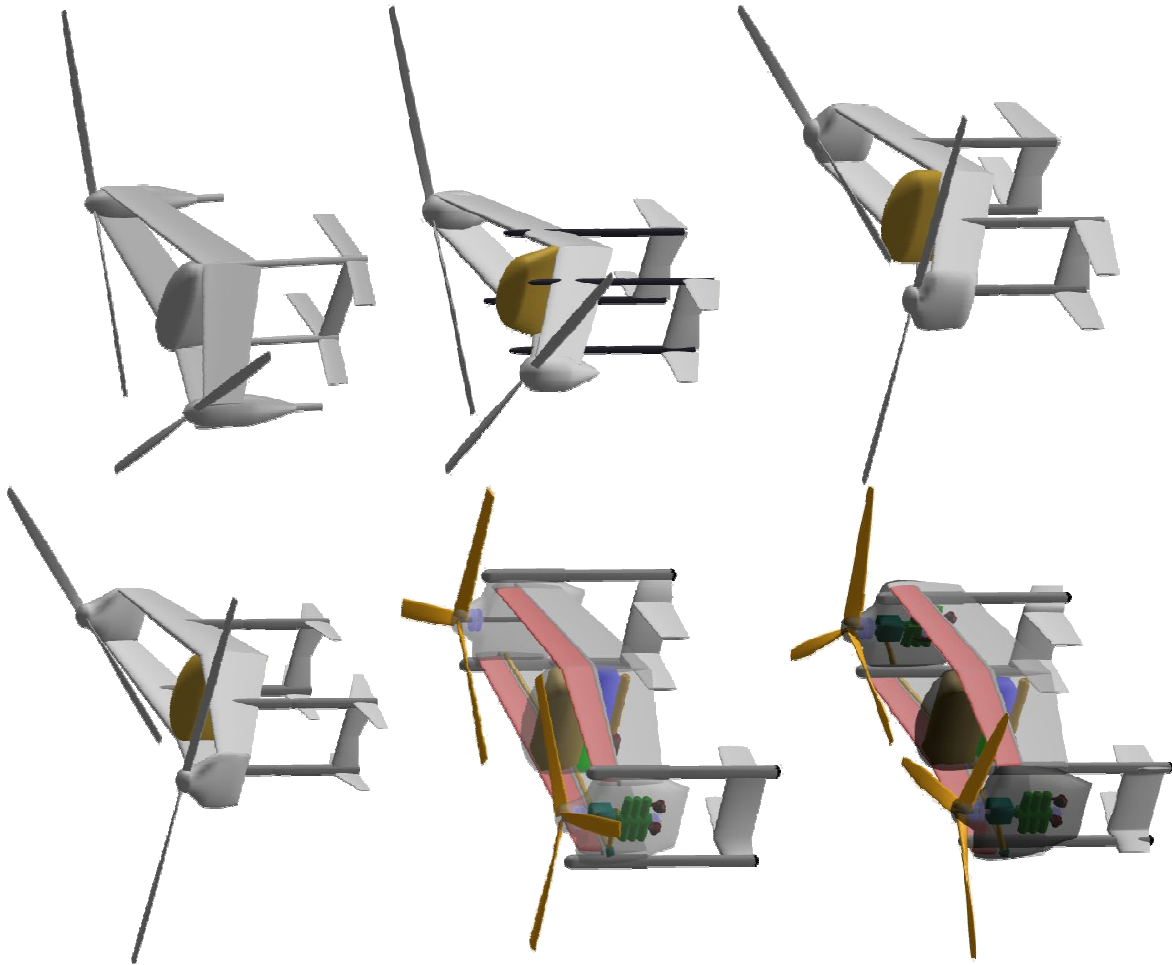


Figure 5-1: Dragonfly Development Progression

The fuselage contains a payload bay of 4.5ft x 2.2ft x 1.5ft with a volume of 15ft³ directly centered on the center of gravity. Eliminating the CG excursion was critical to maintain sufficient control power at any payload condition. The payload volume was sized based upon a payload density of 40 lbs/ft³, which is a lower density value based upon comparison with other UAVs currently in production. Fuel is located in four wing tanks located in the D-tube in front of the main spar, providing sufficient fuel volume for 620 lbs, while the design mission requires 579 lbs. The fuel tanks are centered at the vehicle CG location, again to minimize CG excursion to assist with control power. All four fuel tanks are interconnected and pressurized to maintain balanced fuel states in each tank during the mission.

5.2. Dragonfly Engine Selection

Engine type and placement was a major design decision for the dual rotor side-by-side tailsitter configuration. This trade study also compared a single fuselage mounted engine versus twin engines in outboard nacelles. Another key element of this comparison was the need for the turbine engine to incorporate two speeds in the gearbox to accommodate the reduced tip speeds in forward flight. The UEV has very different propulsion needs than the ARV. The RFP specified a three hour loiter over the objective at the maximum endurance speed, while having to provide coverage for a full six hour period. Instead of swapping out at the mid-mission point, a UEV capable of the full six hour endurance would be preferable. The engine selection is driven by specific fuel consumption in loiter at less than 50% power. While the RFP turboshaft has low weight and SFC's at high power settings, the partial power SFC becomes very high in comparison to reciprocating engines. This is especially true in comparison to diesel engines which are able to operate very efficiently at low partial power due to their higher overall pressure ratio and ability to operate below stoichiometric fuel to air ratios.

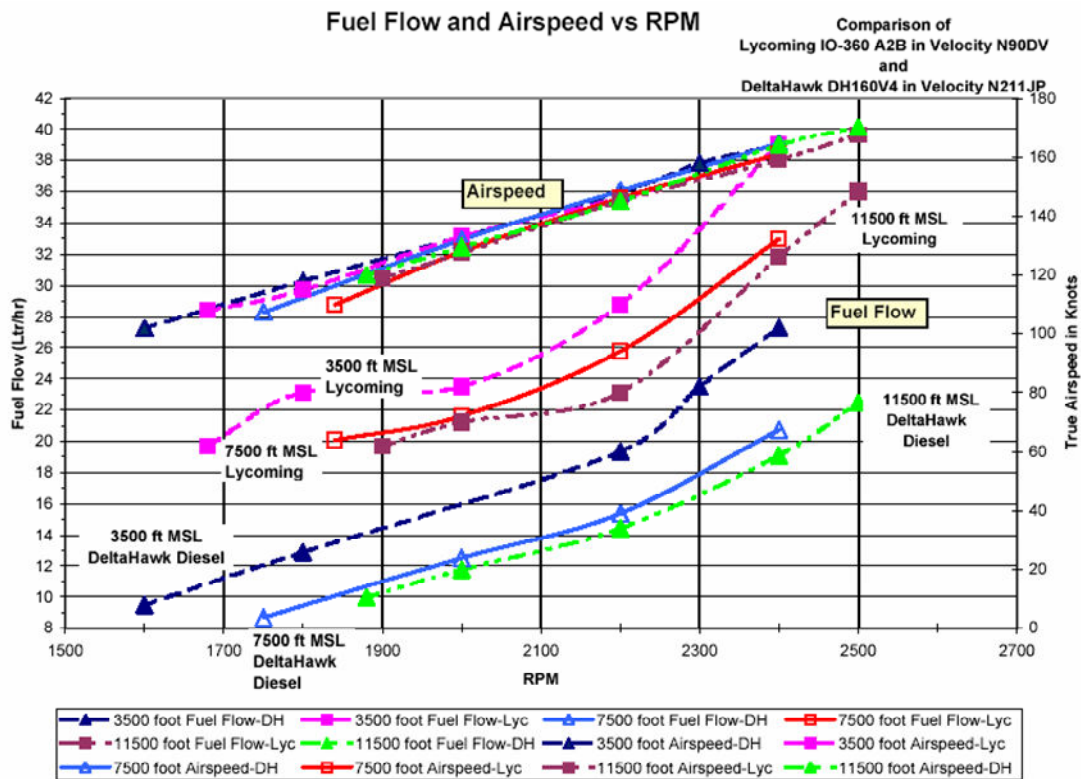


Figure 5-2: Turbo-Diesel Fuel Flow Comparison to Conventional Spark-Ignition Engines²²

There are a number of new small aircraft turbo-diesel engines in the 100 to 400 hp range including flight tested engines developed by Thielert, SMA, Teledyne-Continental, and DeltaHawk. A representative turbo-diesel fuel flow is shown in comparison to a spark-ignition aircraft engine in Figure 5-2 during

flight testing. These aircraft diesels demonstrate over a 30% decrease in fuel consumption, while achieving specific weights of approximately 2.5 lbs/hp.

An advanced two-stroke turbo-diesel funded by NASA, DARPA, and the Dept. of Commerce has completed development which offers improved specific weight over other aircraft diesels. The GSE turbo-diesel has demonstrated an improved specific weight of 1.19 lbs/hp. The key technology differences that the GSE engine offers are a unique pre-chamber cylinder head design that incorporates Self Injection Engine Technology (SIETEC) and a variable compression ratio valve. The GSE engine offers low specific fuel consumption, greater specific output, improved reliability, reduced maintenance, omnivorous heavy fuel capability, improved high altitude and cold starting, and potentially lower cost than other aircraft diesels.

The comparison of the RFP turboshaft engine and the GSE turbo-diesel SFC is shown in Figure 5-3 at the 200 hp size, demonstrating the significant improvement in partial power fuel consumption which is critical to the UEV loitering mission.

5.2.1. Dragonfly Engine Placement

Several engine installations were investigated for the UEV since the two rotor configuration permits either single or dual-engine arrangements. A two-speed gearbox is essential when used in combination with a turboshaft engine because of the need to keep turbine rpm above a lower limit at partial power. The turbo-diesel is able to avoid requiring a two-speed gearbox, but at the price of having less power available at the lower tipspeeds. However, since the UEV does not have a dash or high-speed requirement, this is not an issue for the cruise or loiter conditions. A comparison of resulting engine plus fuel weight of the possible integrations is shown in Table 5-1, indicating that two turbo-diesels offered the lightest vehicle mission weight, even though the engine weight is significantly higher than the turboshaft. The single engine arrangements require a full-time (full power) cross-shaft from the fuselage engine to the rotor pylons. Since the UEV is unmanned and the blades do not intermesh, a cross-shaft was not considered essential to the mission, with rotor power balancing performed electronically across the two engines.

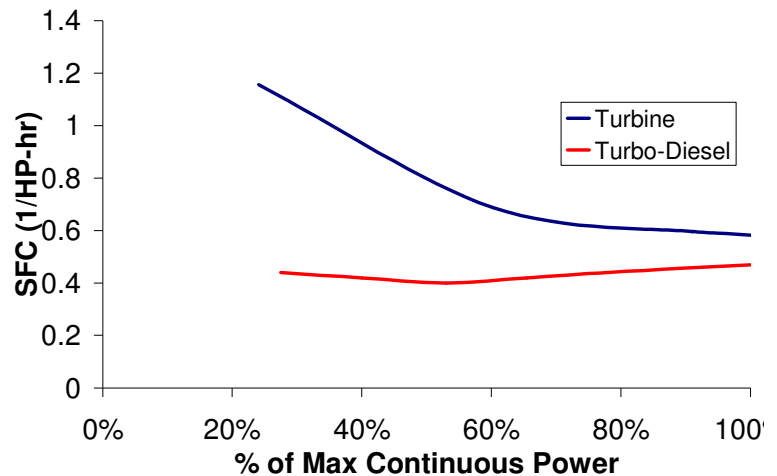


Figure 5-3: Comparison of Turboshaft and GSE Turbo-Diesel SFC at a 200 HPW Size

Table 5-1: Comparison of Turboshaft and Turbo-Diesel Installations

	(1) GSE Diesel	(2) GSE Diesel	(1) RFP Engine	(2) RFP Engine
Engine (lbs)	451	451	119	153
Prop Subsystems (lbs)	0	0	33	38
Gearbox (lbs)	70	70	116	116
Crossshaft (lbs)	114	0	112	0
Fuel Weight (lbs)	521	501	728	834
Engine + Fuel (lbs)	1156	1022	1108	1141

The turbo-diesel gearbox design will utilize a gearbox reduction ratio of 4.6 cutting engine rpm transferred to the rotors from 4000 to 863. An optimization of the hover, cruise, and loiter tipspeeds was conducted, with power matching of the engine rpm at those conditions.

5.3. Dragonfly Aerodynamic Design

5.3.1. Dragonfly Airfoil Selection

The airfoil utilized for the UEV is a newly developed section for General Aviation aircraft developed by Andrew Hahn at NASA Langley. The ASH-17 is a 17% thickness to chord ratio airfoil that is designed for a high C_{Lmax} with low pitching moment. Figure 5-6 shows a comparison of the ASH-17 airfoil with the NLF-0215, as well as several other popular low speed airfoils. Scaled data was developed in Drela's MSES code with constant span and chords scaled proportionally to the C_{Lmax} of each specific airfoil. The C_{Lmax} of the ASH-17 is 2.15, which is also slightly inferior to the NLF-0215 with ten degrees of flap but the ASH-17 provides an improved L/D at maximum endurance

5.3.2. Dragonfly Wing Type Selection

The length requirement on Barracuda is 15.5 feet. This places a severe span limitation that eliminates a conventional wing from consideration. A traditional biplane design was considered but wing mounted engines give rise to aero-elastic concerns from wingtip mounted propellers.^{13,14,15,16}

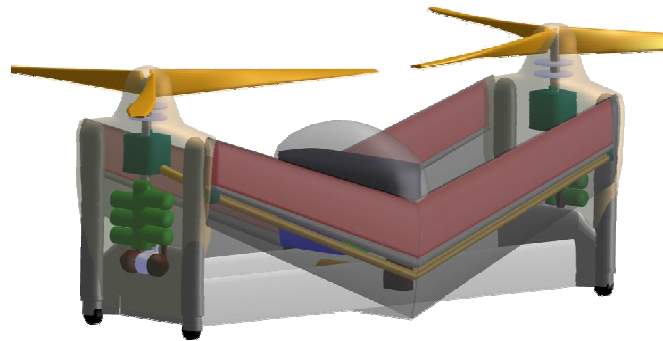


Figure 5-4: Optional Cross-shaft for Engine-Out Flight Capability

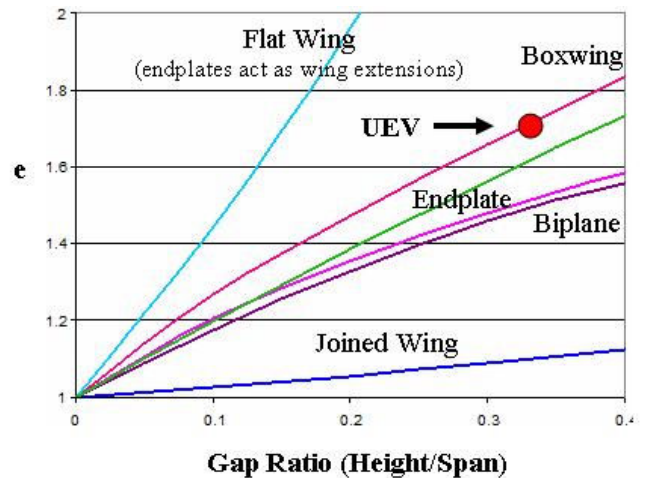


Figure 5-5: Oswald Efficiency Factor for Various Wing Types

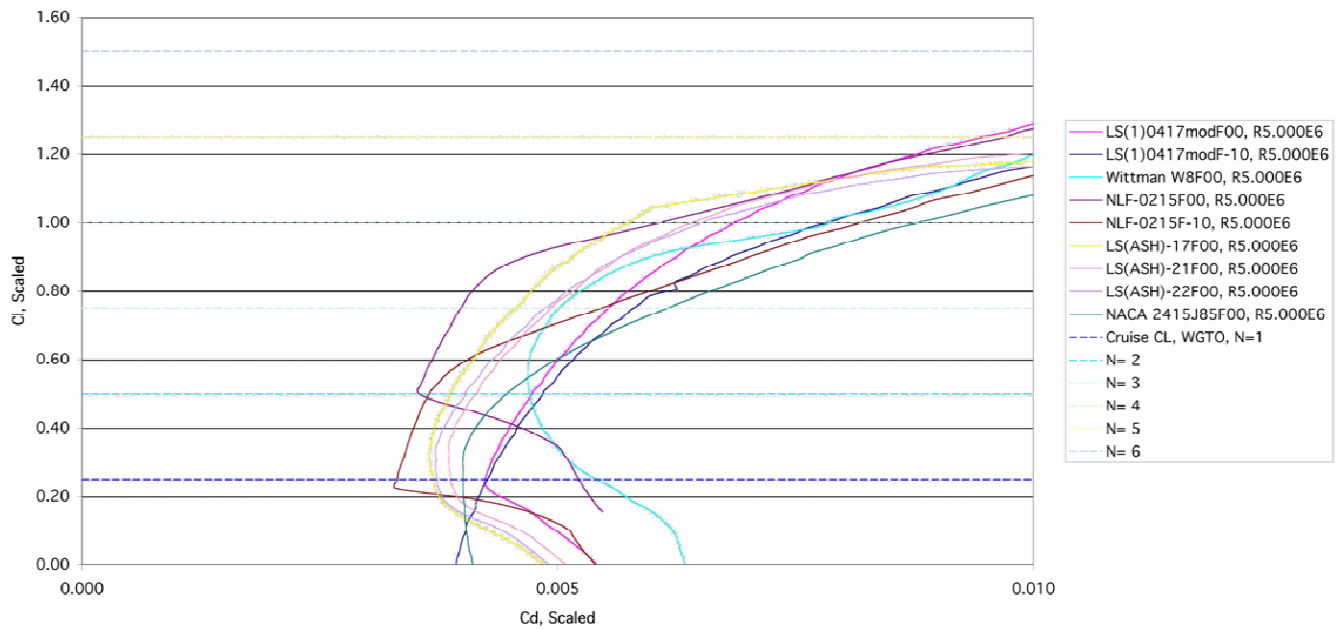


Figure 5-6: NASA ASH-17 Airfoil Drag Polar Compared to Popular Low Speed Airfoils at a Typical Cruise Reynolds Number of Five Million

5.3.3. Dragonfly Induced Drag Estimation

An empirical induced drag method¹⁷ was first utilized in initial sizing of the boxwing, which demonstrated the importance of maximizing the gap ratio (height between the wings divided by the wing span). The gap ratio was maximized based upon the available capsule elevator footprint, with the empirical method yielding an Oswald efficiency factor of approximately 1.7. The effective span multiplier correlates to the square root of the efficiency factor, providing an effective span of 20.9 feet for the 15.5 foot Dragonfly. Empirical estimations were also compared to the use of a bi-plane, endplate and joined wing system.

A vortex lattice code was next utilized to confirm the empirical estimation and optimize the downwash through the twist and camber distribution for the non-planar wing system. A gradient method optimization scheme was added to the NASA Vorview/Vorlax analysis to adjust the twist and camber at each spanwise element across the 3-D lift system. The resulting optimum lift loading distribution is shown in Figure 5-7, with the loading plotted in a mirror fashion for the upper and lower wings. The vortex lattice analysis results confirmed the empirical results, with a 1.67

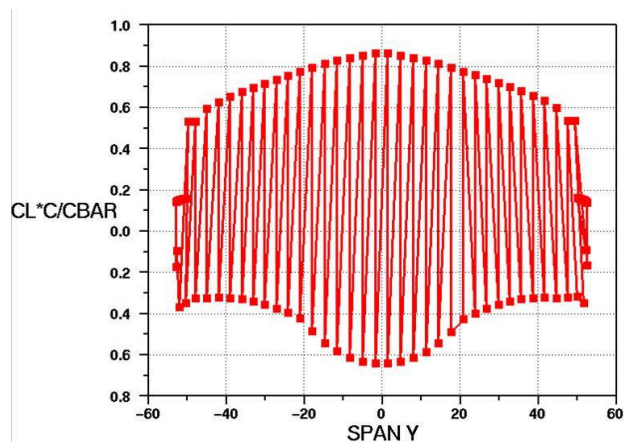


Figure 5-7: Optimized Vortex Lattice Load Distribution

efficiency factor at the design C_L of a 1.25 as compared to the 1.7 initially used. Another significant factor influencing the induced drag is the interaction of the rotor with the wingtip vortex that is shed by the boxwing at the endplate mid-point where the rotor hub is located.

5.3.4. Aero-Propulsive Interaction

One of the most difficult characteristics to analyze was the aero-propulsive interaction of the wingtip vortex and wingtip prop/rotors. Wind tunnel tests demonstrated induced drag reductions of 20 to 30% at typical cruise C_L 's and typical aspect ratios of approximately six to eight as shown in Table 5-2²³.

Table 5-2: Induced Drag Reduction from Wingtip Mounted Propellers

	C_{Di} Props Off	C_{Di} Props On	% Improvement
Optimum	0.02003	0.01310	52.9%
Elliptical	0.0191	0.01383	38.1%
Trapezoidal	0.02240	0.01528	46.6%
Triangular	0.02685	0.02425	10.7%

An empirical method was developed that simplified the propulsive efficiency improvement to a function of only the normalized C_L . The normalized C_L is merely the C_L at the operating condition divided by the 3-D C_{Lmax} of the configuration. At the maximum loiter condition, the benefit of the wingtip vortex/rotor interaction is approximately 1.25, or resulting in a 25% reduction in induced drag. This benefit decreases to less than 10% at the best range speed conditions.

5.3.5. Dragonfly Tail Design

Wing and tail sizing were determined through the transition analysis, which is described in detail in the controls section. Due to capsule space requirements, the Dragonfly height is limited to 7 ft. In order to maximize the tail moment arm, the tails are mounted to extending landing gear struts. A total translation of 4.5 ft is achieved through pneumatic pressurization of the landing struts after take-off, which provides a moment arm of 7.5 ft from the tail aerodynamic center to the center of gravity. An articulating horizontal tail is required in order to orient the tail surfaces appropriately during low speed forward flight so that a transition moment may be achieved at the minimum conversion speed of approximately 80 kts. The tail surfaces are arranged as a box-tail structure to maximize the aspect ratio and aerodynamic effectiveness while providing a stiff structure during the 70° transition maneuver to minimize aero-elastic flexure. Sufficient control power is achieved through the combination of rotor cyclic and tail surfaces. The wing is sized to be 80ft² to provide sufficient lift at the minimum transition

speed with a stall C_L of 2.1, while providing an efficient loiter C_L of 1.25 and a V_{br} C_L of 0.56. The wing is equipped with 40% chord full-span ailerons separated into three sections.

5.4. Dragonfly Rotor Design

Engine size is driven by the high hot hover requirement. Large diameter rotors have lower hover power requirements resulting in a lower weight engine. Increasing the diameter requires intermeshing but this causes BVI which can significantly increase the acoustic signature. In addition, the sensor package would be required to always go through the rotors. A one foot gap at the fuselage midpoint resulted in a finalized rotor diameter of 13.5 feet.

5.4.1. Dragonfly Rotor Blade Design

The RF software used for Cipher was used to model Dragonfly. Combined blade element momentum analysis was used to optimize the twist and taper distribution. The code was modified to allow for a nonlinear twist distribution. Nonlinear twist is essential to account for the drastically different inflow conditions between hover and forward flight. The best balance between hover, endurance, and cruise was determined to consist of a taper ratio of 0.5 from 80% radial location to the tip. This impact of the non-linear twist and taper is shown in Figure 5-8. With a linear twist distribution the inner 50% of the blade produces negative lift and results in a significant increase in power required for forward flight. Dragonfly has an inboard linear twist of -55 degrees changing to -16 degrees at the 70% location, and use of an inboard VR-7 airfoil changing to the VR-8 airfoil at the 70% location.

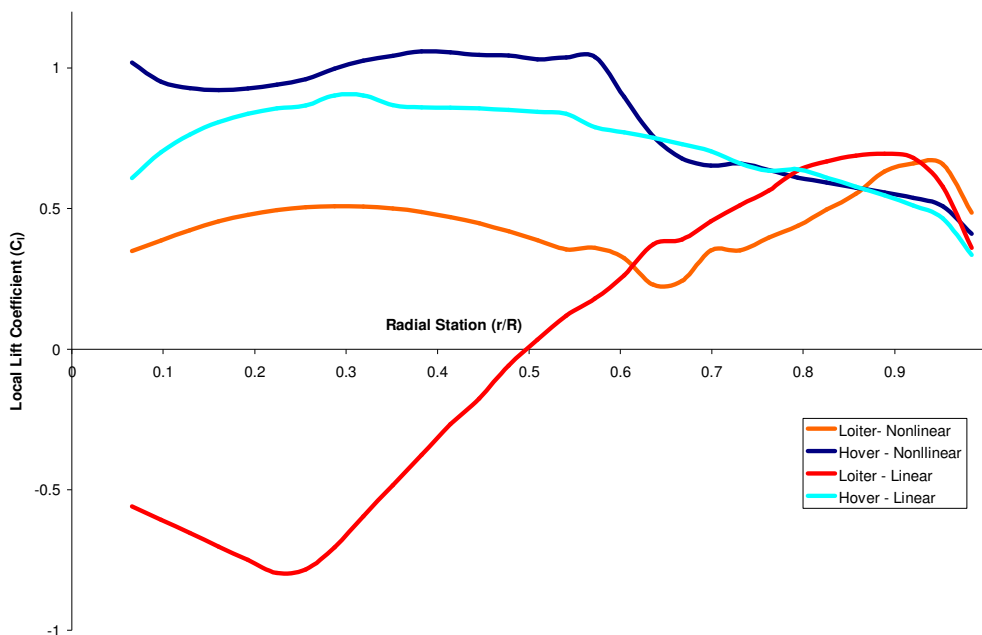


Figure 5-8: Non-Linear and Linear Twist Comparison at the Hover and Loiter Flight Conditions

5.4.2. Dragonfly Tip Speed Selection

Slowing the rotor is problematic for conventional helicopters due to rotor flapping and instability since the rotor plane is operating edgewise into the forward flight velocity. However, slowing the rotor for tilt rotors or the tailsitter UEV does not share this problem since the rotor is operating as a propeller with the rotor plane symmetrically facing the velocity flow field. Therefore, the rotors tip speed on the UEV can be drastically reduced to achieve improved forward flight performance. Wind tunnel data from V-173 demonstrated stability without flapping for similarly sized rotors down to 166 ft/sec²⁴. Dragonfly's endurance tip speed was limited to 200 ft/sec since variable engine gearing was not utilized, and power available was reduced as the engine rpm was decreased to accommodate the lower tip speeds. This low loiter tip speed also dramatically reduces the acoustic signature. A lower tip speed could have been utilized aerodynamically, but the power available at the low tip speeds would have been further reduced due to operating at a lower engine rpm. A variable gearbox would provide significant advantage to the UEV for forward flight performance, especially the ability to achieve a dash at maximum speed, however the increased cost, complexity, and maintenance of a variable gearbox was not warranted. Figure 5-9 shows the significant reduction in power required that is achieved through the use of different tip speeds for loiter and endurance.

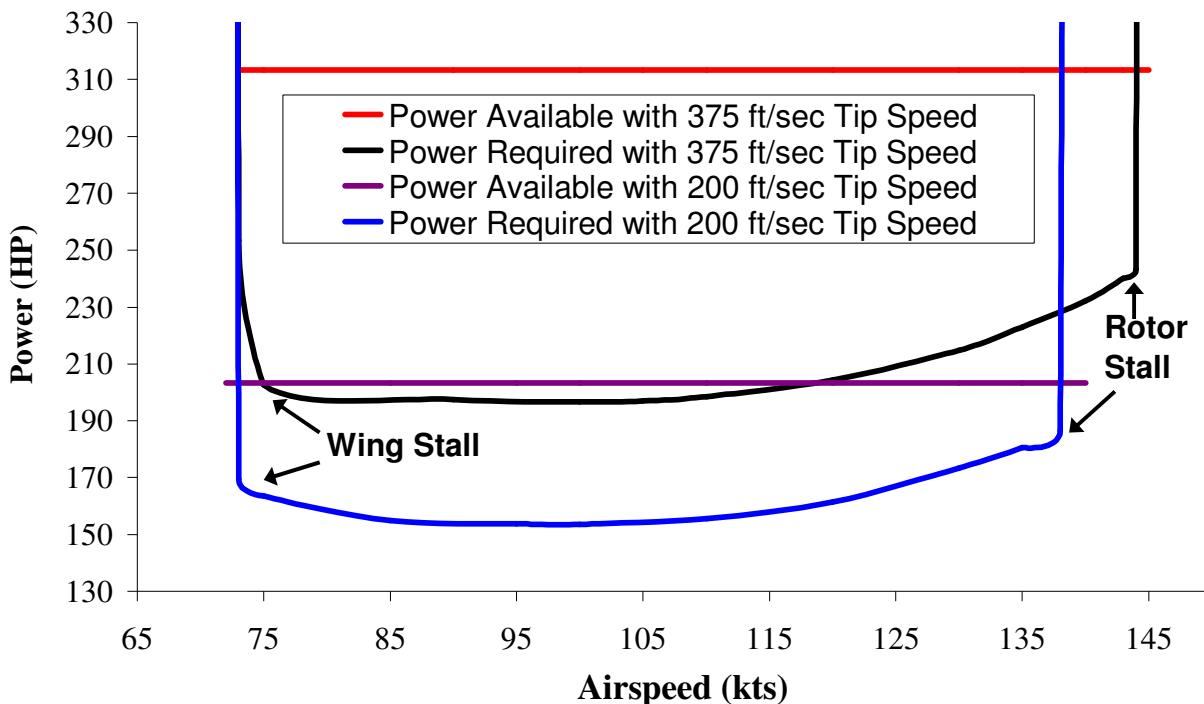


Figure 5-9: Dragonfly Power Required at Cruise and Loiter Tip Speeds

6. Performance

6.1. Cipher Flat Plate Drag Breakdown

The drag was developed using an empirical handbook aircraft build up method. Each component was compared against known data, and the reference area associated with the known shape C_D from Horner²⁵ was used to calculate the equivalent flat plate drag area.

The fuselage was compared to a body of revolution with a l/d ratio of 2.5 at the cruise Reynolds number. The tail boom, vertical and horizontal tails were calculated using flat plate skin friction drag. However, since the tail boom has some pressure drag from the aft close off, the additional pressure drag was calculated using a rounded nose cylinder to approximate the fuselage ahead of the boom.

Landing gear drag was comparable to tube sections in free stream air, and boxes for the

fold mechanism. The hub drag was approximated by a large flat cylinder with a d/h of 1.5. Cooling and momentum, interference, and excrescences drag were approximated by adding 5% to the total drag of the aircraft.. The total flat plat drag of $7.15ft^2$ is relatively high for an aircraft of this gross weight, but it is due to the high drag of the folding landing gear and large five bladed hub which are both necessary.

6.2. Dragonfly Flat Plate Drag Breakdown

The flat plate drag was calculated using the component wetted areas, lengths, thickness to chord ratios, and thickness induced acceleration and separation terms. Component Reynolds numbers were used to determine the laminar and turbulent coefficient of friction, with laminar flow only present on the top and bottom wing leading edge up to the quarter chord. Table 6-2 shows the complete breakdown and comparison to the Glasair III, which is a 2400 lb General Aviation aircraft with a 25ft span and 80ft² wing area^{26,27}.

Table 6-1: Cipher Drag Buildup

Equivalent Flat Plate Drag	Total sq.ft.
Fuselage	2.49
Tail boom	0.35
Rotor Pylon and Transmission Fairing	0.05
Horizontal Tail	0.02
Vertical Tail	0.02
Landing Gear Folded (overall)	0.15
Perpendicular Members to Airflow	0.89
Box Members	0.65
Main Rotor Hub and Mast	-
Hub	1.10
Mast	0.49
Cooling and Momentum	0.31
Interference Drag	0.31
Excrescences (Antennas, Steps, Gaps)	0.31
	7.15

Table 6-2: Dragonfly Drag Buildup

	Dragonfly	% of Total Drag	Glasair III	% of Total Drag
Wing	0.569	25.6	0.623	36.7
Fuselage	0.327	14.7	0.501	29.5
Engine Pylon	0.529	23.8	-	-
Landing Gear	0.115	5.2	-	-
Horizontal Tail	0.175	7.9	0.157	9.2
Vertical Tail	0.191	8.6	0.101	5.9
Misc	0.318	14.3	0.318	18.7
Total	2.2		1.7	

6.3. Cipher and Dragonfly Mission Breakdown

The mission summary for the sizing mission for Cipher and Dragonfly are shown in Table 6-3 and Table 6-4.

Table 6-3: Cipher Mission Summary

Phase	Time (min)	Velocity (kts)	Power (HP)	SFC (1/hphr)	Fuel Required (lbs)
Idle	4	-	81	0.857	4.64
Hover	2	0	297	0.444	4.41
Cruise	67.47	124	282	0.453	144.40
Hover	4	0	275	0.455	8.35
Cruise	67.74	124	276	0.456	142.40
Hover	2	0	264	0.461	3.96
Reserve	20	61	147	0.614	30.13
Total (Including Reserve)	167	-	-	-	338.29

Table 6-4: Dragonfly Mission Summary

Phase	Time (min)	Velocity (kts)	Power (HP)	SFC (1/hphr)	Fuel Required (lbs)	L/D
Idle	4	-	60	0.810	3.24	-
Hover	2	0	343	0.436	4.98	-
Cruise	64	142	246	0.420	101.97	8.14
Loiter	360	82	108	0.421	276.91	5.80
Cruise	61	137	216	0.420	92.76	8.11
Hover	2	0	278	0.467	4.18	-
Reserve	20	76	85	0.421	11.88	6.78
Total (including Reserve)	488	-	-	-	495.92	

6.4. Cipher Autorotative Performance

The Height-Velocity diagram was calculated based on the procedure in NASA TN D-4536²⁸ and shown in Figure 6-1. The autorotative rate of decent is also shown compared to the Schweizer 333. While Cipher has a low tip speed and low inertia rotor, the rate of decent is comparable to the Schweizer.

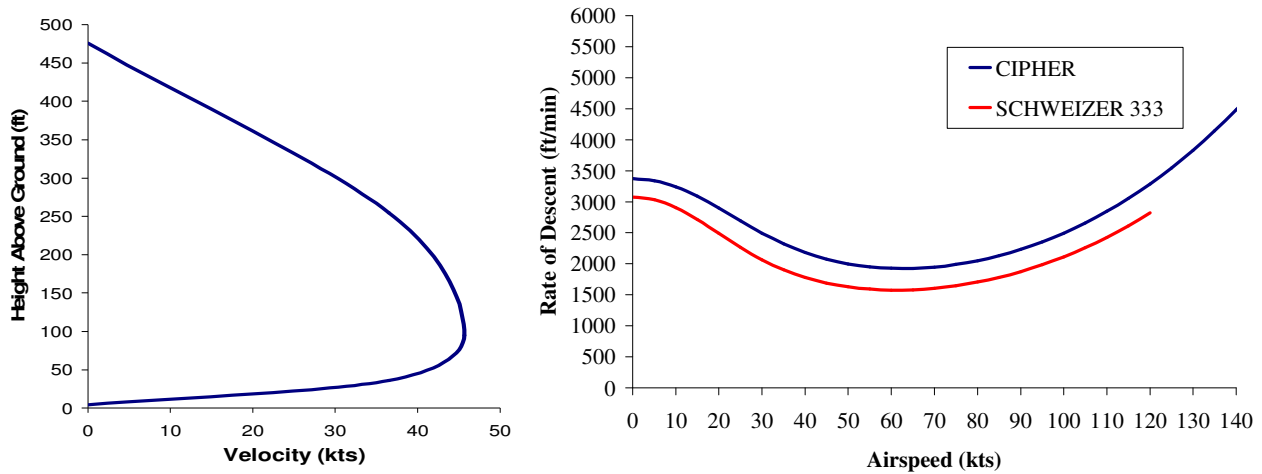


Figure 6-1: HV Diagram and Autorotative Rate of Decent

6.5. CIPHER Performance

The power required verses airspeed is shown in Figure 6-3. The maximum horsepower available is limited by the transmission limit of 329 hp. The maximum airspeed is 129 kts at sea level and increases to 140 kts at 7500 ft. The endurance speed is 62 kts at sea level. The retreating blade compressibility and retreating blade stall limits the maximum speed and altitude using simplified methods.¹²

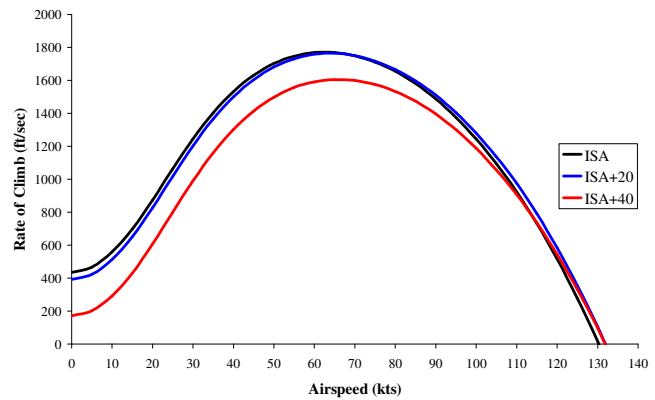


Figure 6-2: Cipher Rate of Climb

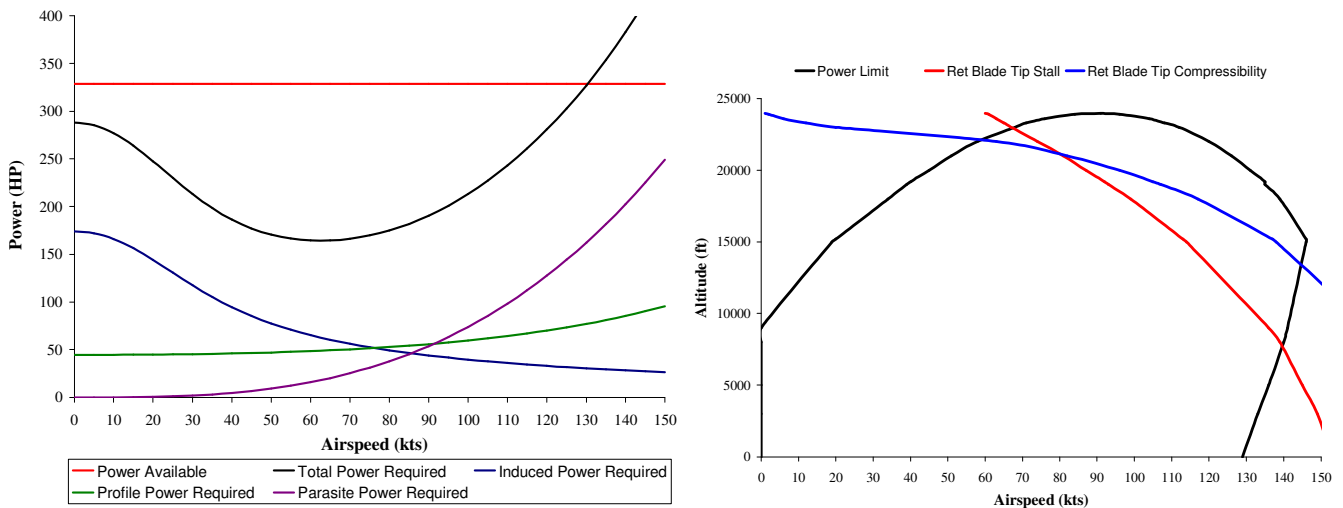


Figure 6-3: Cipher Power vs. Airspeed and Power vs. Altitude (ISA and Max Gross Weight)

6.6. Dragonfly Performance

Dragonfly performance is shown in fixed wing mode in Figure 6-4. The low speed is limited by wing stall while the maximum speed at sea level is limited by rotor stall. As tip speed is increased, the power requirements and maximum altitude increase.

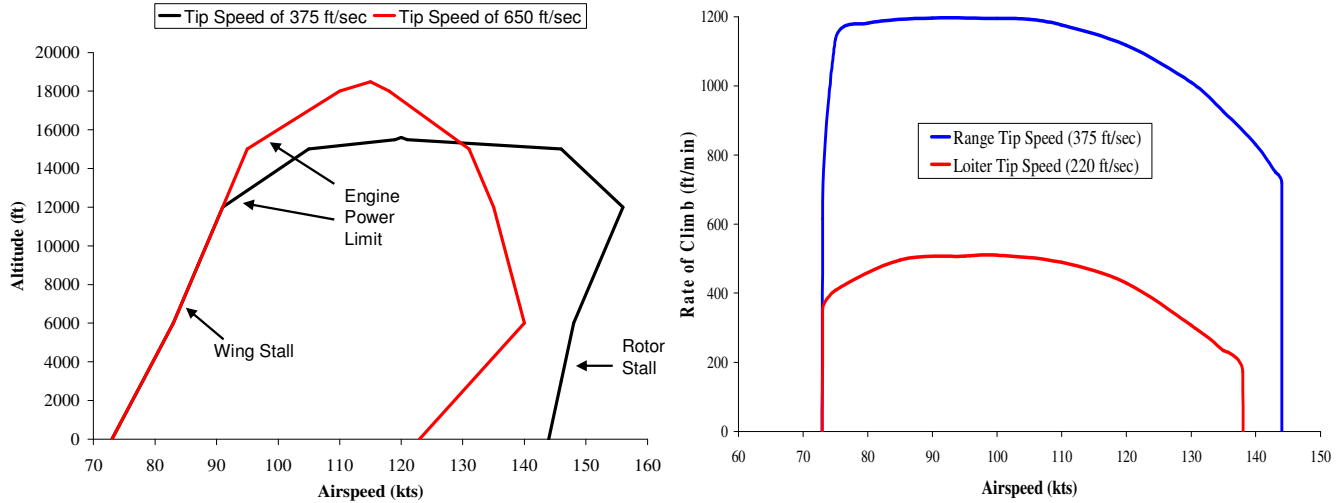


Figure 6-4: Dragonfly Forward Flight Performance

6.7. CIPHER and Dragonfly Hover Performance

The engines for CIPHER and Dragonfly were sized for 6000ft/95F hover. This resulted in HOGE ceilings as shown in Figure 6-5 with the weights going from empty to maximum weight.

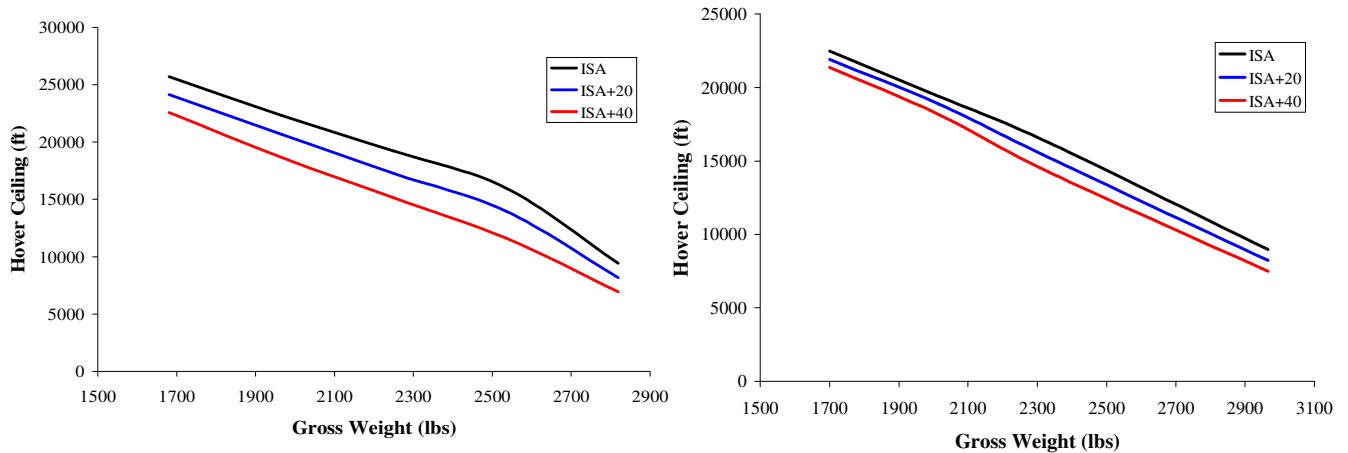


Figure 6-5: CIPHER (left) and Dragonfly (right) HOGE Performance

6.8. CIPHER and Dragonfly Empty Weight Breakdown

The empty weight calculations were primarily based upon Prouty¹⁰ equations which were recalibrated utilizing detailed weight breakdowns of the OH-6A¹³ and Robinson R-44²⁹. Equivalent technology factors were utilized on both the Cipher and Dragonfly to account for improvements over these production aircraft since they were originally manufactured thirty to forty years ago. The technology factors accounted for approximately a 20% improvement in weights across most components. The additional weight required due to folding was calculated on top of these weights. The weight of the rotor hub and rotor blades were taken from the final optimized structural design. Ballistic Protection (BAPS) was added to the front of the aircraft to provide protection for the SOF soldiers and flight computers. The wing weight was calculated based on a NASA equation developed for strut braced and boxwings, and the fuselage and landing gear weights were built-up based on wetted areas, structural thickness and loading³⁰. The turbo-diesel engine weight was supplied from the manufacturer based upon the current flight weight articles that are undergoing flight testing by NASA³¹. The turbo diesel engine weight includes all liquids and accessories, including cooling, starter, and turbocharger.

Table 6-5: Cipher and Dragonfly Weight Breakdown

Component	Cipher Weight (lbs)	Dragonfly Weight (lbs)
Main Rotor Blades	56	64
Main Rotor Hub and Hinge	107	78
Vertical Fin	2	9
Horizontal Stabilizer	7	46
Tail Rotor	20	n/a
Additional weight due to NOTAR	148	n/a
Tail Folding Motor	10	n/a
Body (fuselage)	220	70
Landing Gear	64	58
Nacelles	11	58
Engine Installation	115	592
Propulsion Subsystems	25	0
Drive System	99	80
Cockpit Controls	13	n/a
Systems Controls Boosted	16	17
Instruments	11	12
Hydraulics	18	18
Electrical	179	166
Avionics	300	300
Air Conditioning and Anti-Ice	18	19
Wing	n/a	111
Passenger Seats (2)	50	n/a
Ballistic Protection	100	n/a
Crashworthy Fuel System	9	13
Payload (Including Soldiers)	800	600
Empty Weight Contingency (5% of Empty Weight)	84	86
Empty Weight	1680	1711
Fuel Weight	338	570
Gross Weight	2818	2966

6.9. Cipher Center of Gravity Travel

The extremes of center of gravity travel are shown in Figure 6-6. The CG stays within two inches of the mast for all loading conditions. The most extreme loading condition is a full fuel but no soldiers or equipment on board. This is not required of any current aircraft and increased the emphasis on requiring that the soldiers and their equipment be very close to the mast.

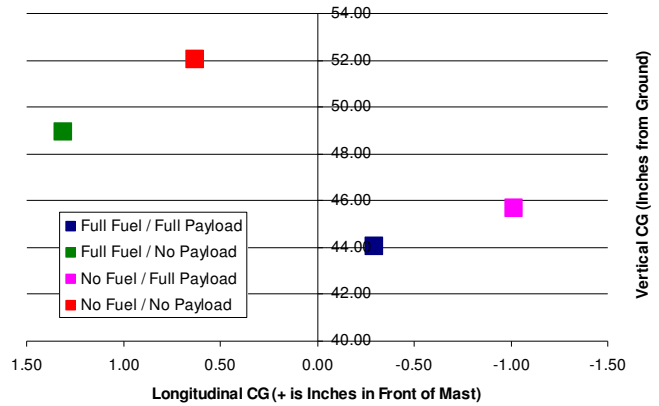


Figure 6-6: Center of Gravity Travel

6.10. Overall System Reliability

Stochastic Petri Nets (SPN) were used to analyze the reliability of the six hour deployment mission using @SPN, a software developed by Dr. Vitali Volovoi^{32,33}. Petri Nets are graphical tool for modeling complex time dependent systems. Each token represents a vehicle, either a Barracuda or a Cipher. Each state is represented by a circle with transitions to other states through gates.

For the Barracuda, three different types of errors were analyzed and are summarized in Table 6-6 with the Petri net shown in Figure 6-7. Failures in the control system and the mechanical systems are repairable with two and one hour mean time to repair respectively.

Table 6-6: Barracuda Failure Sources

Failure Type	Failure Sources
Pressurization	Failure of watertight seals
Control	Failure of ballast tank, thrusters
Mechanical Systems	Failure of elevator, hatch

The errors for Cipher are summarized in Table 6-7 with the Petri Net shown in Figure 6-8. For the Cipher, the aircraft could have an error during start up, a mechanical error in flight, a flight computer failure, enemy fire, and landing errors. The probability of a failure due to mechanical and enemy fire was assumed to be the same as the sum of all US Military helicopters from 2003-2006 in Iraq³⁴. While all the combat record in Iraq of all US Military helicopters is not that representative of the missions that Cipher will be used for, it is the most representative number available. The remaining probabilities were used from a variety of sources^{35,36,37,38}.

Table 6-7: Cipher Failure Sources

Failure Type	Failure Sources
Startup	Warning light, folding
Mechanical	Engine failure, hydraulics, transmission, electrical generator
Flight Computer	Software, hardware
Enemy Fire	Direct fire
Landing	Rollover, obstruction, landing gear failure

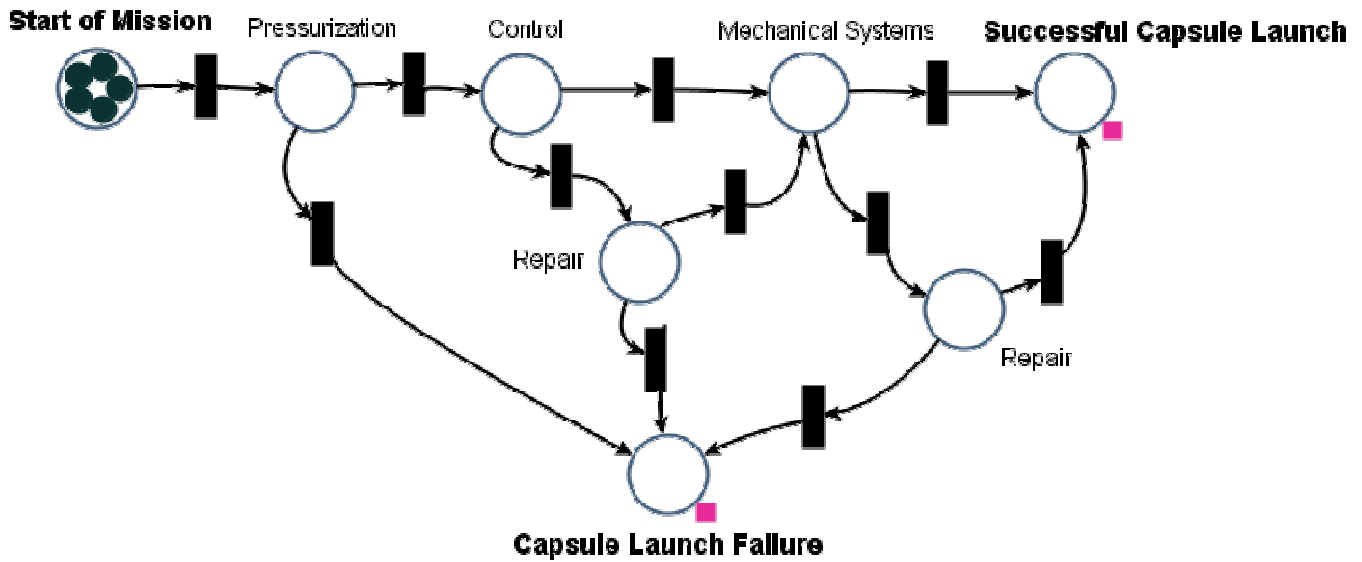


Figure 6-7: Petri Net for a Barracuda Capsule

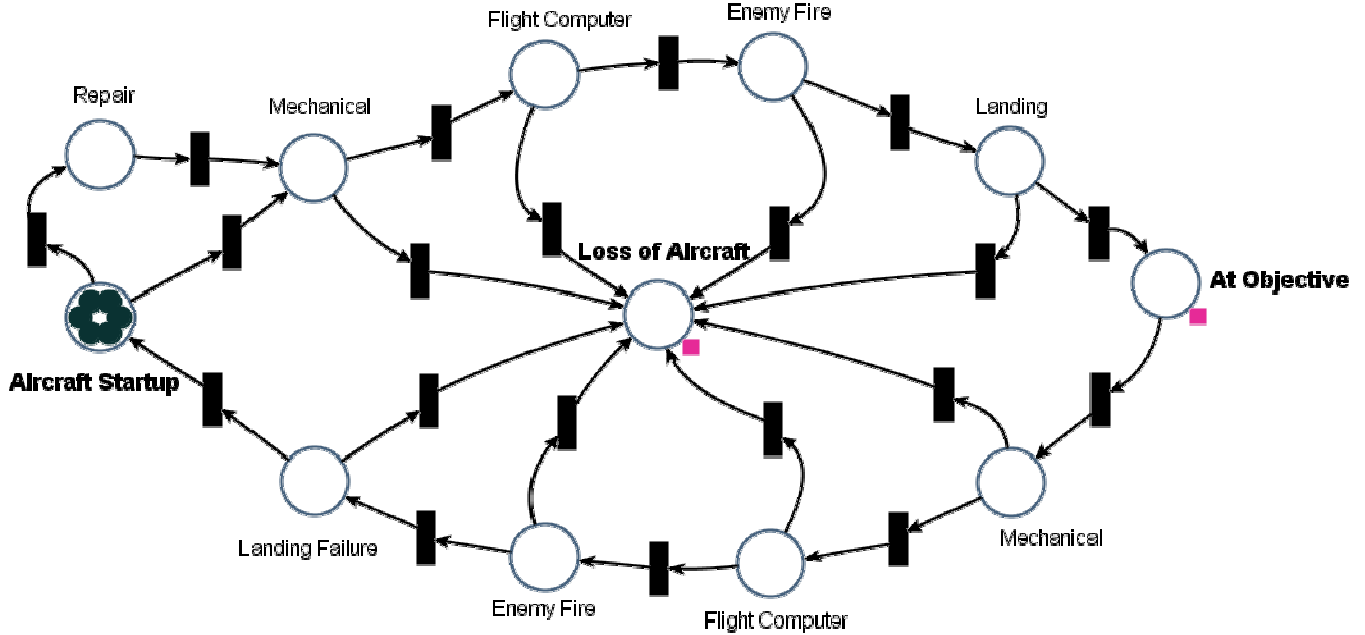


Figure 6-8: Petri Net for a Cipher Aircraft

Monte Carlo analysis was run for 1,000,000 iterations. It was found that the Barracuda was the primary source of error. It was calculated that there is an 88.75% chance that all capsules would be able to successfully reach the surface in 30 minutes to deploy the first aircraft. A repairable failure in either the water pump, elevator, or control system accounted for the majority of the problems. Repairing these failures improved the probability that all five capsules would be ready to deploy all of their aircraft to 94.95. For the maximum deployment mission of 28 Ciphers in 6 hours, there is an 86.77% chance that all 112 SOF's can be deployed without a single failure. Allowing for repairing a delayed Barracuda or Cipher, Petri Net analysis showed a 93.46% chance that all soldiers can be deployed inside the 6 hour window.

7. Rotor System Design

7.1. Cipher Rotor Blade Aerodynamic Design

7.1.1. Airfoil Selection

The airfoil selection was limited to airfoils with available C81 aerodynamic data. This data is required by the blade element code and DYMORE and eliminated recently developed proprietary airfoils such as the SC2110 and SSCA09 used on the UH-60M Growth Rotor Blade³⁹. The C81 tables available to the team were the NACA0012, NACA0015, NACA23012, VR7, VR8, SC1095, and SC1094R8. For Cipher main rotor, the SC1095 and SC1094R8 were chosen. They outperformed the NACA airfoils and have a less severe pitching moment than the VR8. They have a lower critical mach number which delays the onset of HSI and drag divergence. The SC1094R8 has a higher maximum lift and pitching moment due to its smaller leading edge nose radius than the SC1095. It is located on the inner 95% of the rotor blade. The SC1095 is located on the tip because of the importance of lower pitching moment near the tip.

7.1.2. Twist

The twist distribution of the main rotor blades is a balance between hover and high speed requirements. Twist improves the inflow and lift distribution while reducing the induced power requirements. Most helicopters have linear twist rates from -8° to -14° . At high speed, a high negative twist rate has high drag near the root of the rotor and can increase vibrations. Due to the high lift requirements on the retreating blade, the advancing blade is often at negative angles of attack.

Manufacturing composite rotor blades makes nonlinear twist distribution easier. Several thousand UH-60A Blackhawks and its derivatives have been produced with a nonlinear twist distribution for the past thirty years. The UH-60A blade twist and the Cipher blade twist are shown in Figure 7-1⁴⁰. Both aircraft have linear region with an equivalent twist rate of -18 degrees for most of the rotor blade. Near the tip of the rotor blade, the nonlinear region begins. This region was approximated with a second linear twist of 25° for use in the sizing and analysis codes. The primary purpose of increasing the pitch of the rotor blade near the tip is to avoid the large negative lift region on the advancing blade in high speed flight.

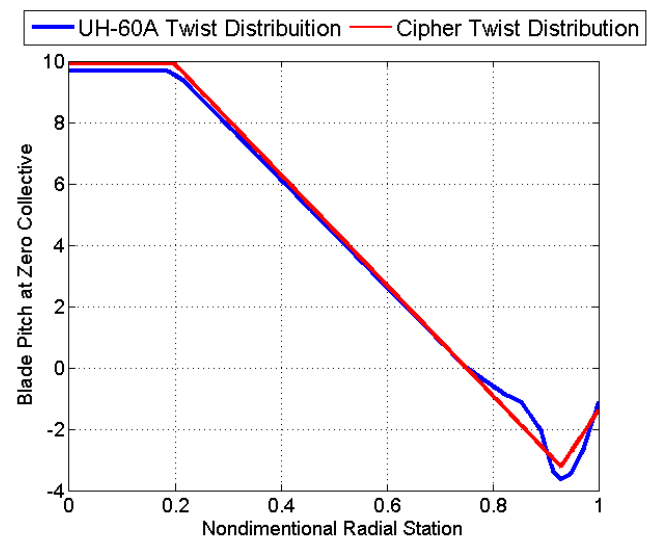


Figure 7-1: Nonlinear Twist Distribution

7.1.3. Taper

A 5/8 taper was chosen beginning at $r/R=0.95$. This was chosen using a Sikorsky developed Landgrebe Wake Model based CBEM model using C81 tables for the SC1095 and SC1094R8 airfoils. Taper allows a more uniform lift distribution and helps defuse the tip vortex.

7.1.4. Sweep

The rotor blade has two linear leading edge sweep angles. Sweeping the rotor blade decreases the Mach number normal to the rotor blade and delays the onset of supersonic flow. Supersonic flow on the advancing blade is the source of High Speed Impulsive noise. HSI and two rotor blades are the dominating features of the distinctive acoustic signature of the UH-1

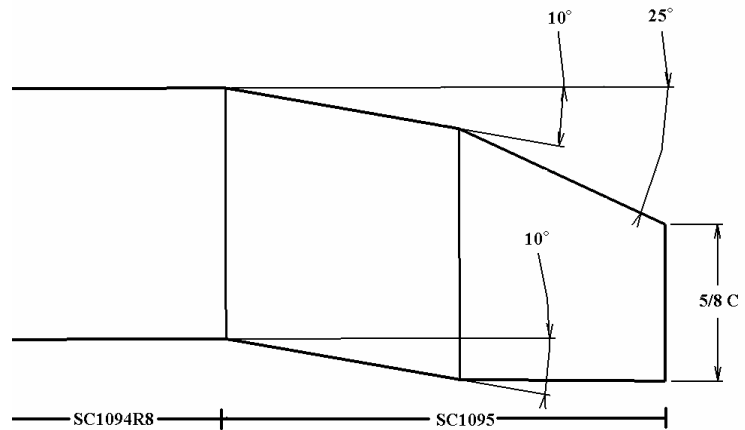


Figure 7-2: Rotor Blade Tip Design

Huey and the AH-1 Cobra. The blade is swept at $r/R=0.9$ by 10° to keep the normal Mach number of the rotor blade below Mach 0.7 at 120 kts. This is below the critical Mach number for the SC1095 for the small positive and negative angles of attack. At $r/R=0.95$, the 5/8 taper begins which increases the sweep to 25° .

7.1.5. Anhedral

Anhedral was used to improve the performance while reducing the acoustic signature. Anhedral releases the tip vortex lower than a rectangular blade. This reduces downloading on the tip which increases thrust while reducing the power requirements⁴¹. Releasing the tip vortex lower also helps reduce BVI in descending flight.⁴² Anhedral tips have been shown experimentally to reduce the power required by 7% in hover and up to 10% in forward flight and reduce the acoustic signature^{43,44}. A 20° linear anhedral was chosen similar to that on the Sikorsky Growth Rotor Blade.⁴⁵

7.2. Rotor Blade Structural Dynamic Design

7.2.1. Blade Material

The blade structure was designed to achieve the stiffness distribution required to carry the centrifugal force, both steady and oscillatory flap, lead-lag, and torsional moments. Composites are superior to metals in terms of specific strength, fatigue life, and damage tolerance. Suitable composite ply layups can provide the blade with favorable structural couplings. The composite materials considered are in Table 7-1. Kevlar is the lightest among the materials considered. However, it is susceptible to ultra-violet radiations and requires more complex bonding techniques. For the superior specific stiffness and

specific strength characteristics, CYTEC 5250-4 IM7/6K was chosen for the blade material.

Table 7-1: Material Properties of Possible Composite

Material	Density (slug/ft ³)	Young's Modulus (lb/ft ²)	Shear Modulus (lb/ft ²)	Cost (\$/lin. yard, 48" W)
CYTEC 5250-4 IM7/6K	3.43730	3.384E+09	1.224E+08	22.50
Graphite/RP46	3.11506	3.254E+09	1.066E+08	20.50
Kevlar-49	2.79273	2.592E+09	9.672E+08	16.50

7.2.2. Blade Structure

The two shear spars of the blade as shown in Figure 7-3 can sustain most of the shear in the blade. Three channel sections provide additional strength to the blade structure and maintain the airfoil shape of the blade skin. Blade skin is made of ten [0°/±45°] plies laid symmetrically and provides torsional stiffness. To avoid aeroelastic instability, a small lead balance weight was placed near the leading edge to move the center of mass and elastic axis closer to the aerodynamic center.

7.2.3. Blade Sectional Properties

A CATIA model of the airfoil was imported into ANSYS, a commercial finite element analysis tool. After finalizing the inner structural design for the blade, the areas were defined as shown in Figure 7-3. The origin of the coordinate system is located at quarter chord of the blade. The x-axis is along the span, y-axis is along the chord line, and the z-axis is vertical. VABS, Variational Asymptotic Beam Sectional Analysis, a code developed by Dr. Dewey Hodges at Georgia Tech, was used to compute the sectional properties of the main rotor blade.^{46,47} Table 7-2 shows the sectional properties of this design, with the balance weight. These properties were used for the DYMORE model for the rotor blade and hub static and dynamic analysis.

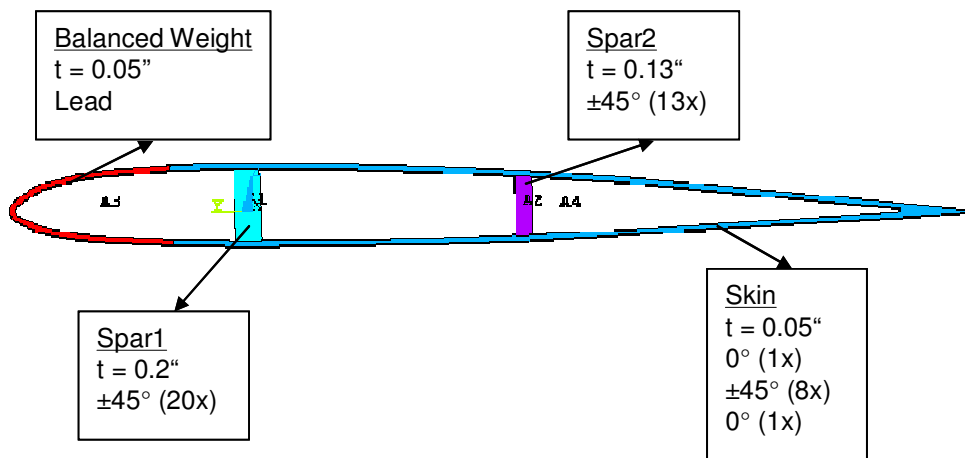


Figure 7-3: Blade Section Design

Table 7-2: Sectional Properties of Rotor Blade

Material	CYTEC 5250-4 IM7/6K	Graphite/RP46
Sectional Mass (slug/ft)	3.474E-02	3.282E-02
Axial Stiffness (lb)	6.540E+06	6.171E+06
Flap-wise Bending Stiffness (lb-ft ²)	3.173E+03	3.000E+03
Chord-wise Bending Stiffness (lb-ft ²)	3.498E+05	3.284E+05
Torsional Stiffness (lb-ft ²)	7.818E+03	7.518E+03

7.3. Blade Loads Analysis

The blade root cross-section is the most critical span-wise station of the elastic blade. For this reason, six components of unit load are put into the VABS input file of the blade root cross-section. These were used to scale the results to any values and superimpose them to the actual loads. The sets of loads are shown in Table 7-3. For each loads set, VABS is run to get the 3-D stress and strain for each Gaussian integration point of the cross-section. ANSYS is then used to develop contour plots for the Tsai-Wu stress and strain. Results of stress visualization for each sample are shown in Figure 7-4 and results of strain visualization for each sample are shown in Figure 7-5.

Table 7-3: Test Cases

Case 1	Case 2	Case3	Case 4	Case 5	Case 6
Unit Load in X	Unit Load in Y	Unit Load in Z	Unit Moment about X	Unit Moment about Y	Unit Moment about Z

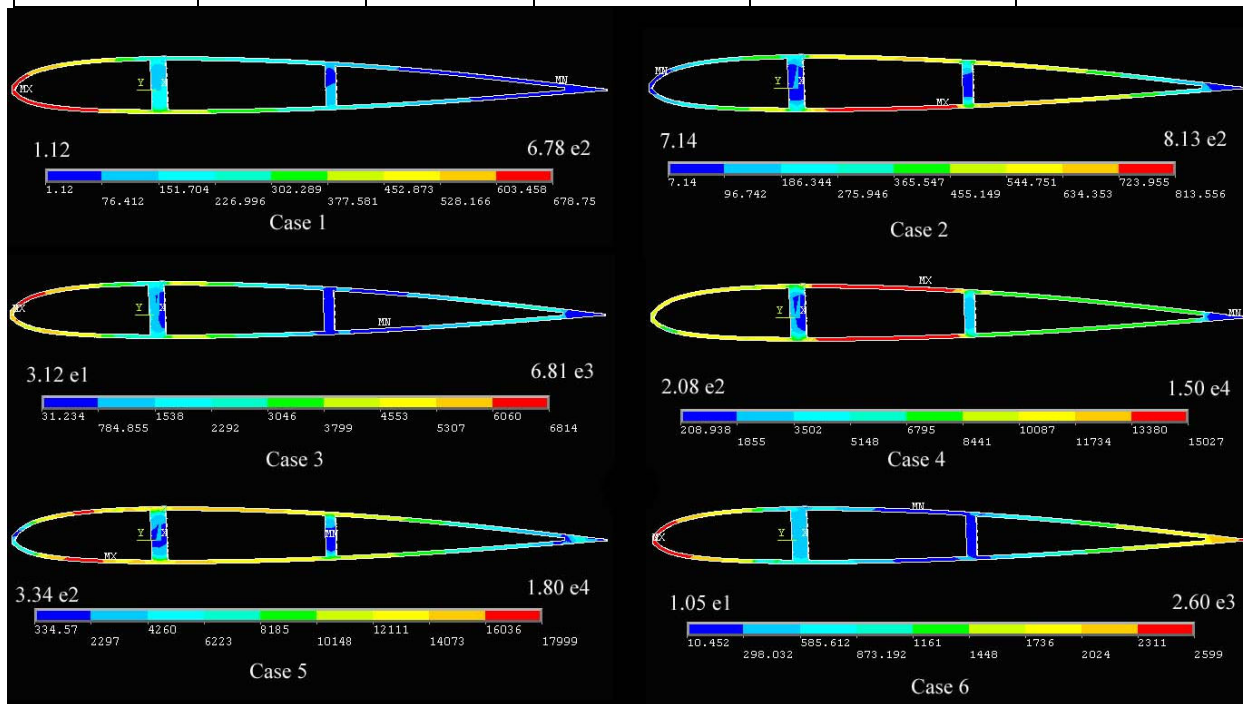


Figure 7-4: Tsai-Wu Stress for Blade Root Cross Section

The allowable strain of CYTEC 5250-4 IM7/6K is 0.004, and the allowable stress is 5.76E+06 lb/ft². After scaling and superimposing the unit loads to become the actual loads, the results are less than the allowable strain for the flight loads. Note that different directions of the load contribute to the results in

different ways. Some loads have positive contribution to the equivalent stress and strain, and the others have negative contribution.

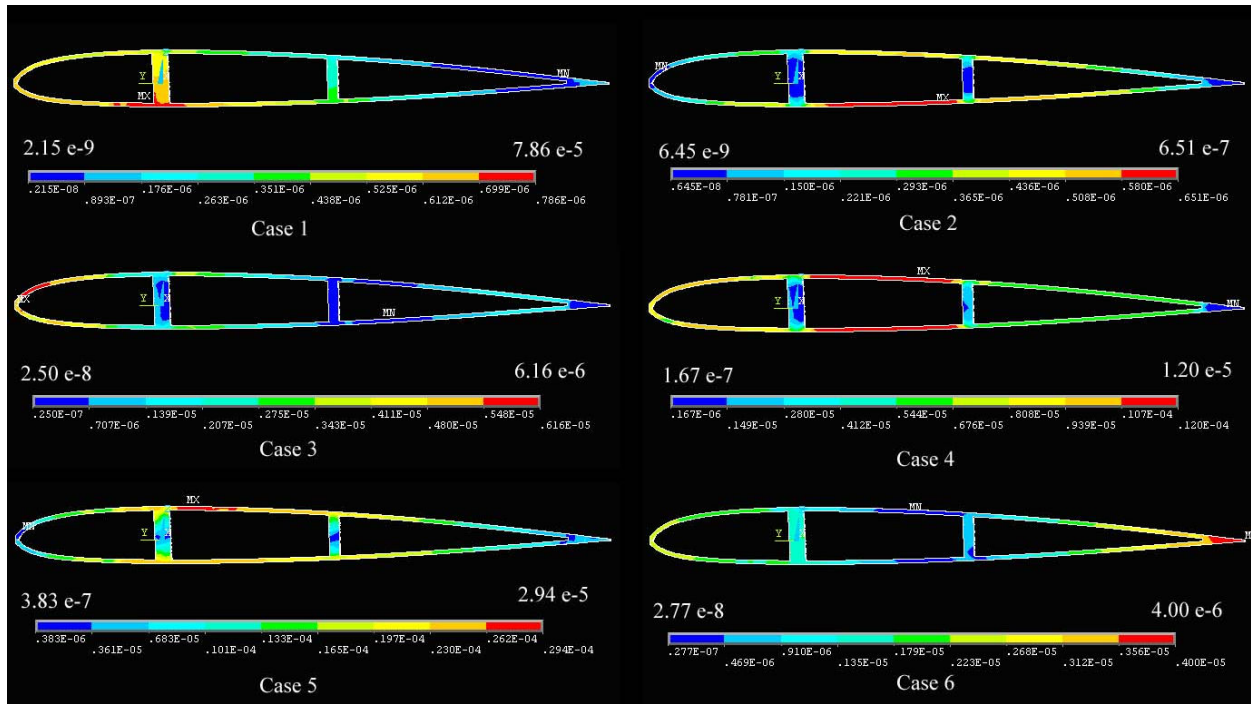


Figure 7-5: Tsai-Wu Strain for Blade Root Cross Section

7.4. Flexbeam Design

7.4.1. Flexbeam Material Selection

The key element in the hub design is the flexbeam design – a combination of elastic straps that allow the blade to experience lead-lag and flapping motions without hinges. The flex beam consists of a core, four flex straps, and four connection parts. The straps are configured to decouple the lead-lag and flapping motions, while the torque tubes are designed to provide blade feathering input. For the purpose of reducing lead-lag stiffness and maintaining enough flapping stiffness, the material selected for the straps and the connection parts is RP46 polyimide matrix/IM7 graphite fibers (Graphite/RP46), because it has a higher stiffness while still maintaining superior structural damping characteristics. Figure 7-6 provides a cross sectional view of the flex beam.

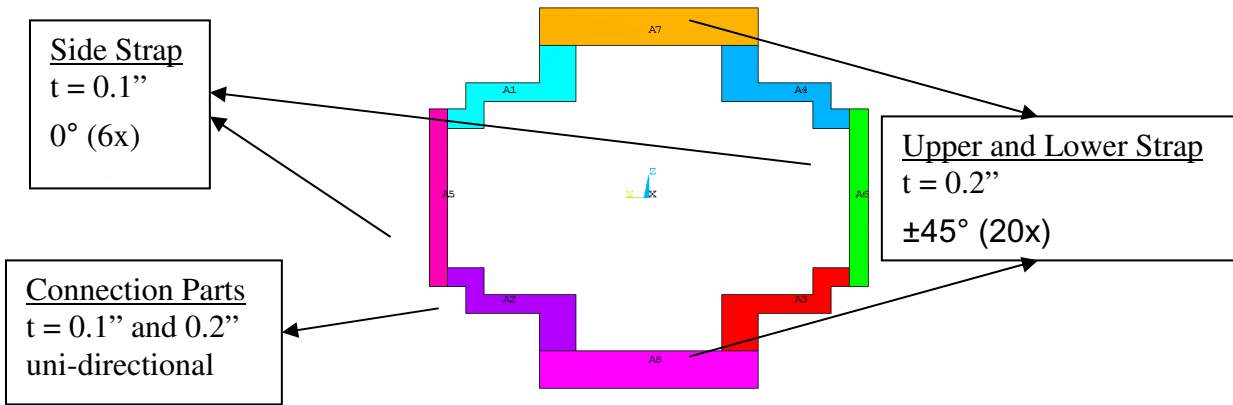


Figure 7-6: Flexbeam Cross Section

7.4.2. Flexbeam Sectional Properties

A CATIA model of the flexbeam was imported into ANSYS. After finalizing the inner structural design for the flexbeam, the areas were defined as shown in Figure 7-6. The origin of the coordinate system is located at the center of the flexbeam. The x-axis is along the span and positive going into Figure 7-6. VABS was used to compute the sectional properties of the flexbeam. Table 7-4 shows the sectional properties of this design.

Table 7-4: Sectional Properties of Flexbeam

Property	Graphite/RP46
Sectional Mass (slug/ft)	2.520E-02
Axial Stiffness (lb)	1.579E+07
Flap-wise Bending Stiffness (lb-ft ²)	3.682E+04
Chord-wise Bending Stiffness (lb-ft ²)	7.200E+04
Torsional Stiffness (lb-ft ²)	6.616E+03

7.5. Flexbeam Loads Analysis

The root cross-section is the most critical span-wise station of the flex beam. The Tsai-Wu stress and strain on the flex beam was calculated in a manner similar to that of the blade. Results of stress visualization for each test case are shown in Figure 7-7, and results of strain visualization for each sample are shown as Figure 7-8. The allowable strain of the material (Graphite/RP46) is 0.0033, and the allowable stress of the material 4.80E+06 lb/ft². After scaling and superposing those unit loads to become the actual loads, the results are less than the allowable stress and strain.

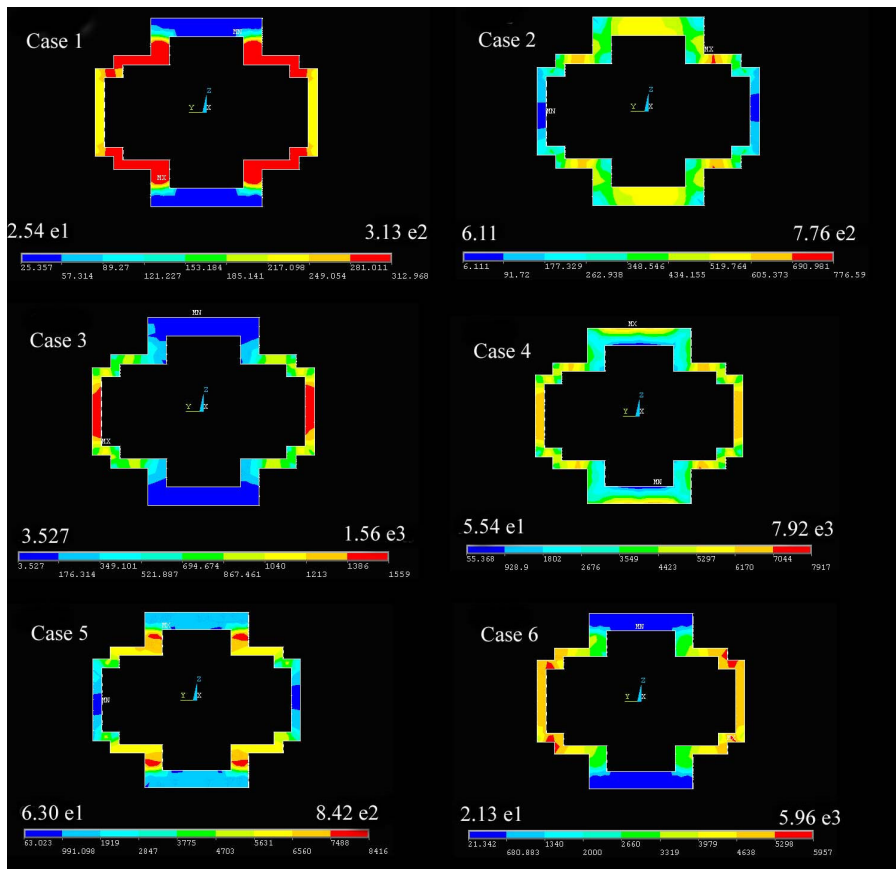


Figure 7-7: Tsai-Wu Stress for Flexbeam Cross Section

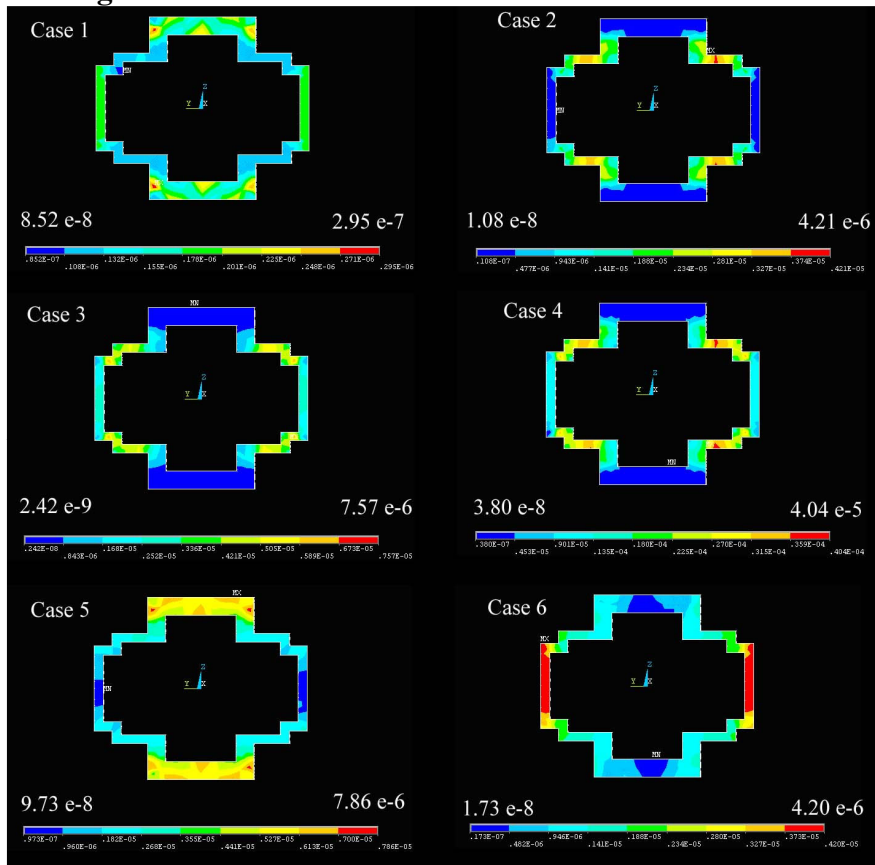


Figure 7-8: Tsai-Wu Strain for Flex beam Cross Section

7.6. Fatigue Life Estimation

The main rotor blade and flex beam were designed for 10,000 hours as the cycle criteria. The fatigue life estimation done for CYTEC 5250-4 IM7/6K, and Graphite/RP46 using material properties, reliability, surface finish, shape factors, and a safety factor of 1.5 as shown in Figure 7-9 and Figure 7-10. The Goodman Diagrams indicate the combinations of mean stress and alternating stress satisfy the requirements of infinite fatigue life design. Each stress combination must remain inside of the safe stress line. A usage spectrum, predicted loads, and vibratory stresses from DYMORE will be used to verify the blade's infinite life.

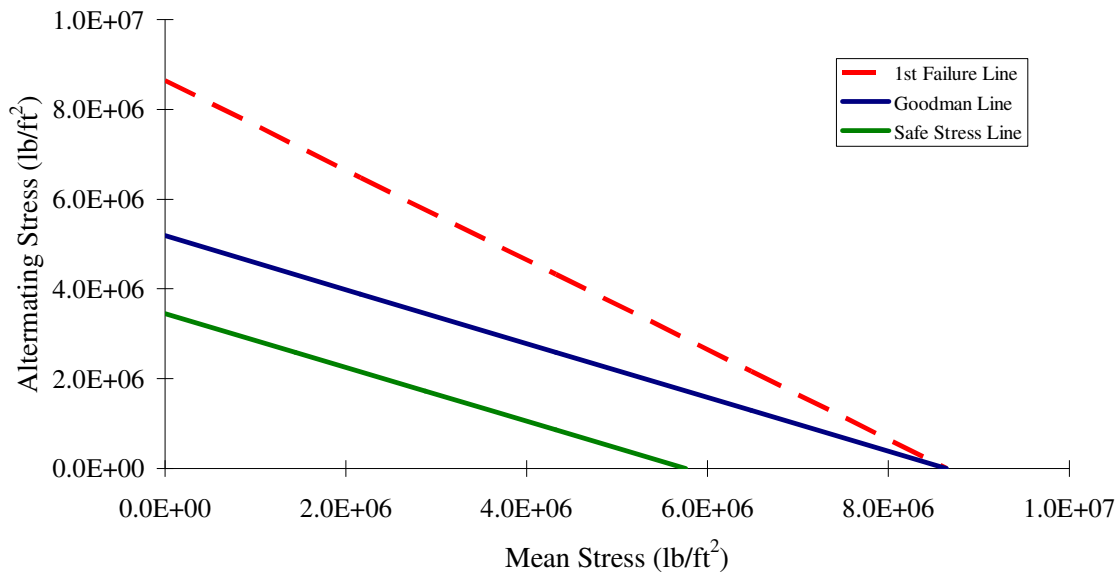


Figure 7-9: Goodman Diagram for CYTEC 5250-4 IM7/6K

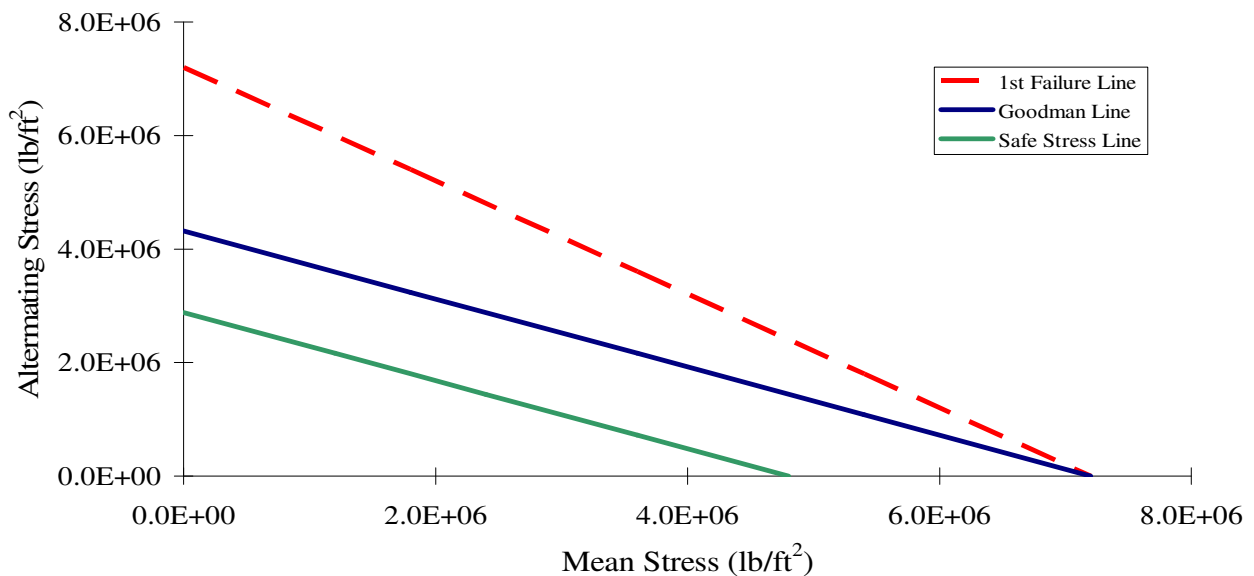


Figure 7-10: Goodman Diagram for Graphite/RP46

7.7. Rotor Dynamics

The dynamic characteristics of the blade and the flex beam were designed to place the frequencies at suitable locations on the fan plot to avoid aeroelastic instabilities. DYMORE, developed by Dr. Oliver Bauchau at Georgia Tech, was used for dynamic analysis to investigate the natural frequencies and perturbation response behavior of the rotor system.⁴⁸

7.8. Static Droop Analysis

As a result of the inherent stiffness in the blade and flex beam design, the need for a static droop stop can also be eliminated. This further simplifies the hub configuration. A static droop analysis was conducted using the slow application of gravity in DYMORE. Figure 7-11 demonstrates a blade static droop of 3.7 in at its tip.

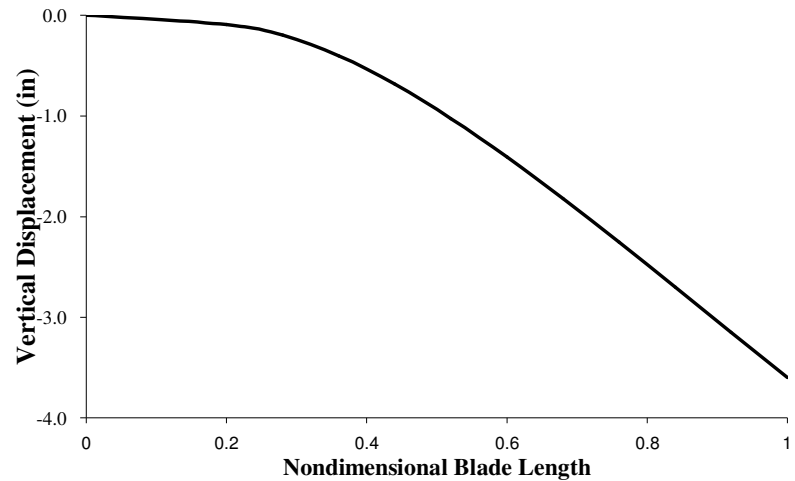


Figure 7-11: Main Rotor Static Droop

7.9. Quasi-Static Analysis

The natural frequencies of the rotor system were determined using quasi-static analysis. The in-plane motion of the blade occurs at multiples of the rotor's rotational velocity. The vibratory excitation frequencies occur based on number of blades. The fan plot in Figure 7-12 shows that the Ciper has no adverse modes near 95% and 105% of the operating RPM as stipulated by FAR 27.1509.

Table 7-5: Rotor Frequencies

1 st Lag	0.831/rev
1 st Flap	1.150/rev
2 nd Flap	2.941/rev
3 rd Flap	5.363/rev
1 st Torsion	6.189/rev

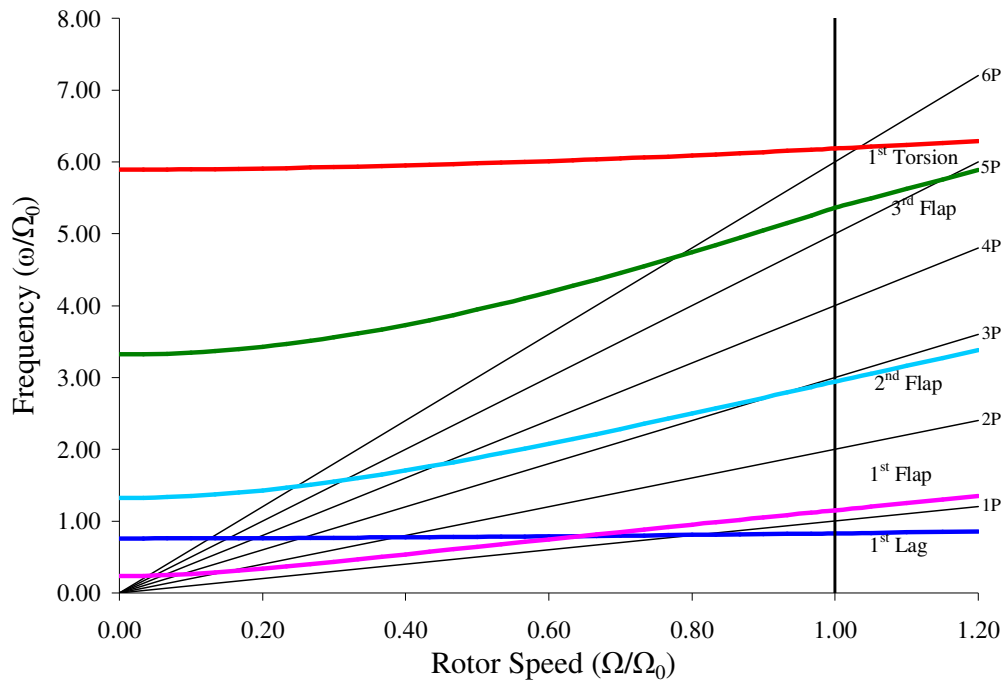


Figure 7-12: Fan Plot

7.10. Ground Resonance

The Cipher uses a soft-in-plane rotor system, therefore the potential for ground and air resonance must be examined. Ground resonance is a destructive coupling of the natural frequencies of the vehicle with the in-plane frequencies. Cipher's combined fuselage and landing gear properties were modeled using a torsional spring with an equivalent torsional

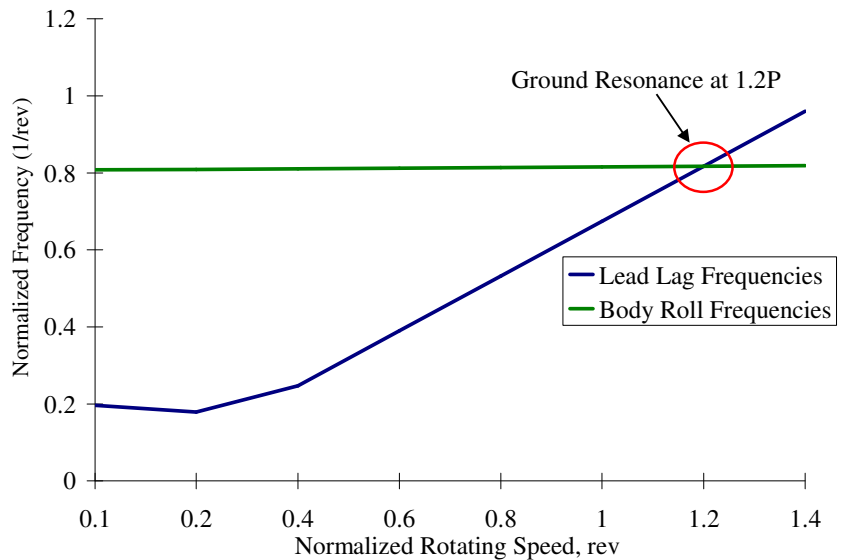


Figure 7-13: Ground Resonance Plot

stiffness of the roll and pitch axis of the vehicle. A linear static analysis was conducted in ABAQUS with an applied pitching and rolling moment of 2 lb-in. An equivalent torsional spring constant was determined and the model was then connected to the inertial frame so that its relative motion could be observed. The DYMORE model results in Figure 7-13 show that the regressive lead-lag mode intersects the body roll mode at 1.20P when the frequencies coalesce, which indicates that Cipher is free of a ground resonance condition within its normal operating limits from 0 to 1.20P. This meets the FAR

27.1509 requirements by covering all operating rotor speeds up to and including 1.05 times the operating RPM.

7.11. Air Resonance

In order to check for air resonance, a model was developed to calculate the angular momentum of the vehicle that results from in-plane rotor excitations during flight. At the instant that the disturbance is applied, it is assumed that the centrifugal force of each rotor blade momentarily acts parallel to surface reference frame. The results indicate that air resonance condition was likely to occur at 1.26P – a value outside of the normal operating envelope for Cipher.

7.12. Blade Pitch Control

Hydraulic piston actuators control pitch of the non-rotating swash plate. Thin hydraulic lines connect the pistons to the hydraulic pump, and the whole system mounts on the top of the transmission housing. The whole system is compact and only requires electrical inputs rather than mechanical linkages, thereby reducing weight and volume.

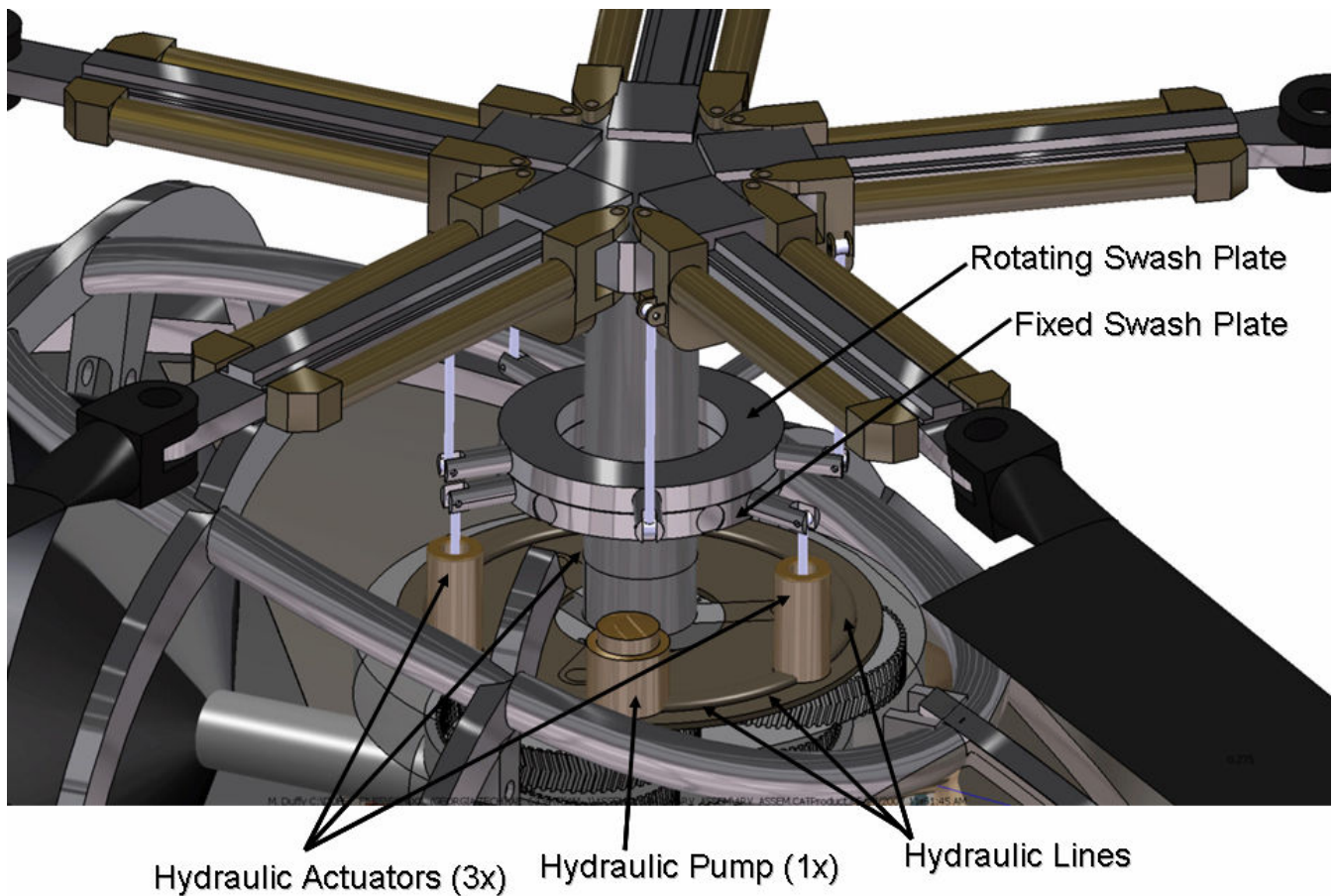


Figure 7-14: Rotor Blade Pitch Control

8. Acoustics

Due to the emphasis on stealth, a detailed acoustic design analysis was performed. Table 8-1 has a brief description of the major sources of noise on a rotorcraft and summarizes the action taken to reduce each source of noise.

Table 8-1: Acoustic Sources

Primary Rotorcraft Noise Sources	Possible Noise Reduction Methods	Action Taken
Main Rotor Harmonics	Modulated Blade Spacing, Increasing number of Rotor Blades	Five Rotor Blades
Loading	Increase Blade Area, Increase Number of Rotor Blades	Increased Solidity and Used Five Rotor Blades
Thickness	Use Thin Airfoils, Lower Tip Speed	Use of SC1095 and SC1094r8 airfoils, Low Tip Speed
High Speed Impulsive (HSI)	Reduce Tip Speed, Low Forward Flight Speed, Thin Airfoils, Sweep	Low Tip Speed of 650 ft/s, Moderate Cruise Speed, Sweep, SC1095 and SC1094R8 airfoils
Blade Vortex Interaction (BVI)	Defuse Tip Vortex, Anhedral, Active Control, Double Swept Blade Tip	Swept, Tapered, Anhedral Blade Tip
Tail Rotor Interaction	Modulate Tail Rotor Blade Spacing, Enclose Tail Rotor, Eliminate Tail Rotor	Use of NOTAR eliminates Tail Rotor
Engine	Engine Placement, Active Control	High Engine Placement

8.1. Main Rotor Harmonics

The main rotor harmonics are due to the periodicity of the main rotor. The primary method of reducing the perceived noise from the main rotor harmonics is to increase the number of rotor blades. This decreases the loading and collective on each rotor blade and decreases the pressure perturbation in the wake behind each rotor blade. Increasing the number of rotor blades also makes the distinction between each rotor blade less perceived by the human ear. In addition to increasing the number of blades, the spacing between each blade can be modified. This is similar to the modulated spacing on the tail rotor of the AH-64 Apache. NASA recently undertook a program to apply modulated the blade spacing to the main rotor blades⁴⁹. The five rotor blades were spaced between 65 and 79 degrees apart such that the magnitude of the main rotor harmonics was decreased by approximately 2dBA. There is an associated power increase that reduced the available payload by 12%. This power increase and the additional difficulty in performance and dynamic analysis eliminated this from the design of Cipher.

8.2. High Speed Impulsive Noise

HSI occurs when small sonic booms occur on the advancing rotor blade. It has distinct forward directivity and can dominate the acoustic signature at high speeds. The Cipher rotor tip is swept and the tip speed is low so that the normal Mach number is always less than Mach 0.7.

8.3. Blade Vortex Interaction

BVI occurs when the vortex from the previous blade gets near the following rotor blade. This causes an impulsive pressure perturbation that increases in magnitude the closer to the blade. This is especially prevalent in descending cases. BVI is prevalent in level flight for multiple rotor systems. Its effect can be decreased by defusing the tip vortex. This is accomplished by unloading the tip. The taper, sweep, and anhedral can accomplish this as shown in Figure 8-2. There are several active techniques to reduce BVI. Active flaps and smart materials have been shown to reduce the BVI noise but they require significant power for actuation and can reduce the aircraft reliability.⁵ The Cipher uses a tapered anhedral tip to reduce the strength of the tip vortex.

8.4. Tip Speed Reduction

Reducing the tip speed of the rotor in forward flight can reduce the acoustic signature but it also reduces the autorotational performance and rotor stability. A low tip speed of 650 ft/sec was selected for the acoustic benefits of low tip speed. Reducing the tip speed further was considered by reducing the RPM of the engine near the objective where reducing the acoustic signature is most critical. This increases the specific fuel consumption and reduces the power available but that would be acceptable for a limited time period. However, it would have made the first lead-lag frequency too close to the reduced rotor frequency. This increases the loads on the flexbeam above the design loads so reducing the tip speed was eliminated.

8.5. Computational Analysis

The computational fluid dynamic code TURNS (Transonic Unsteady Rotor Navier-Stokes Code) developed by Baeder and Srinivasas^{50,51} and enhanced with Symmetric Total Variation Diminishing (STVD) scheme at Georgia Tech^{52,53,54}. This was used as a final check on the hover performance predicted by the sizing code and the Landgrebe wake model. It was found that the hover performance predicted by the sizing code over predicted the power by 3-5% and the Landgrebe wake model under predicted power by 5-8% compared to the TURNS results. The computational grid used was a C-H 161x89x61 grid with 60 points in the wake cut. The surface grid is shown in Figure 8-1.

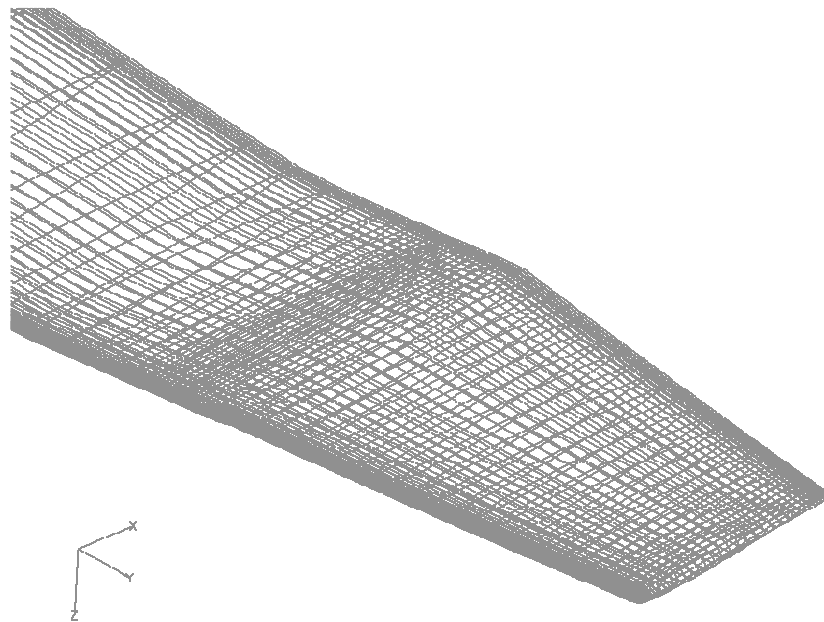


Figure 8-1: Computational Surface Grid

TURNS was run for a standard rectangular rotor blade and the designed blade for Cipher to judge the success in defusing the tip vortex. As shown in Figure 8-2, the size of the tip vortex was diminished. The rectangular tip gives a well defined vortex core with a maximum vorticity magnitude of 2.4 at a vortex age of 5 degrees. The swept, tapered, anhedral tip reduces the overall size of the vortex and the maximum vorticity magnitude to 1.65. Reducing the intensity of the tip vortex reduces the BVI noise.

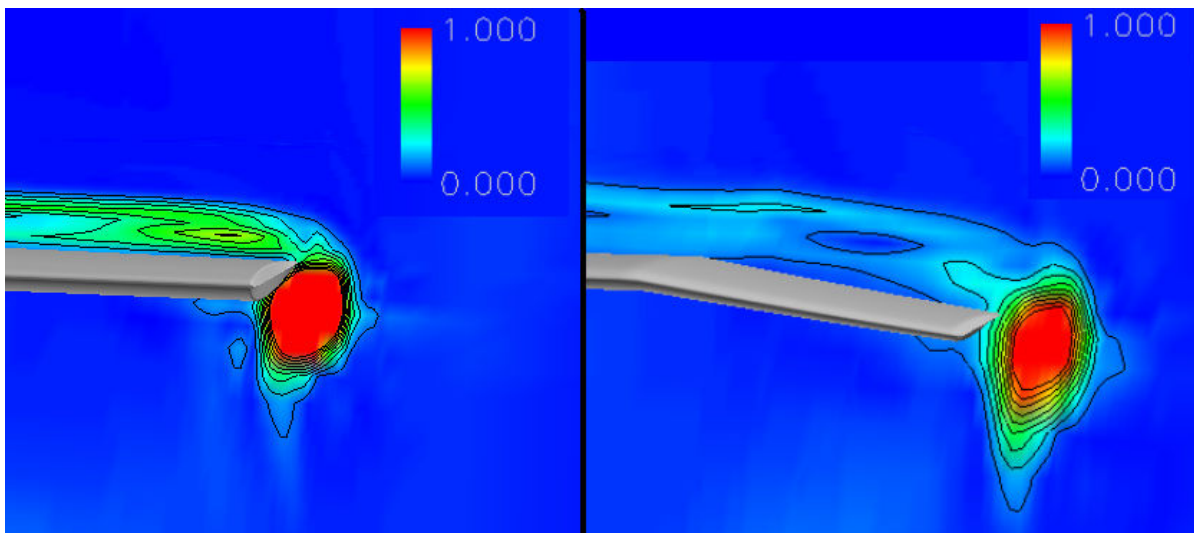


Figure 8-2: Vorticity Contours at 5 Degrees

8.6. Computational Acoustic Analysis

The industry standard program PSU-WOPWOP was used to analyze the acoustic signature of the Cipher and Dragonfly^{55,56}. It is based on the Farassat's integral representation of the Ffowcs Williams-Hawkings equation⁵⁷. The acoustic signature of Cipher and Dragonfly was calculated using compact

loading at 81 spanwise locations in 3 degree azimuthal increments. Each observer location was calculated for three rotor revolutions. The compact loading was calculated using the DYMORE structural model of the rotor blade and hub with dynamic inflow and C81 tables for aerodynamic data.

8.7. Acoustic Results

Figure 8-3 shows the calculated 65 dBA contours for the Cipher and Dragonfly. Cipher was calculated to have a slightly larger footprint than the MD 520N. This is due to the slightly higher disk loading. The spikes in the footprint for the Bell Jet Ranger and AS350B are due to HSI which has been eliminated in Cipher by having a low tip speed, swept tips, and nonlinear twist to reduce the negative pitch on the advancing blade. The Dragonfly has a very small footprint about 400 feet wide. This is due to the thickness noise which radiates in the plane of the rotor with the loading noise radiating outward. The thickness noise itself is very small due to the very low tip speed during endurance. The loading noise is very small due to the low thrust requirement. When flying at the endurance speed, the 65dBA contour for the Dragonfly disappears.

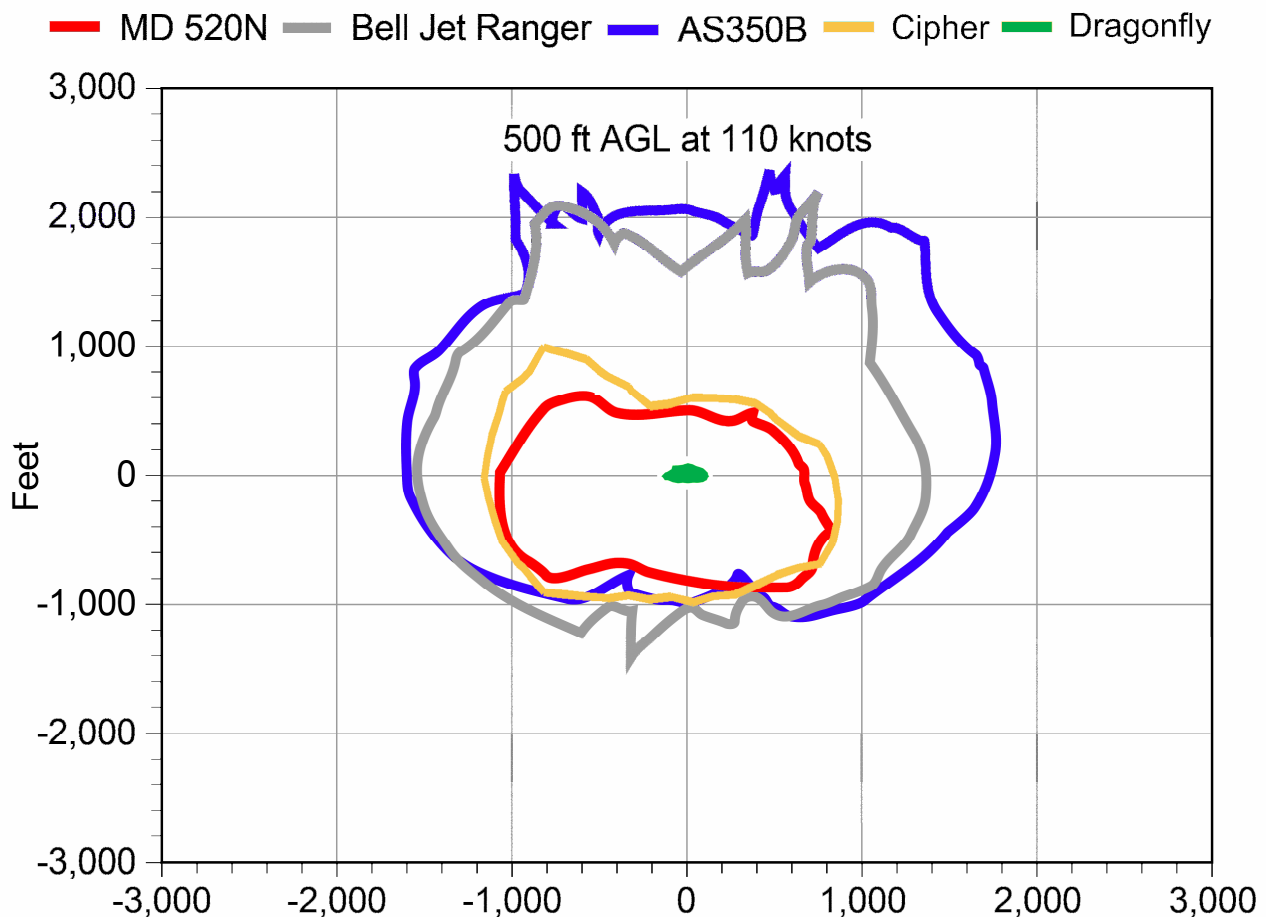


Figure 8-3: Calculated Acoustic Footprints at Maximum Gross Weight (65dBA Contour)

9. Propulsion

9.1. Cipher Engine Selection

The RFP provides advanced scaleable engine data that is representative of likely 2020 values. If the RFP engine is not used, the RFP allows for a 20% improvement in specific fuel consumption and specific weight over current engines. Figure 9-1 shows the SFC of several current engines with the 20% SFC improvement over a range of horsepower. Over the preliminary range of horsepower, the RFP engine has superior specific fuel consumption. The technology improvement for current engines was not used for the turbo diesel.

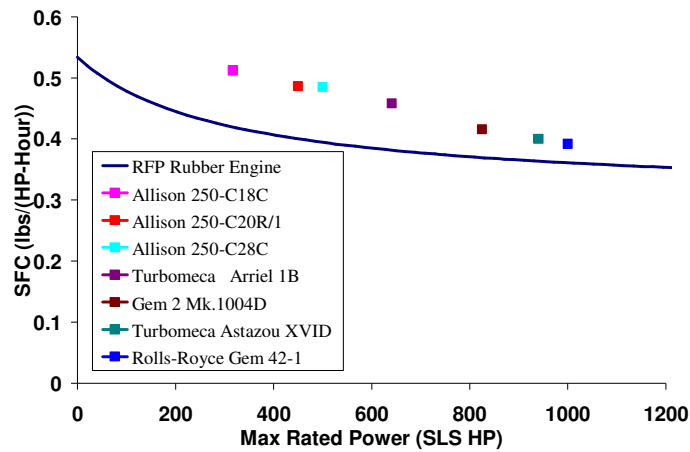


Figure 9-1: RFP Engine SFC Compared to Current Engines with 20% SFC Improvement

9.2. Engine Installation Losses

The final iteration on gross weight optimization and power required yielded the final values for engine data shown below in Table 9-1 and Table 9-2. In addition to all power required by the main rotor, NOTAR, and transmission, several additional power considerations were taken into account. First an accessory power requirement of 10 hp was added to the total power required before installation losses. Post installation losses result in an 8% total reduction in power: 1% inlet loss due to duct friction, 3% inlet pressure loss due to particle separator, 1% exhaust back pressure do to friction, and a 3% exhaust back pressure drop due to infrared suppressor.

Table 9-1: Cipher Uninstalled Engine Data

Scaled Engine Data at SSL	Symbol	Power (HP)	SFC (lb/hp-hr)
Max Rated Power	MRP	499	0.4157
Intermediate Rated Power	IRP	465	0.4234
Max Continuous Power	MCP	380	0.4454
Partial Power (50% MRP)	PRP	249	0.5138
Idle	Idle	99	0.8644

Table 9-2: Dragonfly Turbo Diesel Uninstalled Data

Scaled Engine Data at SSL	RPM	Power (HP)	SFC (lb/hp-hr)
Max Rated Power	4000	249	0.450
Cruise Power	2308	143	0.382
Endurance Power	1354	84	0.409

9.3. Transmission Design

To reduce the weight of the transmission, it was designed for the maximum horsepower from the high hot hover condition. This reduced the weight of the transmission by 45 lbs. After the basic design was chosen, secondary factors came into effect including simplicity of design, minimization of parts, noise minimization, fatigue, and cost. The design criteria that the transmission had to satisfy can be found in Table 9-3.

Table 9-3: Transmission Design Requirements

Max Power to Rotor shaft	329 HP
Engine output shaft speed	18,000 rpm
Rotor shaft speed	485 rpm
Total Gear Ratio	37:1

9.3.1. Transmission Configuration

One of the design layouts considered was a 3 stage compound planetary gear box shown in Figure 9-2. This consisted of 3 planetary gear sets with the planet pinions being held stationary. The ring gear of the first planetary set would act as the sun gear for the second planetary gear set,

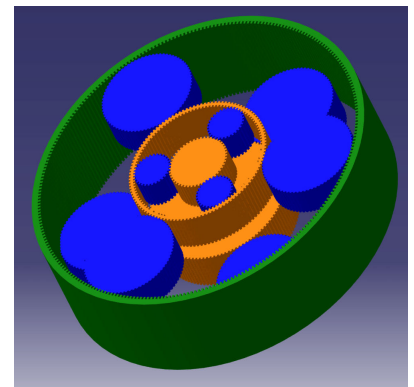


Figure 9-2: 3 Stage Planetary Gear Planetary Transmission Concept

and the second and third planetary gear sets would share the same ring gear. Although this combination would allow for lighter individual gears and higher number of teeth per gear, allowing for better meshing and so lower noise, the overall weight and size was too large.

Therefore the design chosen for the transmission was a 2 set planetary gear set shown in Figure 9-3. This consists of a bevel gear set which reduces the shaft speed and translates the direction into the first sun gear with two planetary gear sets stacked on top of each other. The second sun gear is connected to the first set of pinions

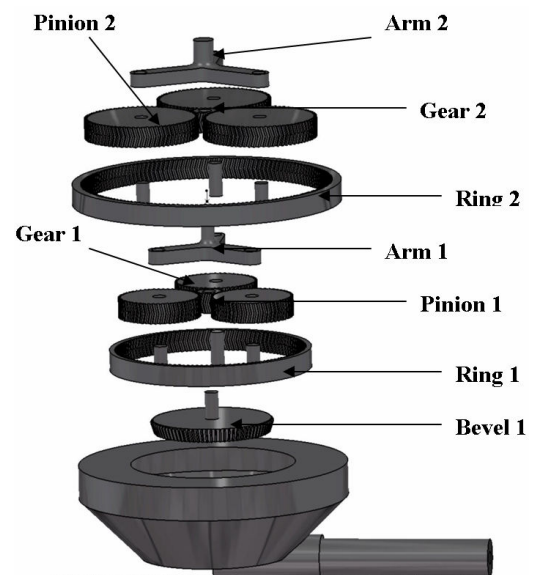


Figure 9-3: Final Transmission Assembly

through the first arm; the rotor shaft would be powered by the second set of pinions through the second arm. Herringbone gears are used due to the fact that they produce counteracting thrust so there is no need for thrust washers. They also mesh better than spur gears which will help reduce noise. A table of the final design details is shown Table 9-4.

The gears were designed using the methods described by Shigley⁵⁸. The face width was chosen from the range between the recommend minimum and maximum face widths which depend on the diametral pitch. The stresses were then calculated using recommended factors and AGMA (American Gear Manufacturers Association) values described by Shigley⁵⁸.

Table 9-4: Gear Dimensions

Gear	Diameter (inches)	Number of teeth	Diametral Pitch	Face Width (in)	Shaft Speed (rpm)	Bending Stresses (kpsi)	Hertz Stresses (kpsi)
Bevel 1	3	27	9	1.1	18,000	1.36	34.1
Bevel 2	9	81	9	1.1	6,000	1.59	19.9
Sun 1	2	18	9	1.5	6,000	52.81	197.94
Pinion 1	6	54	9	1.5	2,000	52.81	114.28
Ring 1	14	126	9	1.5	0		
Sun 2	2	18	9	1.5	2,000	140.41	313.46
Pinion 2	8.25	74	9	1.5	485	140.41	154.36
Ring 2	18.5	166	9	1.5	0		

9.4. Drive System Mounts

The drive system is designed and placed so that minimum volume is required and to ensure that the CG of the Cipher is as far forward as possible. To achieve these design goals the transmission was mounted directly below the rotor mast, and the engine was placed as far forward as possible. In addition, the engine is inline with the NOTAR fan so that minimum shafting to drive the fan is required. The primary loads are sent through structure via motor mounts and transmission mounts. This sends the loads down to the landing gear and into the ground.

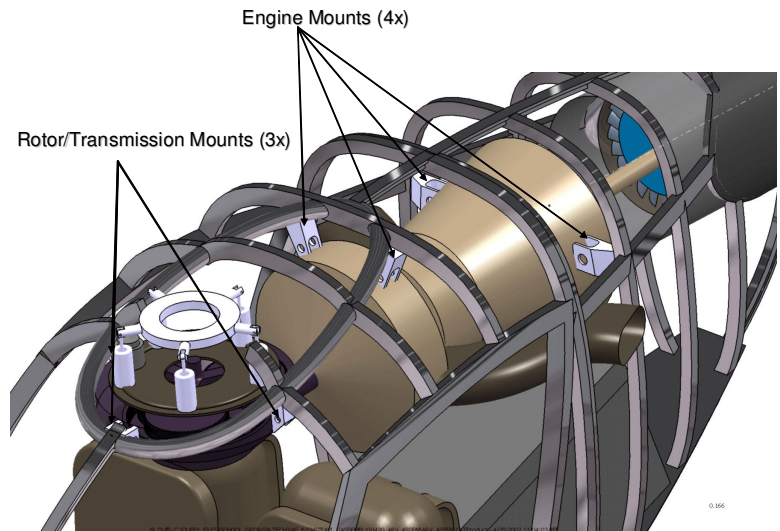


Figure 9-4: Engine and Rotor System Mounts

10. Structural Design

10.1. Finite Element Analysis

10.1.1. Crashworthiness- Limit Load Tests FAR 27.725

Naval Air System document AR-56 mandates that all rotorcraft meet unaccelerated level landings at 12 ft/s.⁵⁹ Following the method presented by Kshitij Shrotri at Georgia Tech, the landing gear was modeled in ABAQUS with all mechanisms locked while being subjected to their limit load, in concurrence with FAR Part 27 and ADS 29: 4.1.23.⁶⁰

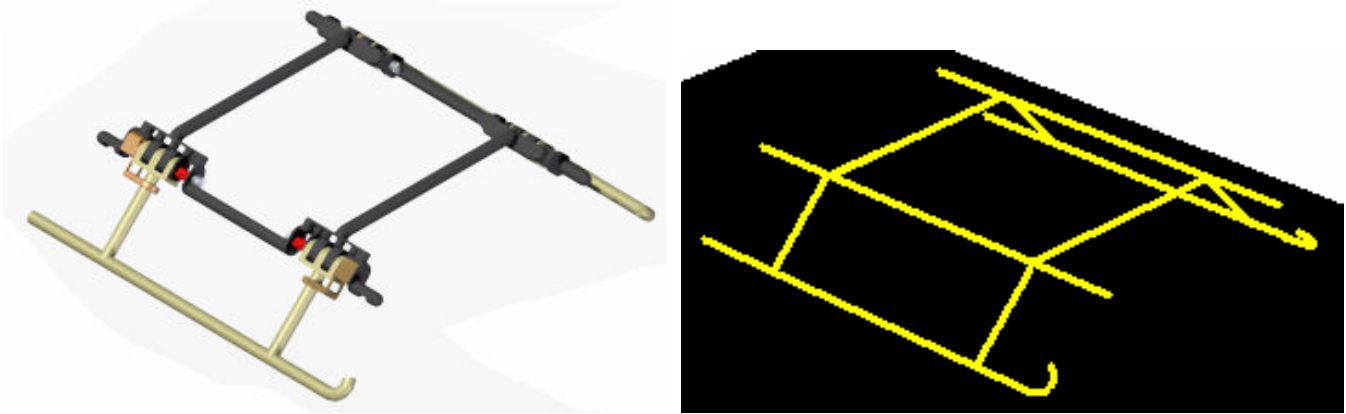


Figure 10-1: CAD (Left) and ABAQUS (right) Landing Gear Models

A 1.5” outer and 1” inner diameter structural steel circular pipe section, based on the Bell 206B design, was selected for the landing gear. Plasticity was included with yielding at 45 ksi and 1% plastic strain at 75 ksi with the ultimate tensile strength being 94 ksi. Beam elements (B31) were used for the landing gear and a single Discrete Rigid Element with reference rigid node was used for the ground for meshing. A 0.01” clearance between the ground and the landing gear was specified in the Dynamic/Explicit analysis. A rigid reference node with an assigned mass and inertia was set at the Ciper centroid representing the fuselage and was connected to the landing gear by rigid beam elements. A Master-Slave Surface-to-Surface Contact was modeled with Static-Kinetic Exponential Decay Friction properties. The static and dynamic coefficients of friction were equal to 0.5 and 0.35, respectively and the decay coefficient was set equal to 0.05.

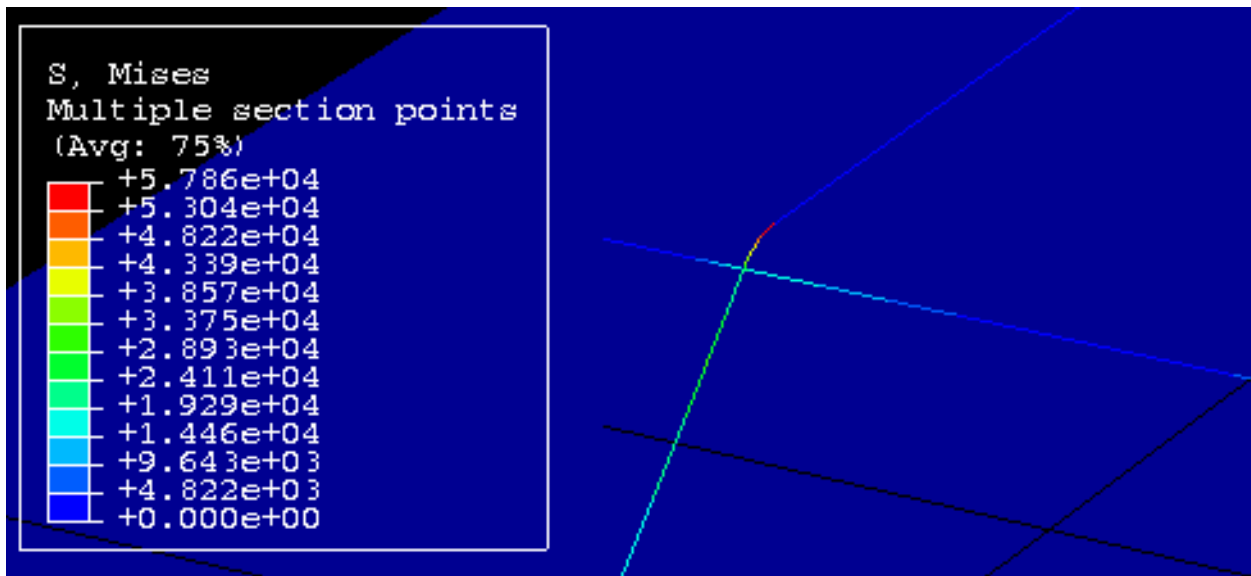


Figure 10-2: ABAQUS Stress Analysis

The skid obstruction scenario was perceived necessary due to the operating conditions typical of this RFP, and was conducted with an additional fixed rigid discrete element fixed perpendicular to the ground. The results of the crash test results are shown in Table 10-1.

Table 10-1: Crash Test Stress Results

Landing Condition (All at 12 ft/s)	Maximum Observed Stress	Maximum Allowable Stress
Level	55.13 ksi	94 ksi
Nose First (8° pitch)	65.24 ksi	94 ksi
Aft First (8° pitch)	63.30 ksi	94 ksi
Skid Obstruction	63.5 ksi	94 ksi
Single Skid Rolling (15° roll)	75.00 ksi	94 ksi

10.1.2. Skid Morphing Model

The skid morphing model incorporated an assembled three part skid. The lower and upper sections were offset by an infinitesimally small gap and connected by a spring/damper connector hinge. The skid was initially placed directly on the ground subjected to a 1g load to not only ensure that yielding did not occur but also to allow for damping sizing at a desired decent rate. Figure 10-3 depicts a fully extended morphing view just before the stepper motors engage. Tangential behavior defined by the coefficients of friction plays a key role in this analysis, thus dictating the morphing skid plate design.

10.2. Fuselage Structural Design

The fuselage structure is shown in Figure 10-3. The primary structure consists of 2" x 2" AI6061-T6 frames with 1.5" x 1" secondary structure. The fuselage structure was designed to sustain a 3.5g pull up while the tail was designed for a 1000 lb load due to a max turn at 120 knots. Figure 10-3 highlights high stress areas denoting the need for additional doublers or filets. The crashworthy seats weigh 25 lbs each and can sustain a 5g load while displacing eight inches. Analysis is shown in Figure 10-3. The structure and corrosion resistant paint allow for operations in adverse climates including desert, artic, and tropical.

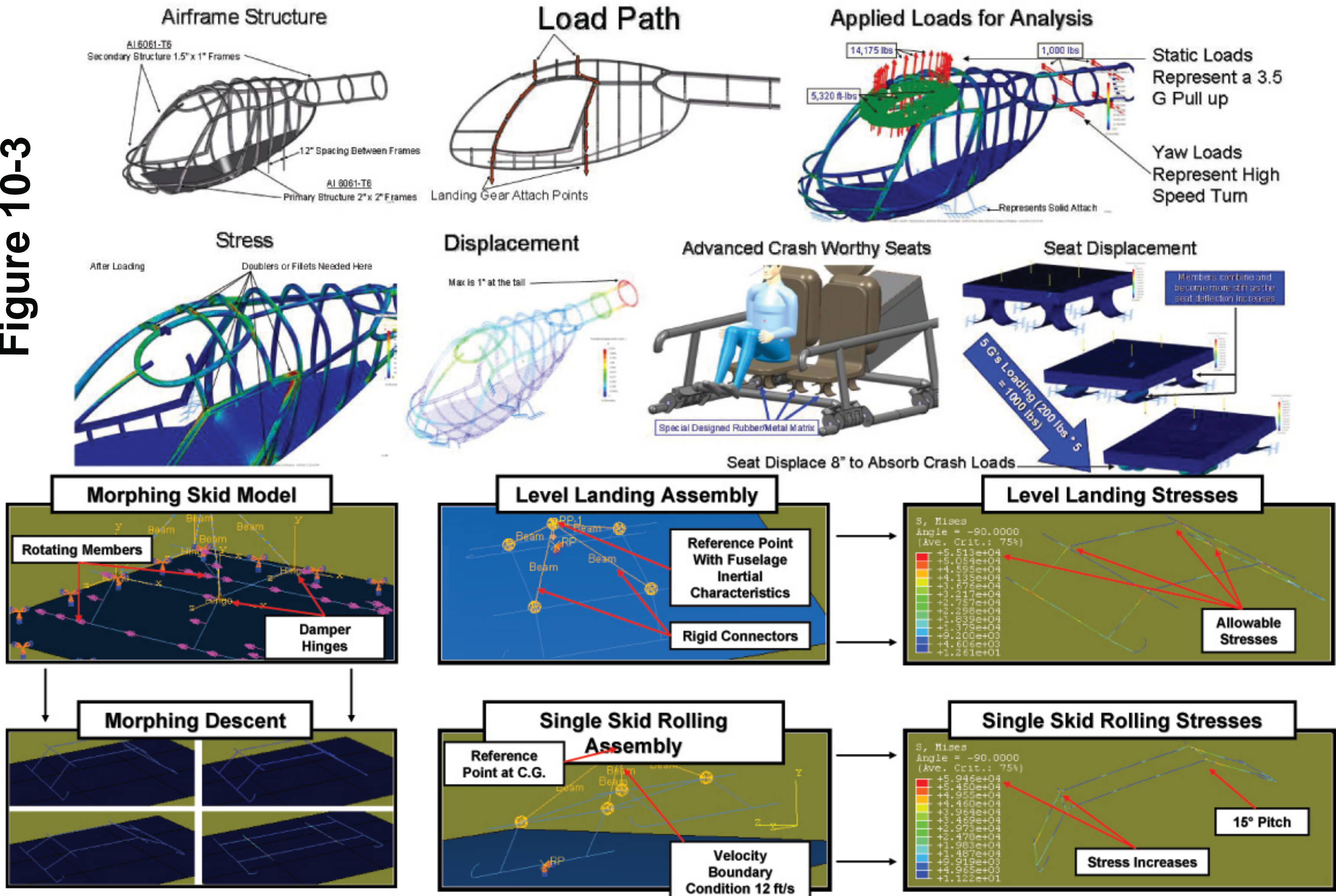
10.3. Dragonfly Landing Gear

The UEV landing gear is based on four spring/damper pneumatic six inches strut systems made of 6061 hollow aluminum tubing to sustain a 12 ft/sec landing without failure. The struts are fully retracted at takeoff and landing to lower the CG and are located at the maximum outside corners of the vehicle to minimize tip-over. Caster wheels are located at the bottom of each strut to permit strut sliding with forward or rearward motion instead of tipping. At takeoff, the struts extend automatically. A 100 psi compressed air tank in the fuselage provides a 10 psi charge to each strut to provide approximately 270 lbs of resistive force in forward flight to ensure the strut stays in the extended position. At landing approach, the struts are de-pressurized to permit retraction as weight is applied to each strut with negligible spring resistance.

10.4. Flotation Capability

The Cipher has a two bag FPT Industries flotation system. This system is similar to that used on a S-92 that enables Sea State 6 capability.⁶¹ The Cipher is not as wide as the S-92 but are only required for Sea State 3. The Dragonfly has large wings and does not have a cabin that can flood so it does not require a flotation system.

Figure 10-3



10.5. Static Tip Analysis

Table 10-2 shows the static tip over analysis of the Cipher at various loading conditions. Even if one leg extends as shown in Figure 10-4, the tip over angle is always at least 20°. The maximum angular tilt on the capsule is less than 2°.

Table 10-2: Cipher Tip Over Analysis

	Location of CG from the Ground			
	52"	49"	45.5"	44"
One Leg Extended	20°	23°	27°	29°
Take-Off	57°	60	63	65
Landing/Flight Mode	38°	40°	42°	43°

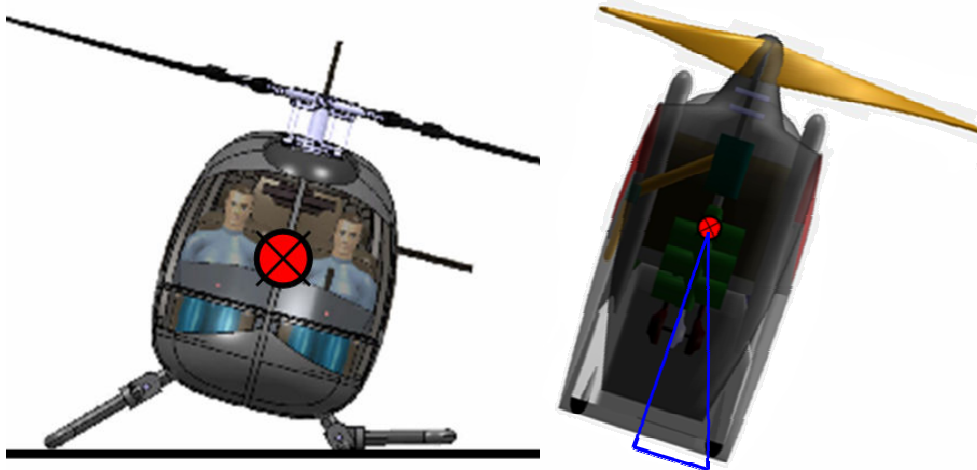


Figure 10-4: Cipher and Dragonfly Tip Over Analysis

The Dragonfly landing gear size and location was determined in order to minimize tip-over, which has typically been a major concern of tailsitters. Due to the low center of gravity location and the wide 16ft x 5ft stance of the landing gear, tip-over is much less of a problem than for previous tailsitters. The landing gear extension was maximized as well by placement of the landing struts within the engine pylon, while minimizing the wetted area and interference drag concerns. Caster wheels are located at the base of the struts to ensure that the struts will slide with any forward or sideslip speeds at touch down and prevent topple over. The wheels also permit the Dragonfly to be maneuvered in the Barracuda capsule by ground personnel as aircraft are positioned on and off the capsule elevator. The tip over angle is 36°, which is much better than previously designed tail sitters.

11. Stability and Control Analysis

11.1. Cipher Trim Analysis

The first step to carry out the stability and control analysis of Cipher is to develop a computer program for the trim analysis. The code is written in MATLAB and uses geometric variables as inputs and trims the helicopter for all flight conditions in between hover and the maximum cruising speed of the vehicle defined as 130 knots.

The trim values for collective, longitudinal cyclic, and lateral cyclic are shown in Figure 11-2. The collective decreases from the hover value as the induced power requirement goes down with forward flight speed. It minimizes around the endurance speed of 60 knots and then increases as parasite drag increases in high speed flight. The longitudinal cyclic, Θ_{1S} , in hover is near zero since the center of gravity is very close to the mast allowing the aircraft to maintain a level attitude as shown in Figure 11-2. The side shaft tilt of one degree reduces the body roll attitude.

The torque required to counter the main rotor is provide by two sources, the NOTAR and the vertical stabilizer. The vertical stabilizer was sized such that the NOTAR is offloaded in high speed forward flight as shown in Figure 11-1. Due to the height and folding requirements, the tail does not completely offload the NOTAR but still provides the majority of the required anti-torque.

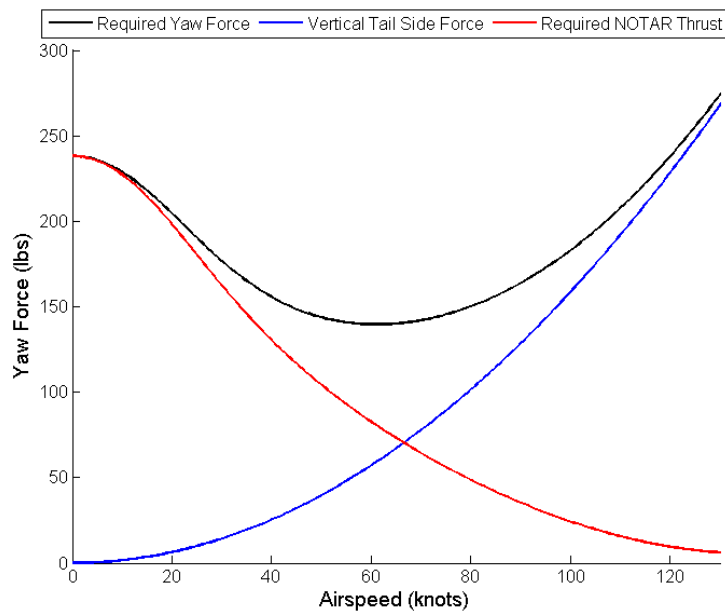


Figure 11-1: Required Anti-torque

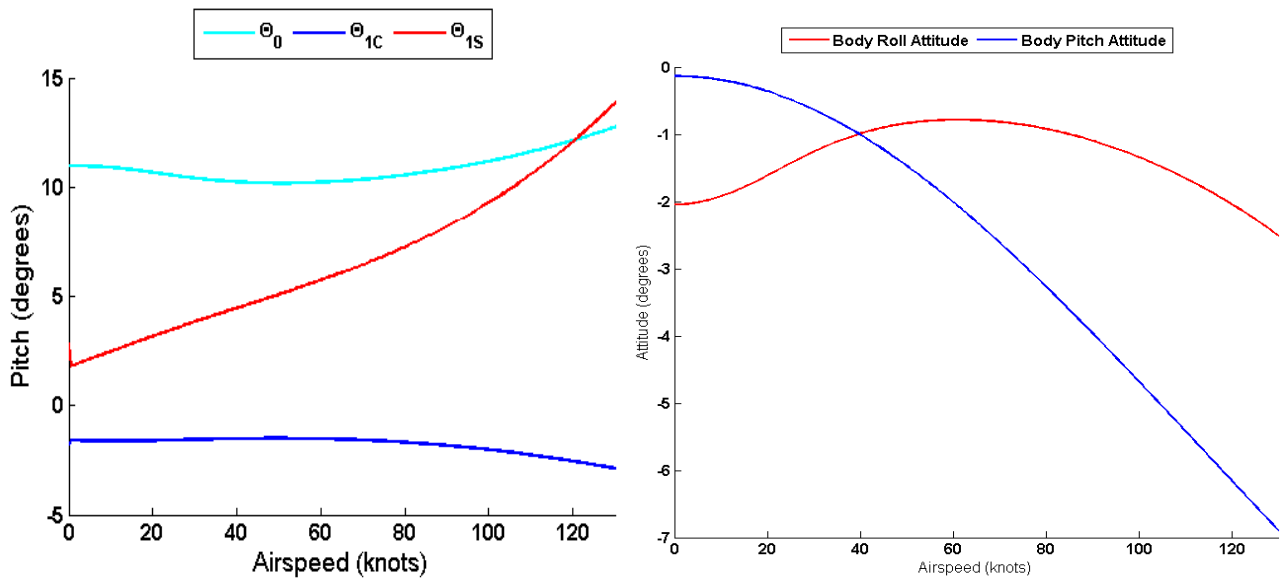


Figure 11-2: Trimmed Rotor Controls and Body Attitudes

11.2. Cipher Maneuverability

In order to get a better idea of the maneuverability of the Cipher, the maximum angular rates were determined using HELCOM energy based equations⁶². The maximum pitch and turn rates are shown in Figure 11-3 and compare well with the maneuverability of other single main rotor helicopters.

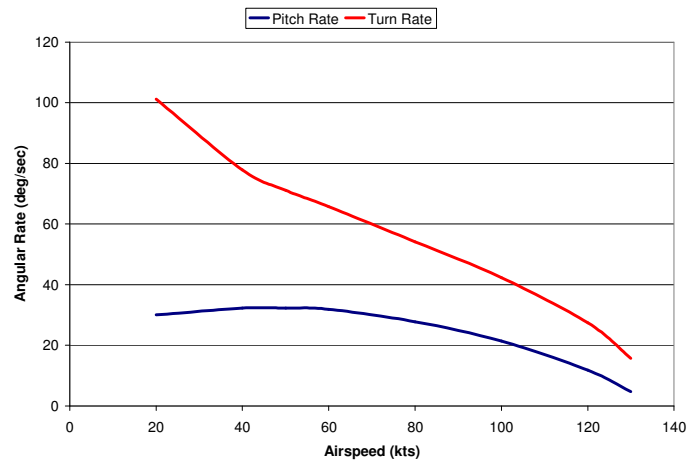


Figure 11-3: Cipher Maximum Angular Rates

11.3. GUST Modeling

In order to assess maneuverability and the ability of the autonomous control system to perform maneuvers, the Cipher was modeled in GUST, a software tool developed at Georgia Tech for controlling autonomous vehicles. GUST allows for mission planning which is then followed by the open control platform of the vehicle. The Cipher’s mission requires both cruise over the ocean, and NOE flight near the objective.

Figure 11-4 shows the final approach trajectory for the sample mission. This trajectory was modeled into the GUST simulator using a model of the Cipher geometric, mass, and engine data. The flightplan is sent to the open control platform represented with the purple line. The yellow line represents the actual flightpath taken by the Cipher. Figure 11-4 shows both the assigned flightplan and the performed flightpath.



Figure 11-4: Mission Plan from Satellite Image to Entering into Computer and Flown Path

Table 11-1: GUST Flightplan and Cipher Flight Results

	#0	#1	#2	#3	#4	#5	#6	#7	#8	#9	#10
Assigned Altitude (ft)	0	1500	15	15	15	15	15	15	15	15	15
Crossing Altitude (ft)	0	1500	18	15	15	14	14	14	15	15	15
Assigned Groundspeed (ft/s)	150	150	20	20	20	20	20	20	20	20	200
Crossing Groundspeed (ft/s)	2	152	27	21	20	19	20	19	20	20	178

11.3.1. Autonomous Control

Cipher and the Dragonfly require an autonomous control system (ACS). For both aircraft, the ACS is responsible for the safety and navigation of the aircraft. The soldiers onboard the Cipher act as supervisors giving commands to the Cipher and Dragonfly which are interpreted by the ACS.

The level of autonomy is the same for both aircraft because the Cipher is required to return to the capsule without the soldiers onboard to direct it. Using the autonomous control level metric developed at the Air Force Research Laboratory⁶³, both the Cipher and Dragonfly have a targeted autonomy level of level six. Table 11-2 shows the autonomy levels in the different aspects of autonomy.

Table 11-2: Autonomy Level

Level	Descriptor	Observe	Orient	Decide	Act
6	Real-Time Vehicle Coordination	On-board sensing supplemented by off-board data	Tactical Assigned Goals	Coordinated Trajectory Planning and Execution	Goal Accomplishment with minimal supervision

11.3.2. Open Control Platform

The ACS of both aircraft consists of an open control platform, adaptive neural network, and user interface. Figure 11-5 shows the ACS of both aircraft. The mission plan is interpreted by the Open Control Platform (OCP), which uses sensor data to determine the best way to accomplish the mission received from the user interface and flight stick.⁶⁴ The OCP then sends control inputs to the adaptive neural network which adjusts the control sensitivity based on the aircraft's orientation. The adaptive neural network then sends actual control inputs to the aircraft. The OCP allows different systems and technologies to interact in a real time environment. The OCP is a control system developed at Georgia Tech for the autonomous control of unmanned aerial vehicles.^{65,66} It allows for configurability, reconfigurability, and integration of different subsystems in order to react and adapt to situational changes.⁶⁷

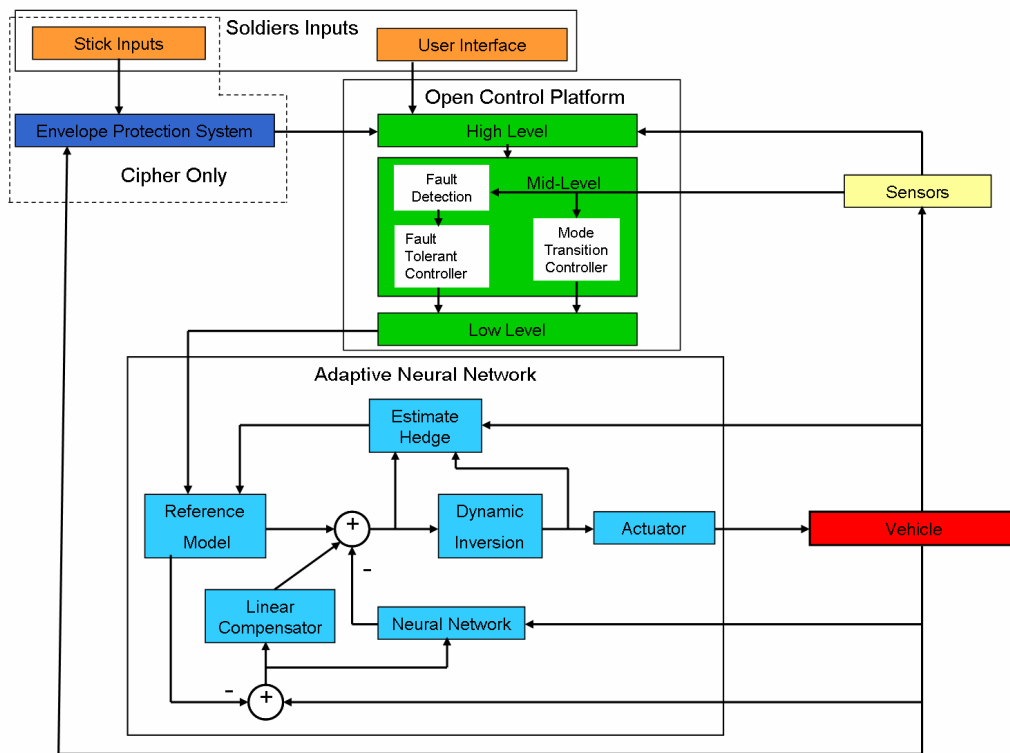


Figure 11-5: Autonomous Control Flow Diagram

Both vehicles require several different modes of flight: takeoff, hover, forward flight cruise, loiter, NOE flight, and landing in addition to emergency aggressive maneuvers. The OCP allows different control systems to take over as necessary; if the OCP detects that a different flight mode is required the controller responsible takes over control of the vehicle from the previous controller. The OCP also links situational awareness systems to the control systems giving the vehicle all the information it needs to fly and conduct the appropriate maneuvers.

The OCP has a control hierarchy, shown in Figure 11-5, which consists of high, middle, and low level controls. The high level controls consist of mission planning and replanning, and choosing the appropriate flight modes to execute the mission plan. The middle level controls are responsible for flight mode transitions, fault detection, and system reconfiguration. The low level controls are the stability and control algorithms for a specific flight mode.

For the Cipher, the control stick inputs made by the soldiers are treated as flight mission plan changes that require flight mode changes. The envelope protection system interprets the stick inputs so that a dangerous flight mode is not activated. This system allows for the soldiers to have as much control of the vehicle as possible without endangering them or the vehicle. After the Cipher drops off the soldiers and returns to the capsule, the vehicle has to fly back with no input from the soldiers. In this flight mode the Cipher's only waypoint is the capsule, and the only mission replanning is based on obstacle and enemy avoidance.

Obstacle and enemy avoidance is based on both high and middle level controls that change the flight path and engage aggressive flight modes as necessary. During obstacle avoidance, an aggressive maneuver flight mode is engaged that allows the vehicle to avoid the obstacle and then return to its flight plan. For enemy avoidance, a new flight path is determined based on both the destination and the location of the enemies. The Cipher is also equipped with several autorotational modes that are activated if the fault detection system detects an engine out. Depending on the flight condition, a different autorotation control mode is activated to perform a safe landing.

The touch screen interface in the Cipher cockpit is capable of controlling the Dragonfly high level mission planning and replanning. However, the Dragonfly is capable of determining its own flight paths and is allowed to do more aggressive maneuvers. While the Dragonfly is loitering over the mission objective, the soldiers on the ground can input mission objectives that it will follow. Once again, the method by which each task is accomplished is determined by the open control platform of the Dragonfly. One of the major high level inputs is keeping the camera and other sensory equipment over a specific target area; the OCP allows the control systems to react to the needs of the sensor equipment to accomplish this mission task.

11.3.3. Adaptive Neural Network

The adaptive neural network is a robust system that allows the vehicle to dynamically change the input gains so that the response to control inputs are uniform⁶⁸. An adaptive neural network learns the appropriate gains for different maneuvers and stores them in memory for future use.

When the adaptive neural network receives inputs from the open control platform the adaptive neural network then attempts to have the aircraft follow the established flight path which is updated in real time as the aircraft progresses. This is done for every maneuver done of the Cipher and Dragonfly. Previous uses of the adaptive neural network, such as the GTMax, have yielded excellent results with autonomous vehicles.⁶⁹

11.4. Control Interface

The main design features of the cockpit and user interface are ease of use and versatility. Because the two soldiers on board are not trained as pilots, their control of the vehicle must be limited, and the user interface should be intuitive. The soldiers have the option to let the aircraft fly itself autonomously using the preprogrammed trajectory while the soldiers perform other mission tasks. The user interface is capable of handling the myriad of tasks the soldiers need to complete in route to the objective. The cockpit features four touch screens that can display mission information to the soldiers. Each screen can be split into two or four separate screens as shown in Figure 11-7. The communications equipment provides over the horizon jam resistant and allows communication between other aircraft and mission command.

Each screen is controlled by command buttons on the left side of the screen. The various “pages” are navigated using command buttons on the bottom of each screen as shown in Figure 11-6. The pages listed on the bottom menu are set by the soldiers from

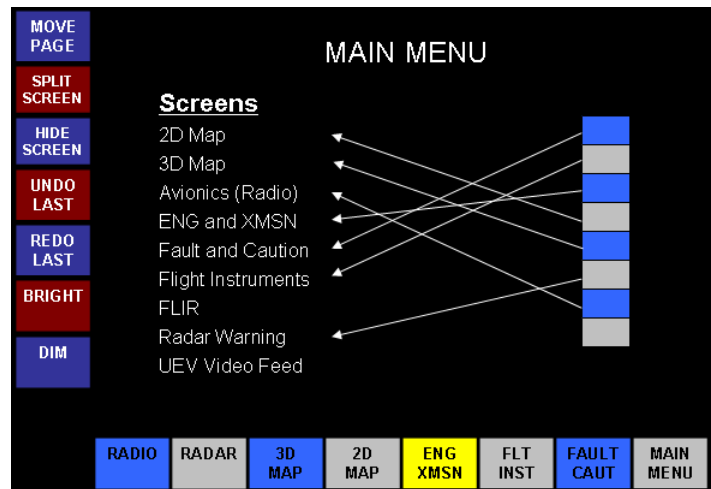


Figure 11-6: Main Menu Screen

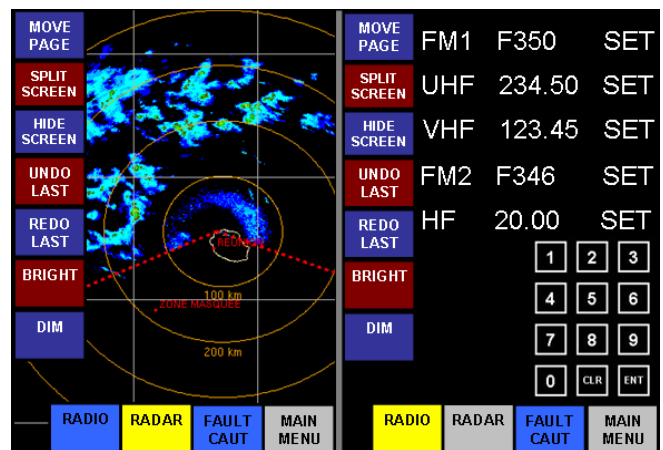


Figure 11-7: Split Screen View

the main menu screen shown in Figure 11-6. The soldiers select the available pages from a drop down list, and select those for the command buttons. Additionally, the soldiers can directly view pages listed in Table 11-3

Table 11-3: List of Touch Screen Pages

Instrument Panel	3-D Moving Map	2-D Map
UEV Video Feed	Common Missile (IR and Radar) and Weather Warning System	Avionics (Radio)
FLIR	Fault Detection/Warning	Engine Instruments

The 3-D moving map is used for waypoint control. A waypoint menu as shown at the top of Figure 11-8 allows for the adding, editing and deletion of waypoints. At each waypoint, airspeed, heading, and altitude are set by the soldiers. If the soldiers do not input specific values for each waypoint, the Cipher will maintain airspeed and altitude. Options for each waypoint such as hover, loiter, and land exist under the “action” menu. The “route” menu allows for the uploading and editing of preplanned waypoint sequences. Upon selecting each menu, a list of options, shown in Figure 11-8, for that menu is shown as well as a numeric keypad that allows for the entry of heading, airspeed, and altitude.

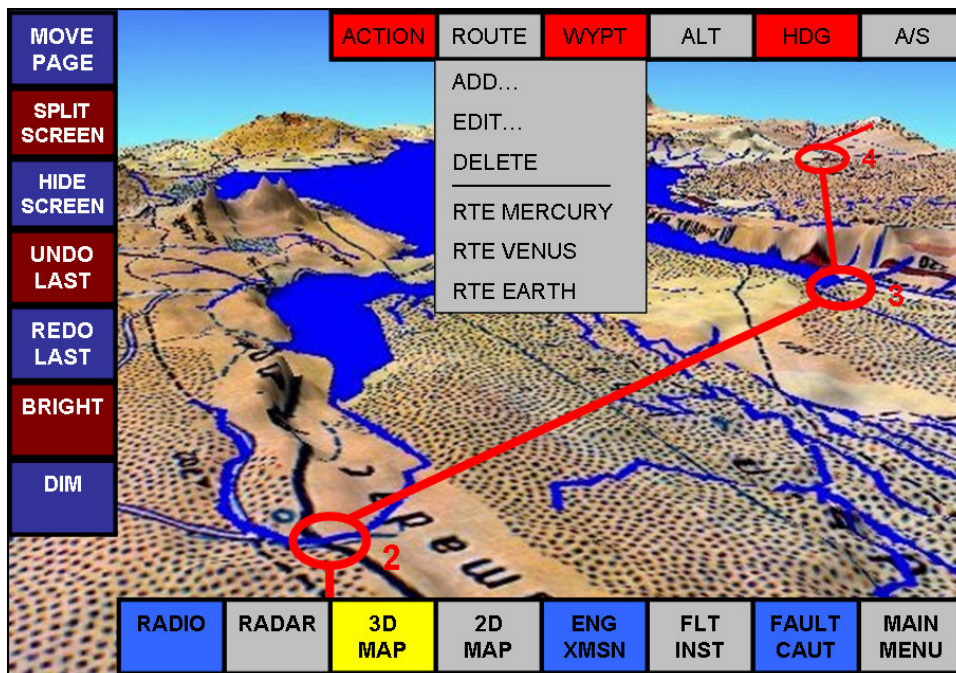
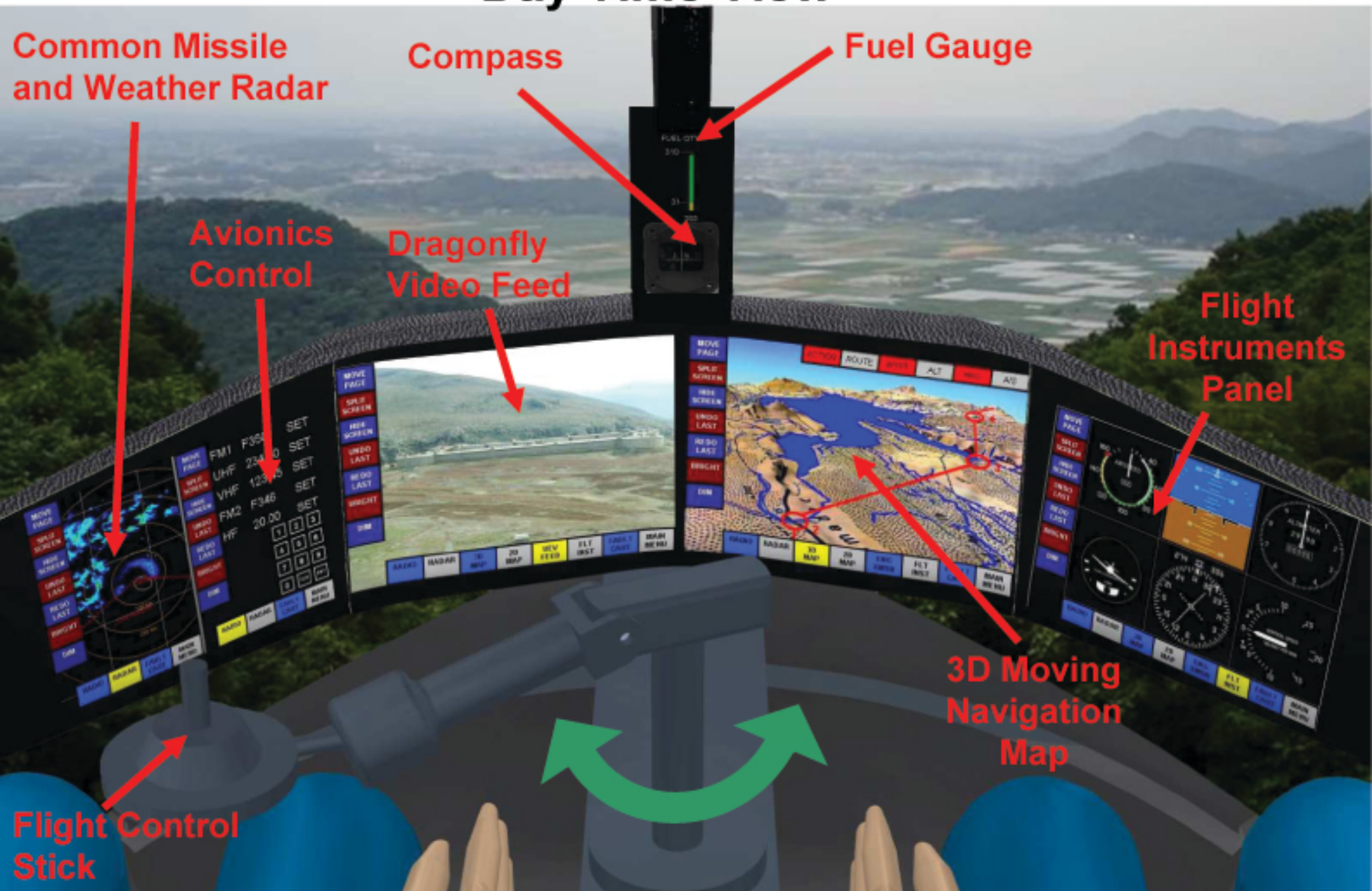


Figure 11-8: 3-D Moving Map

Figure 11-9: Cipher Cockpit Design

Day Time View



Night Time View (NVG Compatible)



11.5. Dragonfly Hover to Forward Flight Transition Analysis

For any tailsitter concept, the transition from hover to forward flight is always of special concern. The takeoff procedure for the Dragonfly is shown in Figure 11-10. A software tool was developed that based on airspeed and pitch angle, changes the tail angle of attack and the rotor thrust vector to balance the longitudinal forces and moments. Multiple velocity solutions were found for each pitch angle creating a velocity corridor as the Dragonfly transitions from hover to forward flight.

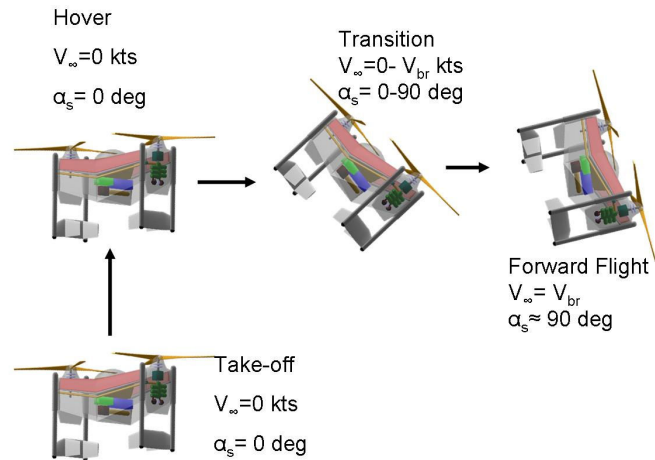


Figure 11-10: Dragonfly Transition

The transition corridor shown in Figure 11-11 gives the range of pitch angles the UEV can fly at a given velocity. Using this software the necessary size of the horizontal tail was determined to be twenty-six square feet.

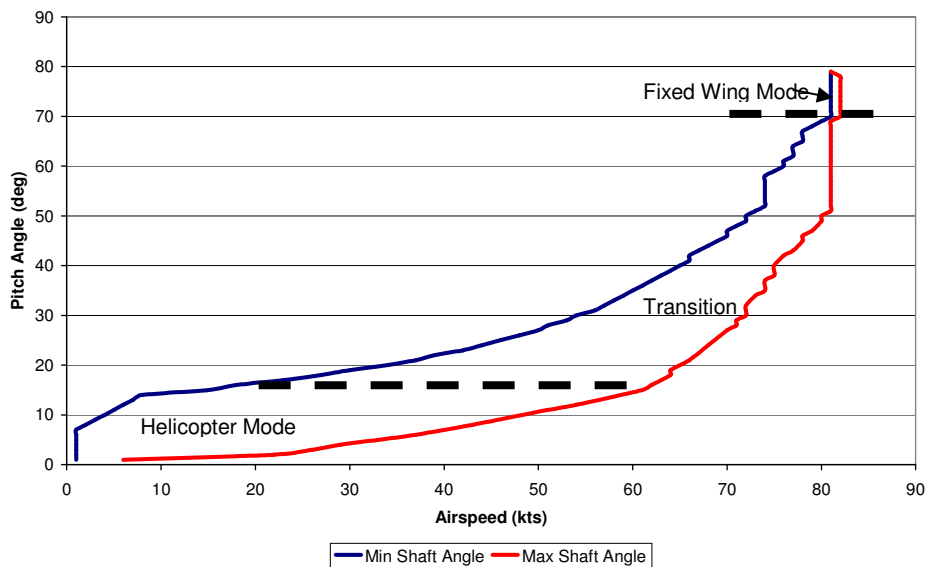


Figure 11-11: Dragonfly Transition Corridor

The wing does not have an incidence angle compared to the rotors; this means that even at steady level flight the Dragonfly will have a nose up attitude. Because of this, when it reaches seventy degrees pitch angle it has essentially fully transferred to forward flight and now functions as a fixed wing vehicle. The red and blue line in the plot represents the minimum and maximum pitch angles, respectively. Any angle between those two lines can result in trimmed flight. At low speeds the UEV can fly at a wide range of velocities without changing pitch angle. This gives the UEV good maneuverability near hover.

12. Cost Analysis

Cost was not a major driver in the conceptual design of the Cipher and Dragonfly vehicles. Based on the current retrofits of the four Ohio class vessels for use in SOF operations, acquisition and operating cost of the aircraft are only a small fraction of the total system cost. Costs are broken out by their major elements with all costs specified in 2007 dollars.

12.1. Submarine Retrofit Cost Estimate

The single largest system cost component is the retrofit of the Ohio class submarines. Since four Ohio class subs have already been modified from a SSBN (Ballistic Missile) to a SSGN (Guided Missile) configuration, this conversion cost is the best source for estimating a sub conversion cost in order to carry the VTOL platforms.

The SSGN modifications were initially funded in 2002, at a cost of \$440 million⁷⁰ for design and development of a conversion that would modify the sub from carrying 24 nuclear ballistic missiles, to carrying 156 cruise missiles and support SOF operations. These modification included shortening of the missile compartment and utilizing the lower portion for SOF storage and crew handling. The SSGNs were designed to carry a minimum of 66 SOF for extended several month missions, or up to 102 SOF for short duration missions. All four Ohio class subs were converted for an additional cost of approximately \$1.2 billion⁷¹. The conversion from SSBN to SSGN is significantly less than that required to go from a SSBN to SSCN (Carrier) capability. Based on these amounts and accounting for inflation, a SSCN design and development modification cost would be \$800 million. A per unit cost to modify each submarine would be \$600 million per SSCN. Therefore, with only a single SSCN sub modification, a reasonable estimate is in the neighborhood of \$1.4 billion.

12.2. Capsule Cost Estimate

The launch and recovery capsule system is even more difficult to estimate since it is a unique vehicle that approaches the complexity of a submarine, but with fewer systems and only shallow water pressure forces exerted on the primary structure. The most similar vehicle that has been developed in recent history that could provide empirical cost estimation is the Advanced Seal Delivery System (ASDS). The ASDS is a mini-sub which was developed for a use with a variety of submarines, and includes the SSGNs, to transport 2 crew and up to 16 SEALs from sub to shore.⁷¹ The vehicle is 55 ton, 65 ft long, 6.75 ft wide, 8.25 ft high and was initially estimated to cost \$80 million per unit.⁷² However, the ASDS currently has over a \$2 billion development cost, with an estimated per unit cost of \$125 million.^{73, 74}

Each capsule weighs about twice as much as an ASDS, but encompasses over 10 times as much volume. The interior power and life support systems are comparable, and provide environmental considerations for a similar number of personnel. However, the capsule elevator, seals, and pump systems provide added complexity and cost over the ASDS. A reasonable estimate for this conceptual study is considered to be \$800 million for the design and development of the capsule, with a per unit cost of approximately \$200 million. For a single SSCN sub modification, capable of utilizing 5 capsules, a total capsule cost estimate is \$1.8 billion.

12.3. Autonomous Flight Control System Cost Estimate

The autonomous control system for both the ARV and UEV is separated from the rest of the acquisition cost since it involves a major investment. A similar control system utilizing the OCP and an adaptive neural network has been flight tested as part of the DARPA Software Enabled Control Program. The control system has also been used to model a fixed wing transition from hover to forward flight.⁷⁵ Examples of semi-autonomous programs such as GlobalHawk, at \$6.3 billion for 51 aircraft⁷⁶, can only be considered indicative of the costing scope for such a sophisticated flight control system that could be flown by non-pilots. The Firescout is the most appropriate control system costing corollary since it involved the use of automating an existing aircraft, the Schweizer 333. The initial contract for the Firescout was awarded in 2000 for approximately \$94 million. Since then, an additional \$314 million has been awarded for FireScout development, with a total of 5 airframes delivered.⁷⁷ The per unit ground station cost excluding this development is estimated to be \$8 million, while the Schweizer 333 currently sells for about \$600,000. This cost differential indicates how expensive the semi-autonomous or autonomous system cost is in comparison to the actual vehicle cost. The recurring cost of the autonomous control system is relatively small since a huge portion of it involves software development and testing verification. The development cost of \$750 million for both vehicles and per unit cost of \$10 million was assumed to account for the increased cost of man-rated autonomy and inflation from the relevant case data.

12.4. Acquisition Cost Estimate

The prior cost estimates were developed qualitatively to put into context the Cipher and Dragonfly development and acquisition costs. Combining the sub modification, capsule and autonomous control system cost yields a total of \$4.15 billion for the development and a single operational SSCN, not counting the vehicle costs. The Bell Helicopter method was utilized for vehicle acquisition cost estimation. Calibrations were performed across comparable light helicopters⁷⁸ and inflated to 2007 dollars. A production volume of 200 Cipher and 200 Dragonfly units was assumed. The RDT&E costs of the vehicles are amortized in the acquisition costs.

The Cipher and Dragonfly acquisition costs are shown in Table 12-1, excluding the autonomous control system which was estimated above. As can be seen, the vehicle costs are a small portion of the overall system cost.

Table 12-1: ARV and UEV Acquisition Costs (2007 Year Dollars)

Component	ARV	% of Cost	UEV	% of Cost
Main Rotor System	68,574	12.6	71,221	15.5
NOTAR Tail Rotor	26,598	4.9	0	0
Fuselage Structure	42,675	7.9	11,355	2.5
Nacelle Structure	8,263	1.5	34,540	7.5
Hor and Vert Tails	3,958	.7	9,975	2.2
Wing	0	0	34,489	7.5
Landing Gear	22,530	4.2	17,578	3.8
Engine System	123,303	23.0	68,632	14.9
Fuel System	7,490	1.4	10,403	2.3
Transmission	61,084	11.4	35,201	7.7
Instruments	16,375	3.1	16,375	3.6
Electrical System	14,997	2.8	15,102	3.3
Hydraulics/Pneumatics	13,334	2.5	6,625	1.4
Furnishings	6,649	1.2	0	0
AC and De-ice	5,661	1.1	5,784	1.3
Ballistic Protection	7,014	1.3	0	0
Assembly, Tooling, Profit	108,022	20.1	121,841	26.5
Total Airframe Cost	536,527		459,121	

Table 12-2: Total Aircraft Development Cost

Component	Cipher	Percent	Dragonfly	Percent
Airframe Cost	536,527	3.95	459,121	3.4
RDT&E Cost	1,104,170	8.15	1,104,170	8.2
Autonomous Control System	11,875,000	87.9	11,875,000	88.4
Total	13,515,697		13,438,291	

Conclusions

The complex nature of the RFP requires iterative aircraft and launch system designs. The system of systems nature of the design solution forces all three components (ARV, UEV, and launch system) to be designed in parallel. Submarine based operations imply that mission stealth is imperative. Severe space limitations on a submarine also place strong emphasis on aircraft compactness. In order to maximize soldiers deployed to the objective the aircraft storage size must be minimized.

In order to improve mission stealth and security, the acoustic signature of each aircraft was minimized during the most crucial aspects of the mission. For the ARV, the most crucial aspect of the mission is the final approach and landing to the objective. For the UEV, the most crucial aspect of the mission is the loiter over the objective. Due to this difference and the long loiter requirement of the UEV, separate configurations were chosen for the ARV and UEV.

Since the SOF soldiers operating the ARV are not trained as pilots and the UEV is unmanned, both vehicles require an autonomous control system. This system is responsible for the overall safety of both aircraft. The soldiers input tactical decisions which are then interpreted and followed by the autonomous control system within the programmed flight envelope.

The Cipher was designed to minimize acoustic signature through low disk loading, low rotor tip speed, and advanced blade tip design. The storage volume of the Cipher is minimized through the design of automatically folding landing gear, rotor blades, and tail. The Dragonfly was also designed to minimize acoustic signature and storage volume. However, since the Dragonfly is not required to land at the objective, the acoustic signature is further reduced by taking advantage of noise directivity by flying in airplane mode and minimizing the rotor tip speed. The dragonfly minimizes storage volume by using a box wing design with extending tail struts and folding rotor blades.

The Barracuda capsule was designed to act independently of the submarine, allowing the submarine to depart the launch area after launching the Barracuda. The low CG of the capsule gives excellent stability during aircraft takeoff and landing.

Overall, the system of systems solution provided by the Cipher, Dragonfly, and Barracuda allows for excellent mission capability while maximizing the overall stealth of the operation and minimizing the risk to the submarine.

References

- ¹ “Advanced Deployable Compact Rotorcraft in Support of Special Operation Forces” 2007 Request for Proposal American Helicopter Society
- ² Dewey, D. B. “Full-Scale Demonstration of Vertical Float Sea-Stabilization Concept, Phase I.” Report General Dynamics San Diego CA, Convair Division
- ³ Interagency Helicopter Operations Guide (IHOG), NFES 1885 March 2006
- ⁴ Smith, Kim “2007 AHS Design Competition Questions” March 2007
- ⁵ Hassan, A.A., Charles, B.D., Tadghighi, H., and Sankar, L.N., “Blade Mounted Trailing Edge Flap Control for BVI Noise Reduction,” NASA CR 4426, February 1992..
- ⁶ “Boeing Noise Certification Tests” <http://www.boeing.com/ids/news/mdc/97-21.html>
- ⁷ Naval Technology SSBN Ohio Class Ballistic Missile Submarine, USA <http://www.naval-technology.com/projects/ohio/>
- ⁸ Voith Schneider Propellers, Voith Turbo.
http://www.voithturbo.com/vt_en_pua_marine_vspropeller.htm
- ⁹ Leishman, J. Gordon, “Principles of Helicopter Aerodynamics” Cambridge Aerospace, 2006.
- ¹⁰ Pouty, R. W., *Helicopter Performance, Stability, and Control* Krieger Publishing. Malabar, Florida 1995
- ¹¹ “Engineering Design Handbook, Helicopter Engineering Part Two: Detail Design” AMCP 706-202 Army Materiel Command, Alexandria, VA
- ¹² Hiller Aircraft Corporation, “Performance Data Report – Proposal for the Light Observation Helicopter” Engineering Report No.60-92.
- ¹³ Group Weight Statement – OH-6A, Hughes Aircraft, Jan 10, 1978
- ¹⁴ Wantanbe, Masatoshi, Takada, Yoshihiro “Prediction Model for Aeroacoustic Noise from Low-Speed Fans AIAA 99-1983
- ¹⁵ Lighthill, M. J. 1952 On sound generated aerodynamically I. General theory. Proc. R. Soc. London A 211, 564-587.
- ¹⁶ Mosher, M., and Peterson, R. L. "Acoustic Measurements of a Full-Scale Coaxial Rotor." AIAA-83-0722, 8th Aeroacoustics Conference, Atlanta, GA, April 1983
- ¹⁷ Brieger, J. T., Maisel, M. D., Gerdes, R., "External Noise Evaluation of the XV-15 Tilt Rotor Aircraft" American Helicopter Society, National Specialists Meeting on Aerodynamics and Aeroacoustics, Arlington, Texas Feb 1987.
- ¹⁸ Hanson, Tom “A Designer Friendly Handbook of Helicopter Rotor Hubs, “1998.

-
- ¹⁹ Peterson, Randall L., “Full-scale Hingeless Rotor Performance and Loads” NASA TM-110356 Ames Research Center 1995
- ²⁰ Cummings, Darold B., Hoisington, Zachary “Dual-mode Air Transportation System (DARTS) Boeing Phantom Works 2002.
- ²¹ MD520 Technical Description http://www.mdhelicopters.com/products.php?id=MD_520N
- ²² DeltaHawk Engines, www.deltahawkengines.com.
- ²³ Snyder, Melvin H., “Effects of Wingtip Mounted Propellers on Wing Lift and Induced Drag”, *Journal of Aircraft*, Vol 6 No 5, p 392-397, Sept 1969.
- ²⁴ Reeder, Brewer FSWT Tests of Vought-Sikorsky V-173 Airplane, NACA TN-2014, April 28, 1942.
- ²⁵ Hoerner, S., *Fluid-Dynamic Drag* 1965
- ²⁶ Validation of PCA2000 – The Glasair III, Optimal Aircraft Design, Technical Note Ref NT04001EN, April 2004.
- ²⁷ Seeley, Brien, Glasair III Flight Test Results, CAFÉ Aircraft Performance Report
- ²⁸ Pegg, Robert, J., “An Investigation of the Helicopter Height-Velocity Diagram Showing Effects of Density Altitude and Gross Weight” Langley Research Center, NASA, Washington D.C. 1968
- ²⁹ Group Weight Statement – R-44, Robinson Aircraft
- ³⁰ Moore, Mark. “NASA/Lockheed Strut and Box Wing Weight Methodology,” NASA Langley Systems Analysis White Paper, June, 1998.
- ³¹ Stevenson, Greg, GSE High Specific Heavy Fuel Engine, NASA Phase II STTR Final Report, March, 2007.
- ³² V. Volovoi, “Stochastic Petri Nets Modeling using SPN@,” RAMS-2006 Symposium, Newport Beach, CA, January 26–29, 2006; Paper 2006RM-166
- ³³ V.V. Volovoi, “Modeling of System Reliability Using Petri Nets with Aging Tokens,” *Reliability Engineering and System Safety*, 84, no. 2 (2004): 149–161.
- ³⁴ Iraq Index: Tracking Variables of Reconstruction & Security in Post-Saddam Iraq The Brookings Institute
- ³⁵ Allan, Nelson S., A Practical Reliability Evaluation of Embedded Avionic Software, Southern Tier Technical Conference, 1987
- ³⁶ Texas Tech University <http://www.physicalplant.ttu.edu/PhyPlant1/StrategicPlans/PPStrategicPlanFY07FINAL.pdf>
- ³⁷ Maintenance, Replacement, and Reliability: Theory and Applications By A. K. S. Jardine, Albert H. C. Tsang

-
- ³⁸ G. Griffiths, N. W. Millard, S. D. Mcphail, P. Stevenson, P. G.Challenor “On the Reliability of the Autosub Autonomous Underwater Vehicle” Southampton Oceanography Centre. Underwater Technology, July 2001.
- ³⁹ Yeo, Hyeonsoo., Bousman, William G., Johnson, Wayne., “Performance Analysis of a Utility Helicopter with Standard and Advanced Rotors” American Helicopter Society Aerodynamics, Acoustics, and Test and Evaluation Technical Specialist Meeting, San Francisco CA, January 23-25 2002
- ⁴⁰ Yeo, Hyeonsoo., Johnson, Wayne, “Assessment of Comprehensive Analysis Calculation of Airloads on Helicopter Rotors” Journal of Aircraft Vol. 42, No. 5, 2005
- ⁴¹ Joncheray, Ph., “Aerodynmics of Helicopter Rotor in Hover: The Lifting-Vortex Line Method Applied to Dihedral Tip Blades” Aerospace Science and Technology, 1997 N1, 17-25
- ⁴² Hoad, Danny R., “Evaluation of Helicopter Noise Due to Blade-Vortex Interaction for Five Tip Configurations,” NASA Technical Paper 1608. AVRADCOM Technical Report 80-B1, December 1979.
- ⁴³ Dessoper A., LafonP., Phillippe J.J. and Prier J., “Effect of an Andedral Sweptback Tip on the Performance of a Helicopter Rotor,” 44th Annual Forum of the American Helicopter Society, Washington D.C. June 16-18 1988
- ⁴⁴ Santa Maria, O.L., Mueller, A.W., “Acoustics of UH-60 Blackhawk with Growth Rotor Blades” American Helicopter Society Annual Forum, 1997
- ⁴⁵ Voirun, B.H., Herter, J.R., Nuttall, J.C., and Trainer, T.N., “Growth Main Rotor Blade Feasibility Demonstration Test Program,” 51st Annual forum Proceedings, American Helicopter Society, Fort Worth, TX 1995
- ⁴⁶ Hodges, D. H., Atilgan, A. R., Cesnik, C. E. S., and Fulton, M. V., “On a Simplified Strain Energy Function for Geometrically Nonlinear Behaviour of Anisotropic Beams,” *Composites Engineering*, Vol. 2, No. 5 – 7, 1992, pp. 513 – 526.
- ⁴⁷ Yu,W., Volovoi, V. V., Hodges, D. H., and Hong, X., “Validation of the Variational Asymptotic Beam Sectional Analysis,” *AIAA Journal*, Vol. 40, No. 10, 2002, pp. 2105 – 2112
- ⁴⁸ Bauchau, O. A., \DYMORE User's and Theory Manual," Technical Report <http://www.ae.gatech.edu/~obauchau/dymore/dymore.html>, 2003.
- ⁴⁹ Edwards, B., Cox, C., “Revolutionary Concepts for Helicopter Noise Reduction – S.I.L.E.N.T Program” NASA/CR-2002-211650
- ⁵⁰ Srinivasa, G.R., Baedert, J.D., “TURNS: A Free-Wake Euler/Navier-Stokes Numerical Method for Helicopter Rotors” *AIAA Journal* 1993 0001-1452 vol.31 no.5 (959-962)

-
- ⁵¹ Srinivasa, G.R., Baedert, J.D., “Flowfield of a Lifting Rotor in Hover: A Navier-Stokes Simulation”
AIAA Journal 1992. Vol 30
- ⁵² Usta, E., Wake, B.E., Egolf, A.T. and Sankar, L.N."Application of a Symmetric Total Variation Diminishing Scheme To Aerodynamics and Aeroacoustics of Rotors,"American Helicopter Society 57th Annual Forum,Washington D.C., May 9-11,2001
- ⁵³ Usta, E., “Application of a Symmetric Total Variational Diminishing Scheme to Aerodynamics of Rotors,” Ph.D. Dissertation, School of Aerospace Engineering, Georgia Institute of Technology, August 2002.
- ⁵⁴ Vasilescu, Roxana “Rotor Wake Capture Improvement Based on the Controlled Grid Resolution”
AIAA 2006-1151
- ⁵⁵ Brentner, K. S., “Prediction of Helicopter Rotor Noise – A Computer Program Incorporating Realistic Blade Motions and Advanced Formulation,” NASA TM-87721, 1986
- ⁵⁶ Brentner, K. S., Perez, G., Bres, G., Jones, H., “Towards a Better Understanding of Maneuvering Rotorcraft Noise” American Helicopter Society 58th Annual Forum, Montreal, Canada June 11-13 2002.
- ⁵⁷ Ffowcs Williams, J.E., Hawkins, D.L. “Sound Generation by Turbulence and Surfaces in Arbitrary Motion” Philosophical Transactions of the Royal Society of London. Series A *Mathematical and Physical Sciences*, Vol. 264, No. 1151 (May 8, 1969), pg 321-342.
- ⁵⁸ Shigley, Joseph Edward and Mitchell, Larry D. Mechanical Engineering Design. Fourth Edition, McGraw-Hill Company. 1983
- ⁵⁹ Tho, C., Sparks C, Smith, Sareen A., and Johnson, C., “*Efficient Helicopter Skid Landing Gear Dynamic Drop Simulation Using LS-DYNA*,” Bell Helicopter Textron and NAVAIR, American Helicopter Society (AHS) 59th Annual Forum, Phoenix, AZ, May 6-8, 2003.
- ⁶⁰ Rambler, Georgia Institute of Technology, 23rd Annual Student Design Competition 2006
- ⁶¹ GKN Aerospace to Supply Extended Flotation System for S-92 <http://www.aerospace.gknplc.com/PageViewer.aspx?page=S632763687498380000&src=>
- ⁶² Prouty, R, “Helicopter Performance, Stability, and Control”
- ⁶³ Clough, B, “Metrics, Schmetrics! How The Heck Do You Determine A UAV’s Autonomy Anyway?”
- ⁶⁴ Willis, L, Sander, S, Kannan, S, Kahn, A, Prasad, JVR, Schrage, D, “An Open Control Platform For Reconfigurable, Distributed, Hierarchical Control Systems”
- ⁶⁵ Wills, L, et al., “An Open Control Platform for Reconfigurable Control,” IEEE Control Systems Magazine, vol. 21, no. 3, June 2001.

-
- ⁶⁶ Schrage, Daniel P., Vachtesvanos, George, “Software Enabled Control (SEC) for Intelligent UEVs” AIAA 2002-3450
- ⁶⁷ Ingvalson, R., Rotstein, H. P., Kevicky, T., Balad, G. J., “Fault Detection Design for Uninhabited Aerial Vehicles” AIAA 2005-6251
- ⁶⁸ Kannan, S., “Adaptive Control Of Systems In Cascade With Saturation”
- ⁶⁹ Johnson, Eric N., Schrage, Daniel P. “The Georgia Tech Unmanned Aerial Research Vehicle: GTMAX” DARPA Software Enabled Control (SEC) Program
- ⁷⁰ Ohio Class SSGN-726 Tactical Trident, GlobalSecurity.com,
<http://www.globalsecurity.org/military/systems/ship/ssgn-726.htm>.
- ⁷¹ Secret Delivery: Advanced SEAL Delivery System (ASDS), Military.com,
http://www.military.com/soldiertech/0,14632,Soldiertech_ASDS,,00.html.
- ⁷² Advanced SEAL Delivery System, Wikipedia,
http://en.wikipedia.org/wiki/Advanced_SEAL_Delivery_System
- ⁷³ ASDS: The Future of Submarine-Based Special Operations,
http://www.chinfo.navy.mil/navpalib/cno/n87/usw/issue_14/asds.html.
- ⁷⁴ Defense Industry Daily, ASDS Mini-Sub Program Taking on Water, Dec 6, 2005.
- ⁷⁵ Johnson, E., Turbe, M., Wu, A. D., Kannan, S., Neidhoefer, J. C., „Flight Test Results of Autonomous Fixed-Wing UAV Transitions to and from Stationary Hover“ AIAA 2006-6775
- ⁷⁶ Price of Global Hawk Surveillance Program Rises, The Washington Post, December 7th, 2004.
- ⁷⁷ FireScout VTUAV Program: By Land and By Sea, Defense Industry Daily, July 31st, 2006.
- ⁷⁸ Helicopter Acquisition Costs, Field Research Corporation Survey, 2000.